Alma Mater Studiorum
Università degli Studi di Bologna

Dipartimento di Fisica e Astronomia

DOTTORATO DI RICERCA IN ASTRONOMIA

Ciclo XXVI

ENHANCING THE EFFICIENCY OF SOLAR CONCENTRATORS BY CONTROLLED OPTICAL ABERRATIONS

Dottoranda:

ALESSANDRA GIANNUZZI

Coordinatore:
Chiar.mo Prof.
LAURO MOSCARDINI

Relatori:
Chiar.mo Prof.
BRUNO MARANO
Dott.
EMILIANO DIOLAITI

Esame Finale Anno 2014

Settore concorsuale: 02/C1 - Astronomia, Astrofisica, Fisica della Terra e dei Pianeti
Settore scientifico-disciplinare: FIS/05 - Astronomia e Astrofisica

Contents

List of Figures

List of Tables

Summary

Concentrating Photovoltaic (CPV) technology is experiencing a growing interest thanks to the development of solar cells with efficiency continuously improved. At present, the best reported cell has a record efficiency of 44.4% at direct irradiance concentration of 302 Suns. A simple advantage induced by this technology is that, given the collected energy, the concentration performed by optical devices such as lenses or mirrors allows us to replace the area of photovoltaic material with cheaper optical surfaces. Moreover, high efficiency cells are too expensive to be used in non-concentrating applications. In this technology the light is focused using one large reflective element (dish), onto an array of photovoltaic multijunction cells densely packed to form a single detector. The dish tracks the Sun in two-axis during the day and it operates in high concentration mode, i.e. with solar flux up to hundreds times the ambient value. Reflective dish concentrators with diameters ranging from few meters to few tens of meters have been proposed and are at the beginning of their commercial development at typical working concentrations of 500×.

Traditional dish concentrators have paraboloidal shapes. Theoretically, their diameters could reach several tens of meters as the heliostats in the central tower plants, the construction of monolithic mirrors being difficult at these scales. The size generally imposes to approximate the profiles with cheap flat reflecting facets mounted on a common frame and reproducing globally the paraboloidal surface. As for the receivers, standard cells have rectangular shapes and the arrays are groups of cells densely packed together mostly in series and parallels connections. The arrays do consequently resemble rectangular shapes too. When a standard imaging mirror is coupled with a rectangular detector problems arise since it produces a solar image intrinsically circular: with this condition some cells could be obscured if the spot is smaller than the receiver, or part of the light could be lost if the detector is smaller than the spot. Both these effects contribute to a substantial loss in efficiency. Moreover, the corresponding irradiance distribution is bell-shaped in contrast with the requirement of having all the cells under the same illumination. In fact, if the interconnected cells have identical electrical characteristics and experience the same irradiance/temperature conditions, each cell produces the same amount of output current and voltage. Mismatch losses instead occur when interconnected cells experience different conditions, in particular when the cells are series connected. Still few investigations

have been done specifically on current mismatches in dense array receivers under high concentrations. The issue relative to spatial light uniformity is instead widely known for single cells and this requirement is commonly approached by the introduction of secondary optics working as homogenizers but also increasing the system complexity and adding reflection losses, chromatic aberration and mechanical problems as alignment and stability. The presence of a secondary optics is rather useful to increase the acceptance angle leading to a relaxation of tracking and alignment tolerances.

In this thesis work we aim at solving these issues by a multidisciplinary approach, exploiting optical concepts and applications developed specifically for astronomical use, where the improvement of the image quality is a very important issue. The strategy we propose is to boost the spot uniformity acting uniquely on the primary reflector and avoiding the faceting of big mirrors into numerous smaller elements that need to be accurately mounted and aligned. In the proposed method, the shape of the mirrors is analytically described by the Zernike polynomials and its optimization is numerically obtained to give a nonimaging optics able to produce a quasi-square spot, spatially uniform and with prescribed concentration level. The free-form primary optics optimized in this way and validated by a ray tracing software leads to a substantial gain in efficiency without the need of a secondary optics. Simple electrical schemes for the receiver are required in our case. The concept has been investigated theoretically modeling an example of CPV application, including a conceptual development of non-optical aspects as the design of the receiver and of the supporting mechanics.

For the method proposed and the specific CPV system developed, a patent application has been filed in Italy with the number TO2014A000016. The patent has been developed thanks to the collaboration between the University of Bologna and INAF (National Institute for Astrophysics).

Chapter 1

Optics for solar concentrators

1.1 Introduction

The last decades of the past century have been characterized by an increasing dependence on fossil fuels, either for electricity production and transportation. The problems introduced by the uncontrolled overdrive of these kind of natural resources are mainly environmental, related to the limitation of the resources itself, to the waste management and to the necessity of reducing some subproducts, as particles and greenhouse gases, naturally emitted during combustion. The use of solar radiation as energy source is thus assuming an important role in modern society, both at the level of distributed micro generation and of large plants. This resource can in fact be considered as renewable and green in the literal sense of the terms, if we compare the time scale of its availability with the human mean lifetime or if we consider that it can be converted into other forms of energy without any form of pollutants production.

The density of the radiation coming from the Sun is often sufficient to be employed as it is for example to heat water under or around its boiling point of 373°K for different domestic uses. Another employment is to produce directly electricity by flat silicon photovoltaic panels. However, the radiation flux remains too low for other processes involved in large scale energy production where in general the conversion efficiency increases with temperature as the thermodynamics laws suggest.

The necessity of both reaching temperatures of several hundred degrees and of lowering the cost/watt of the energy produced (by increasing efficiency or by substituting expensive materials), led the research to investigate towards the solar concentration technology, particularly after the global oil crisis of the 1970s. Concentrated solar energy has been proving to be a valid mean to start this revolution and produce electricity and fuels (like hydrogen) from a completely renewable source. The operation principle at the base of this technology is to concentrate solar radiation into a focus zone where a light collecting receiver is positioned. As for thermal applications, the main advantage induced by this technology is very straightforward: it allows the use of absorbers with smaller surfaces and lower heat

losses, the latter being proportional to the absorber areas. In concentrated power plants (CSP) where the radiation is initially converted into heat, the receiver is an heat exchanger in which a fluid flows absorbing the radiation. High temperature\high pressure steam is then generated and channelled to drive a turbine. On the other hand, in *Concentrated Photovoltaic* (CPV) plants , the radiation is focused on a target made of high efficiency *cells* of semiconducting materials working under high energy density and producing directly electrical current. In this application, concentrating the sunlight by optical devices such as lenses or mirrors reduces not only the losses but also the area of the expensive photovoltaic materials used. Both the types of systems described have been proven to be technically and economically viable in the production of electricity and heat on demand, but further investigation are necessary to make these technologies economically competitive with the traditional fossil fuels.

We decided to investigate the possibility to improve the efficiency of a specific type of CPVs called dense array system, by introducing a new concepts of optics poorly experimented in the previous solar applications. These systems are relatively recent respect to other photovoltaic concentrators that have been widely investigated and where valid solutions have been found for the same optical problems that we will discuss. The issues discussed in this research will be exposed in Section 1.6, after an brief overview on the theory of solar concentration.

1.2 Thesis purpose and outline

The theory of nonimaging optics is clearly not new, but it has not been fully explored especially in solving the issues of high concentration. This specific branch seems to be principally addressed by secondary focusing devices to maximize the flux at the receiver and at the same time manage the irradiance distribution. The aim of this thesis is to propose a new nonimaging concentrator to replace the classical faceted dish employed in dense array systems. The concentrator has been designed for obtaining a square smooth irradiance pattern avoiding the use of refractive secondary optics (SO) and preventing the necessity of conceiving a complex receiver design in order to boost its conversion efficiency. Both theoretical methods and numerical tools have been implemented and the investigation led to the modeling of a whole CPV system, including a first stage design of non-optical aspects, such as the detector and of the supporting mechanics. The increase in conversion efficiency has been evaluated with a preliminary analytical model of dense array implementing a simple electrical scheme assuming the performances of commercial existing cells.

Throughout this Chapter, we will summarize some crucial aspects to understand the theory of solar concentration, also presenting the main examples of applications studied or built up to now. The open issues treated in this thesis are discussed in the last section of the Chapter, together with the existing solutions.

In the second Chapter, the photovoltaic effect will be briefly described and cells and arrays will be shown in their main aspects above all related to the concentration ratio. We will discuss some physical concepts and operating principles of the standard series/parallel connections and the problem of the non-uniform illumination in cells arrays.

In the third Chapter a new optical approach to solve the mismatches problems relative to the non-uniform illumination of CPV dense array receivers is proposed. We will describe a numerical algorithm based on analytical models, for both the optics and the receiver, appositely conceived to optimize the reflective surface in order to square and smooth the light collected with the aim to enhance the array conversion efficiency. We will show in detail the modeling and the simulations results obtained for the optical part of a specific application. Besides, the receiver electrical scheme appositely developed and its analytical modeling will be also explained, together with the procedures implemented to calculate the system tolerances.

In the fourth Chapter we will show the simulated performance of the designed concentrator, also in comparison with the performance of a monolithic imaging paraboloidal mirror dimensioned for the same collected radiation and average concentration ratio. The method implemented and the conceptual design of the concentrator has been patented in Italy. Mechanical schemes of the patent and procedures to calibrate/align the optics will be presented.

1.3 Basics of optics for solar concentrators

Before going deeply into concentrating optical devices, it is convenient to recall some basic definitions and characteristic quantities related to solar radiation. The different objects that drive the solar concentrators respect to the classical image forming devices have to be understood before starting the design of an optical concentrator.

1.3.1 Relevant parameters and definitions

The solar spectrum above atmosphere can be notoriously approximated by a blackbody spectrum radiating at about 5777°C hemispherically into space. The irradiance value at the atmosphere top defines the *solar constant* and a mean value of 1353 W/m^2 is often found in literature. This constant describes the power received on a unit area (perpendicular to the solar position vector), which is located in free space at the Earth mean distance from the Sun. As the radiation passes through Earth atmosphere, it is attenuated by the numerous scatterings occurring between the solar photons and atmospheric molecules and atoms. As result of these and other effects, three radiation components can be distinguished at the ground; direct, diffuse and reflected. The direct component is radiation travelling in a straight line from the Sun which were not scattered, absorbed or reflected by the atmosphere. The second is the solar radiation which has been diffused by atmosphere and clouds and,

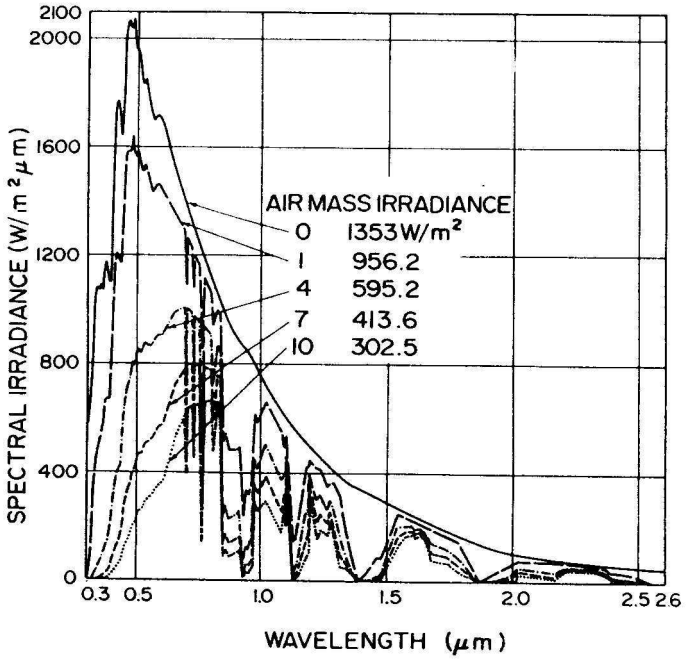

Figure 1.1: Solar spectrum at different air mass values [Tae1976]

as a result, it comes from all directions of the hemisphere. Reflected radiation describes sunlight that has been reflected back by the ground and the clouds. Global radiation is often considered as the algebraic sum of the three components irradiating a flat horizontal surface. Approximately 1000 $\mathrm{W/m^2}$ of the radiation crossing the atmosphere can reach the ground under clear weather conditions. This amount can be considered as a theoretical maximum because the real value impinging on the surface varies depending on the weather conditions, the location on Earth, the period of the year and the altitude of the Sun in the sky.

The only relevant part for a CPV system is the direct beam component, which is proportional to the cosine of the angle between the position of the sun in the sky and the normal to the horizontal surface. The term air mass (AM) often used in the field of solar energy, defines this concept as the ratio of the path length of the radiation through the atmosphere at a given solar zenith angle θ_Z, to the path length when the sun is directly at the local zenithal point. Numerically, the AM number is given by:

$$m = \sec(\theta_Z) \tag{1.1}$$

Fig. 1.1 shows the solar spectrum for different m. AM0 (air mass zero) refers to the absence of atmospheric attenuation. The International Organization for Standardization gives the AM1.5 solar spectrum as the reference value for rating photovoltaic cells and other solar energy components for terrestrial applications. The irradiance in this case is around 960 $\mathrm{W/m^2}$ (often approximated with 1000 $\mathrm{W/m^2}$ in the calculations) and it can be obtained by multiplying the extraterrestrial solar constant for m in the Eq. 1.1, with $\theta_Z = 48.19°$

[NrelWeb].

It is useful to express the density of energy in *sun* units, i.e. introducing a standard irradiance corresponding roughly the sunlight reference value so that: 1 sun = 1000 W/m^2. The power at the aperture and at the receiver of a concentrating system per unit area can be expressed in units of suns.

1.3.2 Concentration ratio and optical efficiency

The concentration is generally operated by optical devices such as lenses, mirrors or combinations of them focusing the light onto a receiver element. Given a quantity of light collected, it is then possible to reduce the area of the active material used by a factor roughly equal to the *concentration ratio*. Literature gives several definitions for it.

The geometrical concentration C_g is the ratio between the projected area A of the entrance concentrator aperture onto a plane normal to the direction of the incoming radiation and the receiver area A_{abs} [Win2005]:

$$C_g = \frac{A}{A_{abs}} \tag{1.2}$$

The areas in Eq. 1.2 can be replaced by widths or diameters squared respectively for linear or rotational system. This definitions considers only the ratio between the two areas chosen but not the effective number of rays emerging form the exit aperture.

Different possible definitions of the geometrical concentration arise from the definitions of both the entrance aperture area and the receiver area [Ben2005]. With respect to the concentrator entrance aperture area, sometimes the fully occupied area A is used, while other times, if a portion of the aperture is clearly inactive by design (for instance, if there is a gap or an obscuration), it is excluded from the aperture area. It should be noted that the concentrator topology may affect the decision of how to define the aperture area. For the receiver area, for example a cell, sometimes the optically active cell area, i.e. that to be illuminated, is used to define C_g, while other times the full cell area is computed. If the entrance aperture is defined by A_E and the cell aperture A_R, four definitions of C_g are possible including or not the active/inactive area for both. Let us highlight two: $C_{g1} = A_{Efull}/A_{Rfull}$ and $C_{g2} = A_{Eact}/A_{Ract}$. The first definition considers both the inactive areas and it is the only useful for estimating material costs, while the second definition is suitable for optical and electrical calculations taking into account only the active zones. As an example, consider the cells in a flat module. In this case $C_{g2} = 1$ but $C_{g1} < 1$, due to the gaps between the cells and the typical non-squared cell contour (if the cell were circular, C_{g1} would equal 0.78, while the typical value for the common cells smoothed at the corners is 0.95-0.98). The example of the flat module is useful to understand the case of dense array CPVs where many cells are closely packed all together to form a single receiver.

The parameter which describes the transmission of rays through the concentrator is the optical concentration ratio or *optical efficiency*. A first definition η_{opt1} is the light power

transmission efficiency through the concentrator up to the receiver surface for light rays impinging at the entrance aperture from a given nominal direction, (usually the normal incidence). It is the ratio between the power at the focal plane and at the collector aperture, which is effectively the dot product of the sunlight density reaching the ground by the apertures considered. This definition is wavelength dependent and cell independent, but it also takes into account the losses due to reflection, scattering, absorption, etc. Other definitions are given in literature but these will be omitted for simplicity.

The definitions assumed in this work are C_{g1} and η_{opt1} as it will be used in Section 3.2. The geometrical concentration will be indicated with the symbol $\times$ or the letter C hereafter. With this notations, a 100$\times$ ideal system with no losses/obscurations, considering its full active areas and supposing an energy density of 800 W/m^2 = 0.8 suns at the entrance aperture, would have an irradiance of $800 \cdot 10^2$ W/m^2 = 80 suns at the receiver.

Another important concept for concentrators that will be analysed in depth in the next section is the *acceptance angle*, that is the angular range over which 100% of the incoming rays are accepted and collected at the receiver. This is an ideal condition, since it is not always possible to construct concentrators for collecting the whole radiation through the entrance aperture. The definition can sometimes include a fewer percentage than the 100%. It is intuitively important that, regardless the definition given, a solar concentrator is designed for an acceptance angle al least of the same angular size of the Sun. We can look at the acceptance angle as an index of the system tracking tolerance as well as of its sensitivity on imperfections of optical surfaces, mechanical alignments, etc.

1.3.3 Limits to concentration

One of the main tasks at the beginning of the investigations on concentration, was to understand how to direct efficiently a bundle of rays in a specific angular cone onto the smallest possible aperture. The result was firstly derived by Winston [Win1969] using phase space conservation, and later by using the étendue definition [Win2005]. Knowing the solar angular size (but in general having a maximum acceptance angle), he showed that it is possible to calculate the theoretical maximum concentration that a system can reach by deriving a generalization of the Abbe sine condition.

The same result has be derived by simple thermodynamical arguments starting from the general definition in Eq.1.2 and using the physical dimensions of the Sun-Earth system, as shown by Rabl in [Rab1975]. In Fig. 1.2 the Sun is represented as an isotropically radiating sphere of radius r, θ_c is the half angle subtended by the Sun, the entrance aperture is A, the absorber aperture is A_{abs} and R is the distance between the aperture and the source. In the the limit $A/R^2 \to 0$ and with $\sin(\theta_c) = r/R$, the light arriving in A is uniformly distributed over the angles smaller than $|\theta_c|$. Supposing the system to be in an infinite empty space and that the source and the absorber are black bodies at temperature T_s and T_{abs} respectively,

the source emits an amount of radiation

$$Q_s = 4\pi r^2 \sigma T_s^4 \tag{1.3}$$

where σ is the Stephan-Boltzmann constant. Calculating the density spread at distance R and supposing no losses between the aperture and the absorber, the power transferred to the absorber is calculated from Eq. 1.3

$$Q_{s\to abs} = A\frac{r^2}{R^2}\sigma T_s^4. \tag{1.4}$$

As for the absorber, it radiates similarly

$$Q_s = A_{abs}\sigma T_{abs}^4 \tag{1.5}$$

and it transfers to the source a power

$$Q_{abs\to s} = \epsilon A_{abs}\sigma T_{abs}^4 \tag{1.6}$$

where ϵ is essentially an exchange factor. Since the second thermodynamic law can not be violated, the maximum temperature reachable by the absorber will not exceed the source temperature and necessarily $\epsilon \leq 1$. In this case the net heat transfer is zero $Q_{s\to abs} - Q_{abs\to s} = 0$ if $T_s = T_{abs}$. Combining in this formula the Equations 1.4 and 1.6 and from the Eq. 1.2, it can be obtained that:

$$C = \frac{A}{A_{abs}} = \frac{R^2}{r^2}\epsilon \leq \frac{1}{\sin^2(\theta_c)} \tag{1.7}$$

The concentration must satisfy this limits for every 3D geometry where the absorber is surrounded by vacuum. Calculating the value for the solar divergence $\theta_c \approx 4.7$ mrad the maximum ideal concentration results in $C \approx 45000$. In case of concentration operated in one

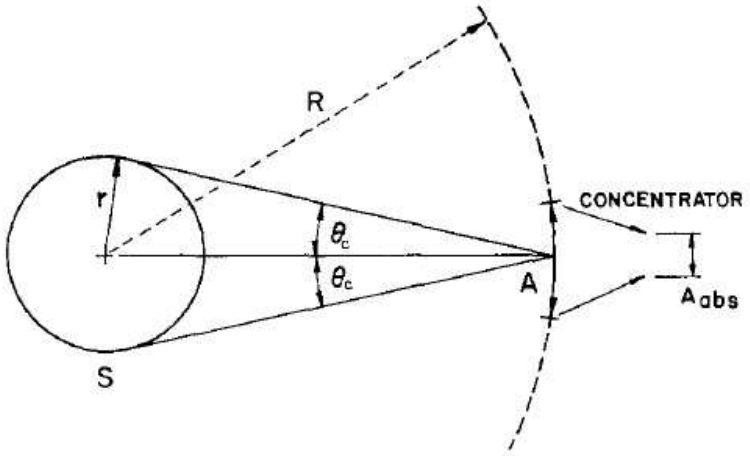

Figure 1.2: Geometrical representation of the Sun-Earth system [Rab1975]

direction (2D concentrators) and if the absorber is surrounded by a medium with refraction index n, the Eq. 1.7 can be generalized by the following:

$$C \leq \frac{n^2}{\sin^2(\theta_c)} \text{ if 3D} \tag{1.8}$$

$$C \leq \frac{n}{\sin(\theta_c)} \text{ if 2D.} \tag{1.9}$$

In the same paper, this arguments are used to show another important result which connect this limit to the f-number $f = \frac{F}{D}$ of an imaging system, this parameter being the ratio between the focal length and the entrance aperture diameter. The focal length F defines together with the angular size of the source, the diameter a of the image which corresponds to the absorber diameter in case of solar concentrators: $a = 2F\sin(\theta_c)$. The concentration factor can be written, thanks to the Eq. 1.8, as:

$$C = \left(\frac{D}{a}\right)^2 = \left(\frac{D}{2F\sin(\theta_c)}\right)^2 = \left(\frac{1}{2f}\right)^2 C_{ideal} \tag{1.10}$$

so that

$$f \leq \frac{1}{2} \tag{1.11}$$

this equation giving the smallest f-number allowed for an ideal imaging collector $f = 0.5$[1].

1.4 Geometrical optics to perform light collection

The concepts and the quantities recalled till now have been derived in the framework of Geometrical Optics, which is the basic tool in designing almost any optical system when the dimensions involved are much bigger than the radiation wavelength. But when dealing with solar concentrator it is important to distinguish between light collection and the classical theory of image formation. We shall refer to the solar concentrators as *nonimaging concentrators*.

Nonimaging optics are devices which do not preserve all the properties of the image: the information about the image is basically lost at the focal plane level but, generally, these optics do not need to reform the Sun image to work at their best. For example in thermal systems, the main goal to be reached is to increase the power density at the receiver and to push it as close as possible to its theoretical maximum. This is because even modest levels of concentration can dramatically increase the temperature at which heat from a solar collector can be efficiently extracted and applied to a thermal process.

We will see in the next subsections the main problems related to light collection, why traditional optics fail and the most recognized example of nonimaging optics. It is even possible to use image forming concentrators with standard shapes, as paraboloidal or spherical mirrors/lenses, but in this case the requirements of conventional imaging are not fulfilled and the scope of increasing collection are approached generally by adding a secondary

[1]The result can be also obtained from the connection between f-number and Abbe sine condition

nonimaging component. For a clearer explanation of the arguments treated here, the reader is invited to consult Winston et al. 2005 [Win2005].

1.4.1 Classical imaging devices and their limitations

Classical imaging devices are lenses and mirrors. As already shown in subsection 1.3.3, an imaging system should have the smallest f-number possible to obtain the maximum collection. That happens for a fixed diameter, by reducing F as much as possible. But for the theory of paraxial optics and using simple ray tracing methods, it is easy to understand that aberrations in imaging systems are difficult to avoid and unfortunately grow for small f-number. Perfect concentrators are theoretically possible to design using spherically symmetric geometry and materials with a quite high reflective index. For example, the Schmidt camera has no spherical aberration or coma because of its aspherical corrective lens. It allows quite fast focal ratio and could be a good concentrator for smaller collecting angles. However the cost and the central obscuration at the aperture are serious disadvantages for its use as concentrator.

It is however possible to calculate the real performance of a typical imaging device respect to the maximum concentration in Eq. 1.8. If we take for example a concave mirror, it is easy to compute the diameter of the exit aperture must be to collect all the rays in the meridian section. This demonstration was performed not specifically for solar concentrators, but in far infrared astronomy to design a field optics to achieve the maximum flux concentration allowed by the Abbe sine inequality and to provide efficient coupling to bolometer-type detectors [Har1976]. Supposing to have a mirror with a spherical section, an entrance

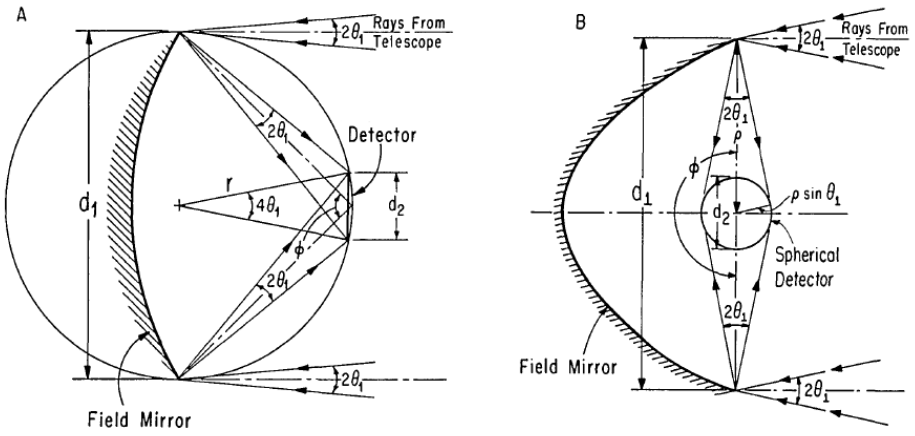

Figure 1.3: Geometrical scheme of reflection for spherical mirrors coupled with flat receivers (A) and tubular receivers (B).

aperture d_1 and a receiver with an aperture diameter d_2 positioned on axis in the focal point as in Fig. 1.3A, we want to find the value of ϕ, which is called the *rim angle* of the mirror, that maximizes C. In other words, we wish to maximize d_1/d_2 under the restriction

that no rays striking the mirror at angles $\leq \theta_1$ (which for us is the solar divergence θ_c already mentioned) miss the detector. Referring to the figure, we see that the detector must be large enough to intercept the divergent beam reflected from the edges of the field mirror. When this condition is satisfied, the edges of the detector and of the field mirror lie on a common circle of radius r. Hence we have $d_1 = 2r \sin\phi$ and $d_2 = 2r \sin\theta_1$ so that:

$$d_2/d_1 = \sin(2\theta_1)/\sin\phi \tag{1.12}$$

From the Equation 1.12 we see that d_2 will be minimized at $\phi = \pi/2$. With this rim angle and for $0 < \theta_1 < \pi/4$, Eq. 1.2 in case of circular apertures taking into account the receiver obscuration becomes:

$$C = \left(\frac{d_1}{d_2}\right)^2 - 1 = \frac{1}{4\sin^2(\theta_1)} \left(\frac{\cos(2\theta_1)}{\cos^2(\theta_1)}\right)^2 < \frac{1}{4\sin^2(\theta_1)} \tag{1.13}$$

For spherical mirrors coupled with tubular receiver (Fig. 1.3B) but also for lenses with flat receiver, the formula can be similarly derived giving the same result as in Eq. 1.13.

This limiting value deduced for imaging systems is less than the 25% of the C_{ideal} for generic optics and it is due almost to the large amount of coma introduced when the entrance aperture is increased in order the rim angle to approach $\pi/2$. For this reason, pure imaging optics alone seems to be not properly suitable for a good solar concentration.

1.4.2 Non imaging optics and ideal collectors

The optical examples shown till now suggest that the condition of forming an image is quite restrictive for a solar concentrator. Since imaging the Sun is not needed for energy conversion purposes, a principle called "edge-ray" has been theorized and then applied to find a useful design method for concentrators. The method consists in mapping the edge rays from the source to the edge of the target, neglecting the behaviour of the rays in the middle [Win2003]. A well known type of nonimaging concentrators has been designed in this way: the compound parabolic concentrator (CPC). The CPC permits the use of low to moderate levels of concentration for solar thermal collectors without the requirement of

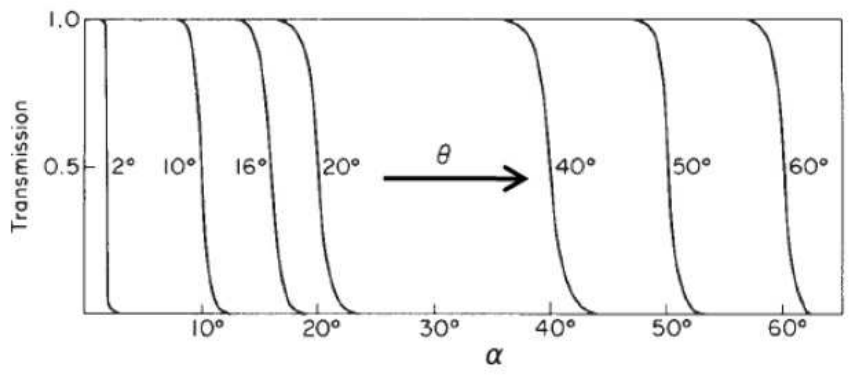

Figure 1.4: CPC transmission curves for difference acceptance angles [Win2005].

diurnal tracking. Nevertheless the CPC has a transmission curve (describing the acceptance angle) which is not exactly a step function as it is expected to be. In a CPC in fact, different rays have different numbers of reflections before they emerge at the exit aperture. Some of them are reflected back and this effect produce the not ideal performance. The CPC transmission curve is shown in Fig. 1.4 for many acceptance design angles θ. The transition between 0.9 and 1 of transmission values occurs in any case in an interval of $\Delta\theta = 3°$.

A very clear example of CPC in a slightly modified configuration is the cusp concentrator integrated in a stationary evacuated tube for thermal applications shown in Fig. 1.5. The "wings" of the concentrator, which are supposed to be reflective, let the light converge on the tube located upon the focus point. In Fig. 1.5A, the details of a specific design are given. In the ray trace diagram 1.5B, the main feature to be noted is the convergence over the absorber tube of the solar radiation within the acceptance angle value for which the collector has been designed ($\pm 35°$). Because the reflector cannot physically touch the absorber, as required for an ideal concentrator, a small radiation fraction is lost in the gap between the reflectors and the absorber [Win2003]. Such a concentrator can however be designed only for very low concentration ratios.

The CPC is the first nonimaging optics conceived, but several other configuration have been implemented and built. The edge-ray design method, which has produced a variety of useful solar concentrators, after some modifications gave birth to new techniques to tailor the concentrators. The tailoring uses numerical integration of a simple differential equation and it is a more general approach that can solve problems beyond the simple acceptance angle, involving other parameters as the receiver geometry, the compactness of the optics, etc. In some conditions, it allowed the construction of two-stage systems with short focal lengths both to increase concentration and to smooth the irradiance profile on the receiver (a problem that will be discussed in detail in the next sections).

1.4.3 Problems related to light collection

To better understand how a solar concentrator should be designed to work at its best, it is useful to categorize two main groups of design problems in nonimaging optics, keeping in mind that the design has to deal with the modification of a given ray bundle. The first group of problems is called *bundle-coupling* and its goal is to design a system in which the input and the output ray bundle coincide. Practically, the objective is to maximize the light power transferred from the source to the receiver pushing the concentration to its limit. The second group of design problems aims to obtain a specific light pattern on a certain target surface at the receiver side. The last type of solutions goes under the name of *prescribed irradiance* and it is common to most of the illumination applications. From an optical point of view, the design of a CPV has to deal both with bundle coupling problem, for approaching the maximum concentration allowed, and with the prescribed irradiance, in order to obtain

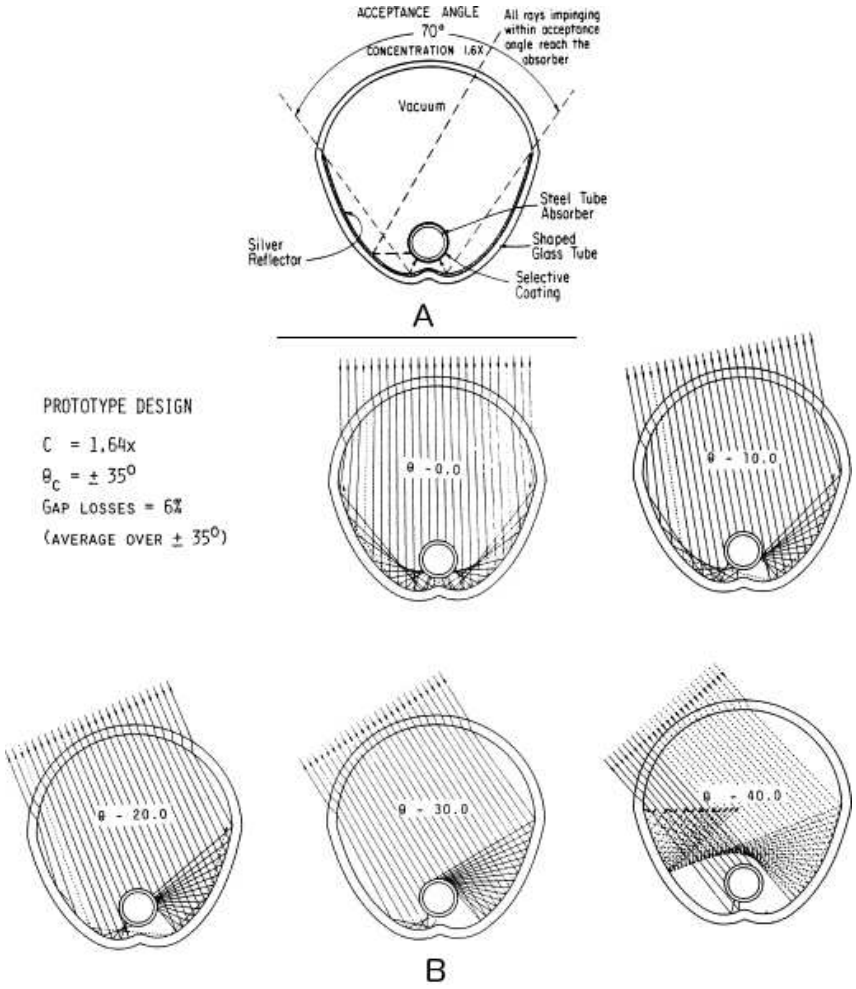

Figure 1.5: (A) Details of a CPC modified, designed for thermal concentraion with evacuated tubes. (B) Ray trace diagram for different incident angles [Win2003].

a uniform irradiance distribution on the PV active area. Of course this is a very difficult task and therefore only partial solutions have been found till now in realized systems.

1.5 Concentrated photovoltaic technology

CPVs are power generating systems where high efficiency PV modules resistant to high energy fluxes and temperatures act as electricity generators in the same way as in flat photovoltaic panels a semiconductor material (like silicon or others) does when directly exposed to the flux of the Sun. The working principle of the CPV technology that makes it also differ from the flat technology is that concentration of sunlight increases the power density of the solar radiation before its conversion into electricity. This is done to increase the total energy collected but above all to replace semiconductors by cheaper materials commonly used for optical components as glass, aluminum, etc. In CPVs, the semiconductors used are complex multi-junction cells appositely engineered to have higher and higher efficiency. Therefore this technology, supposing a research continuously able to

conceive and develop optics to let the cells work at their nominal performance, has great potential for a substantial cost reduction of global systems and consequently of the electricity produced. Some systems are used in a cogeneration mode, since it is preferred, when possible, to recover the residual heat thus increasing the global conversion efficiency.

CPV can be categorized by their energy collection capacity in low (LCPV with C <100 suns), medium (MCPV with 100< C <300 suns), high concentration (HCPV with 300< C <1000 suns) and ultra-high (UHCPV with C >1000 suns) concentrating systems. This is a simplification but can be useful to understand in which regime a system can operate. An optical classification is done between refractive or/and reflective systems depending on the optics used. Geometrically, it is further possible to distinguish between linear and three-dimensional concentrators if the optical concentration is operated respectively in a plane or in space. Three main groups of systems will be described more in detail in the following sections:

- linear CPV;
- single cell point focus systems;
- dense array central receiver systems.

Despite CPV did still not have a great impact in the renewable electricity production, several systems of this type have been developed and several companies producers have recently emerged. For HCPV and LCPV systems the yearly installed capacity increased significantly during the last five years [Wie2012]. Due to the continuous increase in solar cells efficiency, HCPV seems the best future way to face the cost problem, especially if used in sunny environments or in off-grid locations, where the transportation of the fuel to produce energy is the main parameter to determine the local energy cost.

The present status of all operational and pre-operational CPV installations is shown in the CPV World Map 2011 (Fig. 1.6). Figure 1.7 contains the list of the constructors, the working state and the plant size. Another useful and quite recent state of the art of high concentration photovoltaics using III-V multi-junction cells has been reported by Zubi [Zub2009], accounting for more than 20 developed systems commercially available or shortly before market introduction at 2009.

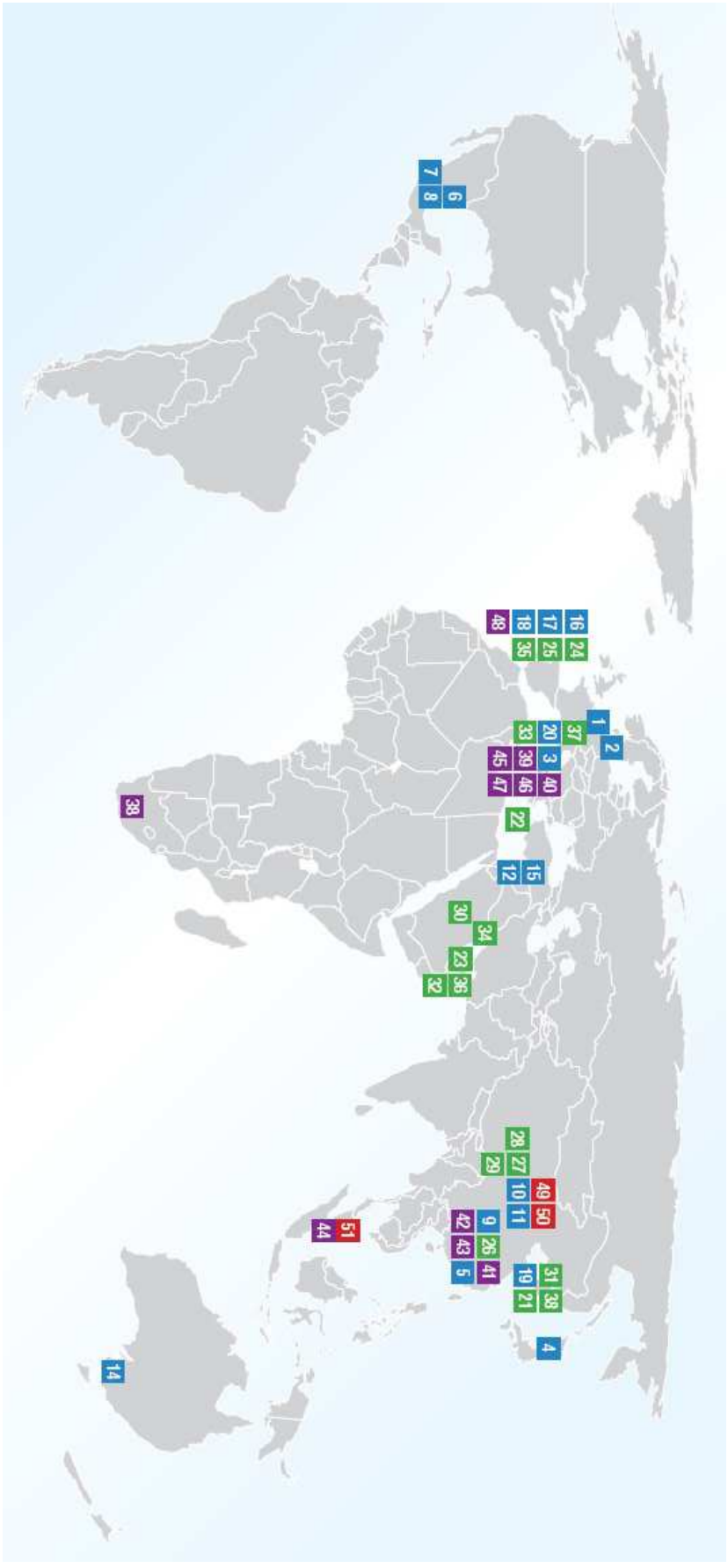

Figure 1.6: Map of the largest operating HVCP and LCPV plants located worldwide in 2011 [PVinsider]

Figure 1.7: List of the largest operating HVCP and LCPV plants located worldwide in 2011 shown in Fig.1.6 [PVinsider]

1.5.1 Linear CPV

Linear concentrators perform concentration only in one direction. These systems mostly are solar troughs with parabolic profile or V-troughs (cavities with V-profiles for very low C) even if some refractive prototype have been proposed, like the linear Fresnel lens by Leutz [Leu1999]. It is a common use to associate the idea of a trough collectors exclusively to the production of heat as they are usually employed in thermal applications using as absorber a metal pipe. This is basically due to their simplicity of fabrication and of working principle, i.e. to heat a fluid in a pipe more efficiently than a common flat heat exchanger. But in the 1990s these configurations started to be coupled with PV linear receivers made by a long string of cells. With the progresses in cells construction going toward higher concentration, ever more attention of both research and market was addressed toward point focus type rather than linear troughs, since linear systems are generally conceived to work in the LCPV-MCPV range, while the former in HCPV mode. These systems normally have only one axis tracking.

EUCLIDES is a reflective parabolic trough concentrator (PTC) that consists of a linear array tracking around a horizontal N/S axis. The system was conceived in the mid-1990s, supported by a fundamental consideration. The background and wide-ranging experience with linear thermal concentrators, such as a projects carried out in the mid-1980s in California, suggested the possibility of transferring the concept to a PV concentrator. Of course, a complete redesign of the system was necessary to fulfil the requirements imposed by a photovoltaic system. The most important change was in the receiver, which needed cost-effective PV solar cells able to work at concentration levels within the range of 20-40 suns. A prototype was designed and installed in Madrid in 1995 with the aim of testing the concept. The structure was 24 m long, consisting of 40 mirrors that cast the light onto encapsulated linear modules at 33× geometric concentration (see Fig. 1.8). The large PV plant experiment that was carried out in Tenerife, highlighted the lack of maturity of the mirror and module technology, but demonstrated the cost potential of the concept [Ant2007][Luq1998].

Another parabolic through has been developed by the Center for Sustainable Energy Systems (CSES) at the Australian National University (ANU), a photovoltaic/thermal (PV/T) collector with geometric concentration ratio of 37×. The so-called combined heat and power solar (CHAPS) collectors consist of glass-on-metal mirrors that focus light onto high efficiency monocrystalline silicon solar cells to generate electricity. Water, with anti-freeze and anti-corrosion additives, flows through a conduit at the back of the cells to remove most of the remaining energy as heat. The energy may either be shed through cooling fins, or be used via a heat exchanger for building heating and domestic hot water. The first commercial scale demonstration installation of CHAPS modular field is a 300 m^2 system providing electricity, sanitary and heating hot water for a residential college at ANU

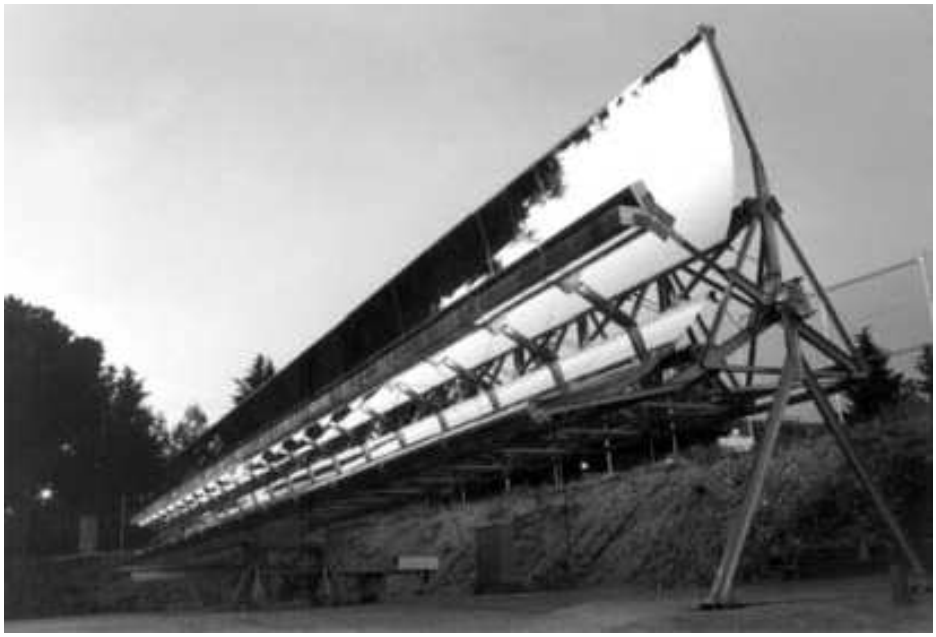

Figure 1.8: Picture of the EUCLIDES prototype installed in Madrid in 1995 [Ant2007]

[Cov2005].

Also in Italy, in the framework of the CESARE project, the construction of a prototype has been carried out in the years 2009-2010 at the Energetic Engineering Department of the University of Florence in collaboration with the National Institute of Optics of the National Research Council (CNR-INO). It is composed of a linear parabolic mirror concentrating the sunlight over an array of PV cells with a concentration around 150×(excluding the shading due to the receiver)[Gia2010]. A particularity of this system was the development of a two-axis tracking in a linear trough to improve the focusing power. The examined system was conceived for residential purposes and to produce electrical energy, heat and solar cooling in order to completely exploit all the light concentrated by the primary mirror, in particular recovering the portion focused out of the cells array. During the last part of the project the implementation of secondary optics to boost the concentration of the pre-existent single stage up to 300× was investigated [Gia2011]. Other two-stage concentrators approaching concentration ratios up to 300× while being tracked around only one polar axis, have been conceived to further reduce the costs relative to the use of high efficiency solar cells [Bru1996][Pra2011].

1.5.2 Single cell point focus systems

In point focus systems many highly efficient solar cells are arranged to form a grid of several hundreds element. Each cell is installed under a refractive element, commonly a square Fresnel lens of some centimetres diameter. These lenses concentrate sunlight hundreds of times and focus it onto small cells, which are connected together in series or in parallels

in different electrical schemes. Between the primary optics and the cells is often placed a secondary refractive element with the scope of smoothing the light pattern over the cell and to increase the acceptance angle. The cells at the concentration involved can reach very high temperature, but since the cells are placed at a certain distance from one another and the area of one cell is very small, a passive air cooling can be efficiently exploited. The tracking is always performed in two axis (as in dense array systems) to better employ the expensive cells and justify their cost.

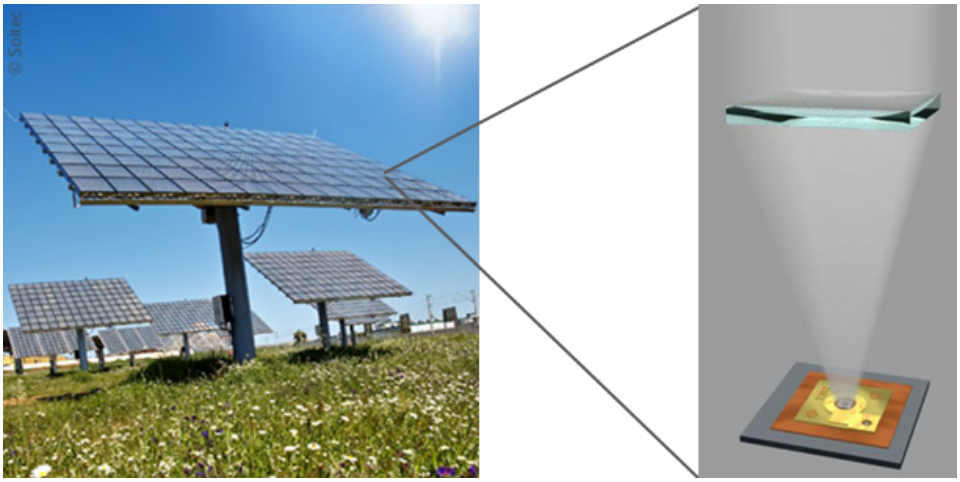

Figure 1.9: Point focus system plant by Soitec company [Soitec]. Besides, the single Fresnel lens which compound the mosaic module.

By far the most diffuse HCPV systems are surely single cells point focusing systems as the one shown in Fig. 1.9, in which the primary optics is a Fresnel lens with typical f-numbers around 0.5. The materials used to made these lenses are mainly plastics (such as PMMA or polycarbonate) injection molded, or silicone on glass substrates. An advantage of this configuration is that lenses protect cells for the external dust and humidity, because they are connected to the adjacent ones to form a unique surface, and their short focal length allows for compact structures. Fresnel lens point-focus concentrators typically employ secondary concentrators to further concentrate light and to homogenize light at the cell surface.

Another primary optics widely used for these concentrators is the mini-dish. The collection unit is a miniature paraboloidal dish (e.g., with a diameter of around 10 cm) that concentrates sunlight into a short glass rod [Feu2001]. The flux distribution of the transported light is homogenized in a miniature glass kaleidoscope that is optically coupled with a small, high-efficiency solar cell. The cell resides behind the dish and can be cooled adequately with a passive heat sink. This scheme can be realized by placing a flat mirror below the focal plane and re-imaging the sun at a recessed plane (a limiting case of the classical Cassegrain optical design often used in telescopes as shown in Fig. 1.10). Fraas et al. [Fra2006] tested in 2006 a Cassegrainian solar concentrator module concept using a primary and a dichroic secondary mirror instead of the flat mirror in Fig. 1.10 to reverse the

focus and to split the solar spectrum into two parts directing the infrared and near visible portions into separate cell locations. An efficiency of 32.9% in standard test conditions is reported measured outdoors for a solar concentrator PV module using dual junction (DJ) cells located at the near-visible focus at the center of the primary and infrared solar cells located behind the secondary. The dicroich approach is going to be another good strategy to enhance efficiency of cells in point focus systems, by using beam splitter to create multiple foci and cheaper cells with single or double junctions.

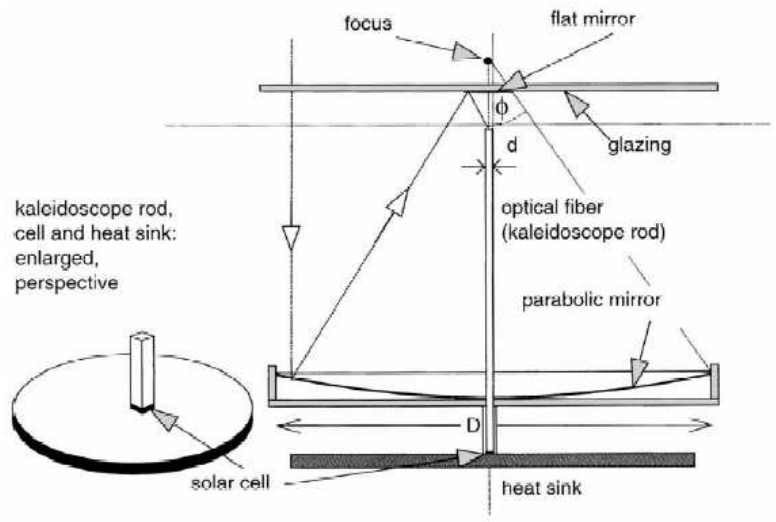

Figure 1.10: Minidish technology including kaleidoscopic rod by Feuermann[Feu2001].

1.5.3 Dense array CPV

Dense array systems focus radiation by using one large optical element, usually a paraboloidal or spherical-like mirror called dish, on an array of cells densely packed one beside the other. A mosaic of low cost mirrors mounted on a parabolic dish frame normally approximates the concave shape and the array of cells is a unique receiver. Under high concentration, PV cells experience a high heat load that will reduce their efficiency if not dissipated adequately. But the fact that the cells are so close each other adds a great problem compared to the case of isolated cells and imposes to cool the detector actively. As already mentioned for single cells systems, the tracking is needed in two axis as the whole structure, optics and receiver solidly, has to point the Sun during its motion. Mirrored dish concentrators with diameters ranging from few meters to tens of meters have been proposed and are at the beginning of their commercial development.

Compared to other CPV technologies such as the common Fresnel lens based systems, the large concentrator dish design seems to be more complex because it involves large-scale optics, active cooling and compact arrays of cells. However, dense array systems appear as a good prospective to increase the concentration factor towards 1000× and beyond. An

Figure 1.11: CS500-5 CPV Dish System produced by Solar Systems [SolSys].

advantage of the reflective optics is indeed the absence of chromatic aberration. Moreover, the single units are suitable to be used alone for medium energy supply (around 10 KW) or to be connected in field for utility scale production. Other advantages: a better optical efficiency if compared to point focus systems because no refractions occur, a lower cell operating temperature (due to the active cooling) and a capability to provide cogeneration of electricity and heat because of the active cooling needed. A significant advantage of concentrator dish systems compared to the other CPV technologies resides in the possibility to change the receiver in case of cleaning, testing or even repair and, as solar cell technology improves, it allows the power station operator to upgrade a concentrator dish PV system to a higher-efficiency receiver at very low cost [Ver2006].

Figure 1.11 shows an austalian dish plant of the Solar System company, one of the most advanced producer of this technology [Kin2006]. The optical concentrator system is designed to operate at 500 suns concentration. The concentrator system consists of 112 mirror panels that are focused onto the receiver composed of 64 sub-modules. Each module is composed of 24 Concentrator Ultra Triple Junction (CUTJ) dense-array solar cells developed by Spectrolab company, totaling approximately 1500 cells. The electrical efficiency claimed is around 30%.

Another commercial system has been developed by Zenith Solar Ltd [Cha2011] in Israel. Zenith dish is shown in Fig. 1.12: it is made by two adjacent dishes, each concentrator comprises 1200 flat mirror facets with total aperture of 11 m^2 that focus the solar radiation onto a dense array of triple-junction 150 mm x 120 mm PV cells bonded to an actively water-cooled heat exchanger. Every mirror facet has a unique shape and their geometrical projections from each mirror impinge on the focal plane to form the spot. The reflection from individual mirrors in the dish does not perfectly overlap; the reflected irradiated flux extends over slightly larger area such that the flux distribution over the PV receiver can be more uniform without embedding an additional optical element. The performance measured in field is reported as 21% electrical and 50% thermal conversion efficiency.

Figure 1.12: Dish System produced by Solar Systems [Qenerg].

1.6 Open issues on dense arrays and existing solutions

The solar cells efficiency is the main driver of the CPV technology. To allow the global system approximating the cell efficiency, an optimization of each part of the system is required: collection optics, photovoltaic array, switches, controllers, current inverters, storage devices and tracking mechanics. A vast amount of research is currently focused on perfecting each of these areas. Some issues about the optics and the receiver, which are the components inherent with the thesis, are briefly discussed in the following.

From the receiver point of view, not all the energy collected can be converted into electricity by the cells. Thermal questions are related to the high flux to dissipate in order to keep the cell working at ambient temperature and to prevent gradients among the cells. Receiver modules have to work in extreme environment then the temperature control of solar cells at high concentrations is a key issue. Short-term efficiency drop and long-term degradation should be avoided by more effective cooling methods. Literature gives various examples of cooling devices [Roy2007][Zhu2011]. Moreover, the very tight packing of cells side by side presents a challenge in providing space for series cell-to-cell wiring, and the placement of bypass/protection diodes. Any space within the array that is used for wiring or other purposes is inactive for cell light conversion, and therefore where valuable concentrated light is wasted.

As for the optical elements, an important issue is related to irradiance distribution over the cells. Several researches validated the idea developed in this work that flux homogeneity

would be the driving force to improve substantially future concentrators for photovoltaic applications. Non-uniform irradiance on the cells degrades the electrical performance thereby reducing conversion efficiency: the worst illuminated cell produces less current than the other cells, limiting the current production of the cells series connected. Moreover, the worst illuminated cell experiences an overheating caused by the dissipation of some current produced by the cells working better and can eventually break out. We will discuss in detail these aspect in Section 2.4.

Another important aspect is that presently available cells and arrays have square/rectangular shape, while the Sun image produced by a traditional imaging element is a circular spot with a similar Gaussian cross-section irradiance distribution. Irradiance pattern should resemble classical detector shape.

The best illumination condition for a dense array receiver is then an irradiance as uniform as possible and, at the same time, a light pattern that trace the natural rectangular/square shape of the array. Generally speaking, uniform flux and pattern shaping are theoretically (partially) possible by redesigning the optics of the primary concentrator [Bur1975], by approximating it with an array of flat elements [Cho2010] and/or by adding SO elements to tailor the flux delivered by the primary[Fu2011][Her2008]. The SOs are the commonly preferred solution in single cell point focus systems [Leu2001][Ben2010][Feu2001] because of the compact dimensions involved. Few commercial systems and data are available involving secondary optics coupled with dense arrays [Rie1996][Ver2006]. The presence of an extra secondary optics would surely increase the acceptance angle leading to a relaxation of tracking and alignment tolerances. However a refractive element would also introduce scattering and absorption losses and would add mechanical complexity to be handled. Since the SOs are made of plastic materials, other not yet solved problems are yellowing and abrasion with age causing lowering of optical efficiency. As reported in the Nrel Technical Report 2012 [Nrel2012], some companies have recently chosen to avoid the cost of SOs by carefully maintaining alignment quality and sacrificing a few per cent in performance under some circumstances. Other research works based on dense array proposed innovative kind of connections or used different kind of cells in the same detector to solve the issue [Sal2011][Loc2010]. A complete and useful review on the non-uniformity problem in CPVs has been recently published [Bai2012].

Chapter 2

High efficiency solar cells and arrays

In the previous Chapter, a brief overview of the main CPV systems has been given and the main problem of how the light has to be collected over the cells introduced (see Section 1.2). To understand how much, under high concentration, a non-uniform illumination may decrease the electrical power output of a cells array, some physical concepts and operating principles of the standard series/parallel connections among cells must be understood. First of all, the comprehension of the photovoltaic effect is essential, since the tuning of the energy bandgaps allows to construct cells with an increasing number of junctions and then of higher efficiency. Multi-junction (MJ) cells and arrays are explained in their main aspects, referring to the state of the art and to an analytical framework that describes the dependence of their electrical parameters from concentration level (that will be used in the next Chapter to model our receiver). Finally, the problems of non-uniform illumination over arrays and cells will be discussed later in these Sections.

2.1 Photovoltaic effect

Solar cells are made starting from semiconductors which are materials made up of individual atoms bonded together in a regular, periodic structure to form an arrangement. In the Periodic Table the semiconductor are in the IV group like silicon and germanium and each atom is surrounded by 4 electrons in the outermost orbital. Other semiconductors can be created from compounds of other groups (as III-V). The electrons surrounding each atom in a semiconductor crystal are part of a covalent bond and it is this type of bond structure that determines the material properties (e.g. the existence of bandgaps). When a semiconductor is struck by a photon with an energy level higher than its specific threshold level, the photon is absorbed and induces the creation of an electron-hole pair. In normal conditions, a recombination occurs very fast. The PV effect is based on this pair creation: for this reason, structures called *p-n junctions* are artificially induced by connecting two

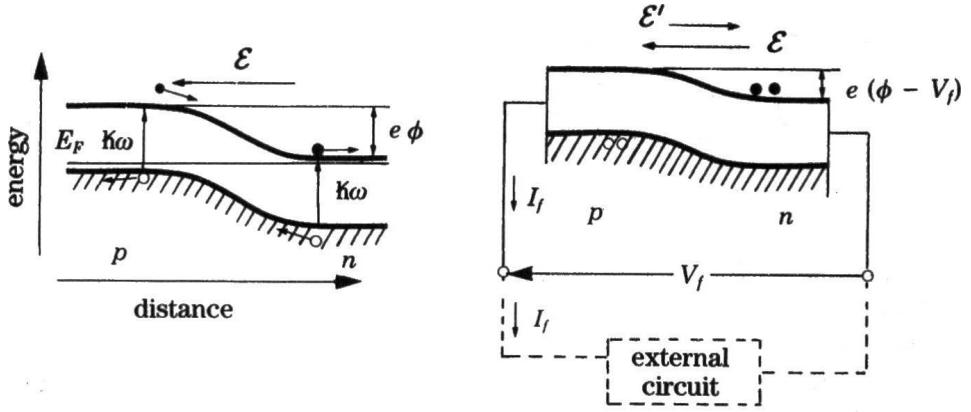

Figure 2.1: Energy levels modification by photovoltaic effect [Her1995].

layers of doped materials. The n-type material is obtained by adding valence five atoms in a semiconductor lattice subtrate; by this doping process we can obtain a new semiconductor rich in negative charge carriers. Similarly, p-type materials are obtained by adding valence three atoms in semiconductor's lattices, creating a new lattice rich in positive charge carriers. When a p-n junction is made by placing in a close contact n-type and p-type semiconductors, a strong recombination process occurs at the interface and a depletion layer is formed in the contact region. This depletion layer creates an electrical field which modifyies the energy band structure of the junction, lowering the threshold level of the energy gap.

An unbiased p-n junction is in equilibrium and it has an energy barrier $e\phi$ and an associated electrical field $\boldsymbol{\varepsilon}$. The electrical field $\boldsymbol{\varepsilon}$ of the p-n junction increases the separation of the pair, accelerating the electrons toward the n-type region and the hole toward the p-type region. So the pair recombination is inhibited and the electric field within the semiconductor altered by a new field $\boldsymbol{\varepsilon}'$ (Fig. 2.1). As a result, the potential at the semiconductor edges is reduced and the electrons and holes are grouped separately by each of two current-collecting electrodes. The decreasing of voltage at the semiconductor terminals induces a current I_f in a circuit external to the semiconductor itself, leaving the p-type region. Ignoring eventual resistive effects, the resulting current I and the voltage V_f will be:

$$I = I_f - I_0 \left(\exp\left(\frac{qV_f}{kT} \right) - 1 \right) \tag{2.1}$$

where I_0 is the characteristic recombination current of that semiconductor and from which the final voltage can be deduced:

$$V_f = \frac{kT}{q} \log\left(\frac{I_0 + I_f - I}{I_0} \right). \tag{2.2}$$

In the Equation 2.1 and 2.2, k is the Boltzmann constant, T the cell temperature and q is the electron charge.

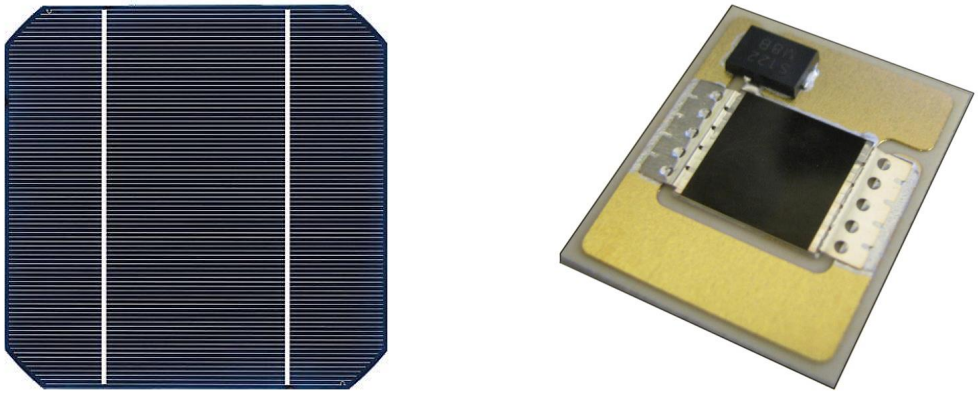

Figure 2.2: Standard pv module for flat application (left) [DirInd]; cells for high concentrations (right) [Spectro].

2.2 Multi-junction solar cells

The first semiconductor to be used in PV systems was the silicon which is today the most common among the standard flat photovoltaic installations. The pure silicon (the most used in cells industry) has a band gap of 1.1 eV, then an electron-hole pairs need a maximum of wavelength in the infrared of $\lambda = 1130$ nm to be produced. The absorbed light is therefore between 350 nm and 1100 nm, but the PV efficiency increases progressively from the infrared to the visible zone. The silicon material in its different forms (monocristalline, polycristalline and amorphous) is almost at the peak of its technological employment reaching industrial efficiencies of 15-17%. Today, efficiency in the laboratory is over the 25% but this improvements will require some years to become commercial.

The cells used in CPV applications are MJ type, originally conceived for space applications. MJ cells have dimensions much smaller than the silicon ones, typically ranging from 1 mm to few centimeters. Fig. 2.2 compares a typical 100 cm^2 silicon cell used in flat PV to a standard 1 cm^2 solar cells on its electrical assembly. The MJ approach to solar cells allows efficiencies far in excess of the best value achievable both in principle and in practice by conventional silicon single-junction cells. A single-junction cell has only one energy band gap E_g for the photons it can absorb, so that the energy above the band gap is dissipated into heat while the energy below the E_g is totally lost limiting the efficiency of any single-junction solar cell. Because the Sun spectrum spans approximately from 300 nm to 4000 nm (above atmosphere), another approach to skip this problem is to imagine the spectrum as composed by several spectral regions trying to convert each region with its own junction having a band gap conveniently tuned. Multiple stacking of solar cells with growing bandgap energies increases the efficiency of the overall device since the solar spectrum is exploited more profitably. Fig. 2.3 shows a schematic representation of the distribution of the solar spectrum photons into the various junctions of a stacked, series-connected three-junction solar cell. The series connections between the junctions are accomplished with

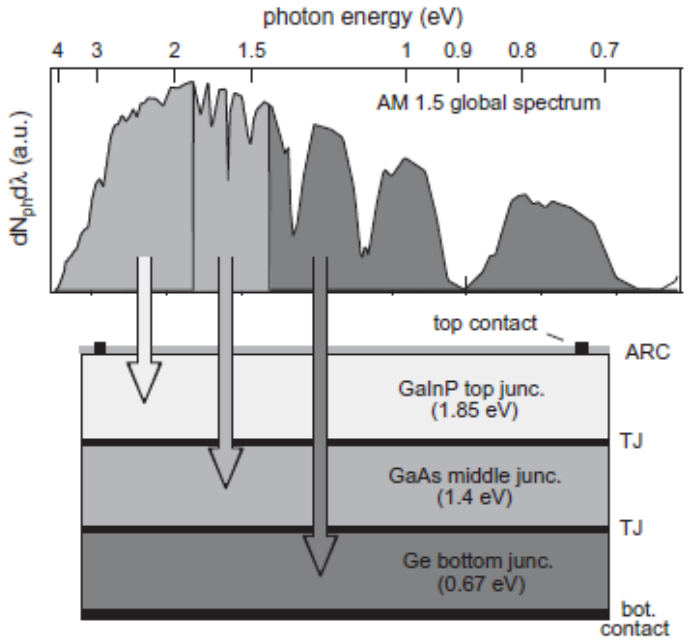

Figure 2.3: Distribution of photons from the solar spectrum into the various junctions of a stacked, series-connected three-junction solar cell [Fri2010].

tunnel junctions (TJ). The anti-reflection coating needed to increase the photons absorption is indicated as ARC.

CPV cells have been introduced in terrestrial application because they have great potential in reducing the cost of the CPV systems. Today, the ultra-high efficiency best reported cell is a 0.165 cm^2 MJ cell having a new record of 44.4% confirmed efficiency at direct irradiance concentration of 302 suns [Gre2013]. At present, the commercial available cells work at typical power density between 500-1000 suns. Typical materials used in junctions are copper, selenium, gallium, germanium, etc. For highly efficient photovoltaic energy conversion the GaInP/GaInAs/Ge structure is largely used.

Ideally, the efficiency of a solar cell increases with increasing concentration, but in practice, at the high currents generated under concentration, all cells experience voltage drops across

Device	Number of junctions	Eff.%	Suns	Area(cm^2)
Si	1	25.0±0.5	1	4.00
GaAs	1	28.8±0.9	1	0.9927
CIGS	1	19.6±0.6	1	0.996
CdTe	1	19.6±0.4	1	1.0055
InGaP/GaAs/InGaAs	3	37.9±1.2	1	1.047
Si	1	27.6±1.0	92	1.00
GaAs	1	29.1±1.3	117	0.0505
GaInP/GaAs/Ge	3	41.6±2.5	364	0.3174
InGaP/GaAs/InGaAs	**3**	**44.4±2.6**	**302**	**0.1652**

Table 2.1: Best demonstrated efficiency for leading solar cells.

internal series resistances that limit the efficiency. Decreased conversion efficiency is observed above 200-450 suns (depending on the construction technology) despite the electrical power delivered raises thanks to the multiplication of the charge carriers [Vos2012][Phi2012]. The efficiency is strongly dependent on the bandgaps of the junctions in a manner determined by the solar spectrum, the detailed dependence of efficiency on bandgap will therefore be different for different spectral conditions. Best demonstrated efficiencies for leading single and multi-junction solar cell technologies are shown in Table 2.1, under one-sun direct and concentrated illumination measured at 25 °C; data are extracted from the last reported efficiency table [Gre2013].

2.3 Theoretical model used for cells and arrays

In this Section we will explain the electrical features of cells and array and the approximated model that will be used in Chapter 3 for designing the receivers. For our aim, it is necessary to investigate how the power generated by an MJ cell is related to the different physical parameters (above all to light concentration) in order to predict the best operating conditions at which the cell should work and to define the performance that our concentrator should have to allow it.

2.3.1 Single and multi-junction cell model

The generic electrical model of a single junction solar cell consists of a current source that depends on illumination in parallel with a diode. The equivalent circuit of a solar cell is shown in Fig 2.4, where the cell behaviour is represented by resistances in series and parallel and V and I are respectively the final voltage and current of the semiconductor. The R_p parallel resistance is a representation of all the charge carriers which do not reach the contacts thus causing a reduction in the output current. The series resistance R_s derives from the carriers crossing the semiconductor before reaching the contacts, then causing a tension drop; R_c is the load resistance. The internal resistances as well as the current flowing

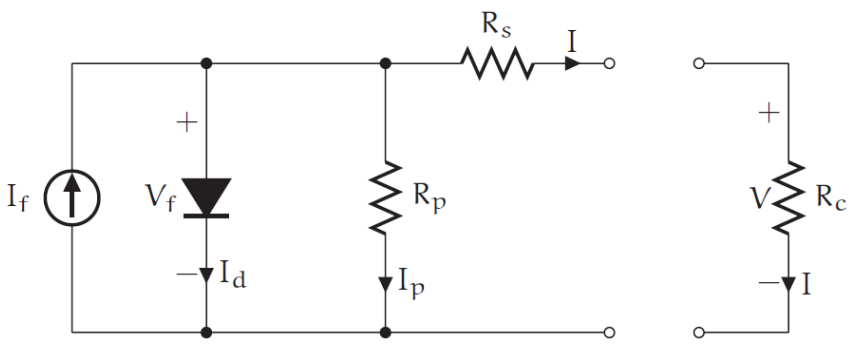

Figure 2.4: A photovoltaic cell equivalent circuit [Men2010].

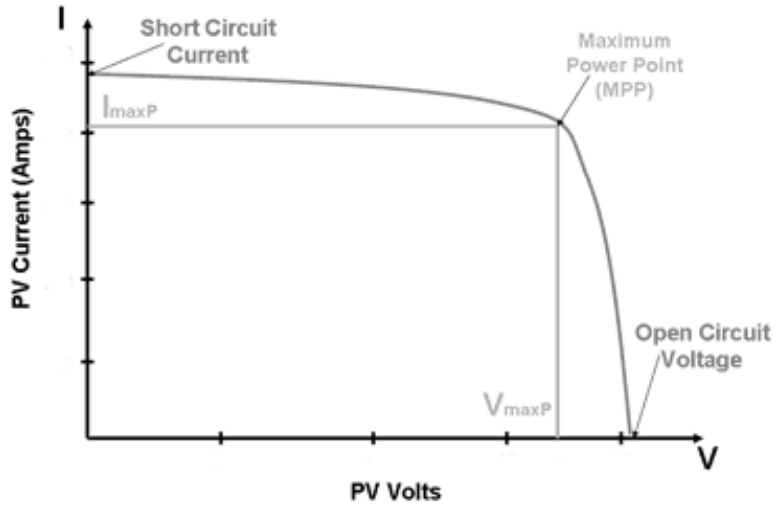

Figure 2.5: IV curve of a generic PV device [Electro]

from the p to the n region and the voltage at their edges (defined in the Equations 2.1 and 2.2) are not easy to be determined.

The cited model can be extended to multi-junction cells as a simple electrical association of the individual models of every subcell. Despite the model is too simple for other modeling purposes, it is able to account for changes in irradiance and, therefore, to predict the performance of solar cells at different illumination conditions by the equations we are going to display.

The IV (nominal current-voltage characteristic) curve for a PV device is shown in Fig. 2.5. In any electronic device, IV graph represents the relation existing among the basic parameters and it is used to model their reciprocal behavior.

Both voltage and current are functions of the light falling on the cell and the relationship between irradiance (density of sunlight impinging over the cell) and output power is complex. As described by the family of curves in the left panel of Fig. 2.6, the short circuit current, that is the intersection of the curves with the vertical axis, has a hard decrement with the decreasing solar intensity impinging on the cell. This effect is caused by the number of photons absorbed by the semiconductor material falling down with a lower concentration level. As a first approximation it can be reasonable to consider that the I_{sc} (short circuit current) is directly proportional to concentration ratio. The open circuit voltage V_{oc} (intersection of the curves with the horizontal axis) varies only slightly with the light intensity and it grows with its logarithmic dependence.

Temperature control of solar cells is a key issue, especially at high concentrations. Short-term efficiency drop and long-term degradation should be avoided by effective cooling methods. Keeping the cell temperature as close as possible to ambient level is an approximation theoretically feasible even for high concentrations when a high thermal load

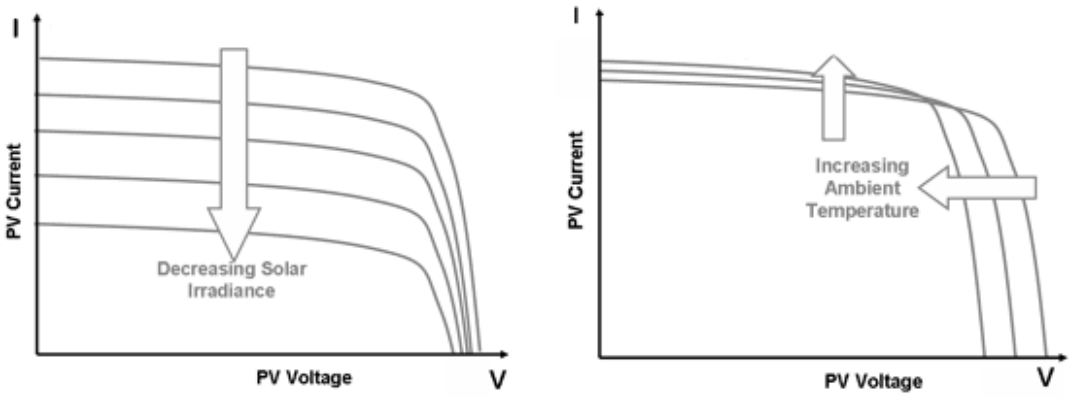

Figure 2.6: Dependence of the IV curve from irradiance (left) and temperature (right) [Electro].

must be dissipated. Nevertheless a certain variability from cell to cell could persist even in case of active cooled systems. The dependence from the temperature is much stronger for the voltage than for the current as shown in Fig. 2.6, right panel. The increase in short circuit current for a given temperature variation is proportionally lower than the corresponding decrease in open circuit voltage.

In this work we assumed an electric model independent from temperature or spectral variation. Since we deal exclusively with reflective elements no chromatic aberration are introduced, so that the last assumption seems realistic. The temperature can also be considered reasonably constant as efficient cooling systems have been shown in literature.

If we suppose to neglect any temperature variation, the physical behavior of a cell here used can be summarized by the following set of equations uniquely depending from the concentration factor $\times$:

$$I_{sc}(\times) = \times \cdot I_{sc}(1) \tag{2.3}$$

$$V_{oc}(\times) = V_{oc}(1) + n_d \frac{KT \ln(\times)}{q} \tag{2.4}$$

$$P_{max}(\times) = I_{max}(\times) \cdot V_{max}(\times) \tag{2.5}$$

$$FF(\times) = \frac{P_{max}(\times)}{I_{sc}(\times) \cdot V_{oc}(\times)} \tag{2.6}$$

$$\eta_{max}(\times) = \frac{P_{max}(\times)}{P_{in}(\times)} = I_{sc}(\times) \cdot V_{oc}(\times) \cdot \frac{FF(\times)}{P_{in}(\times)} \tag{2.7}$$

where P_{in} is the total power received by the cell and $I_{sc}(1)$, $V_{oc}(1)$ are short circuit current and open circuit voltage calculated without concentration at standard test condition (STC) at 1 sun, η_{max} is the nominal conversion efficiency, n_d is the diode ideality factor, which typically ranges between 1 and 2 for single junctions and the rest of the parameters have been already defined in Section 2.1. A more complete model, involving dependences from T and spectral variations can be found in [Dom2010]. Equation 2.6 defines the Fill Factor FF as the ratio between the power at the maximum power point P_{max} (knee of curve in Fig.

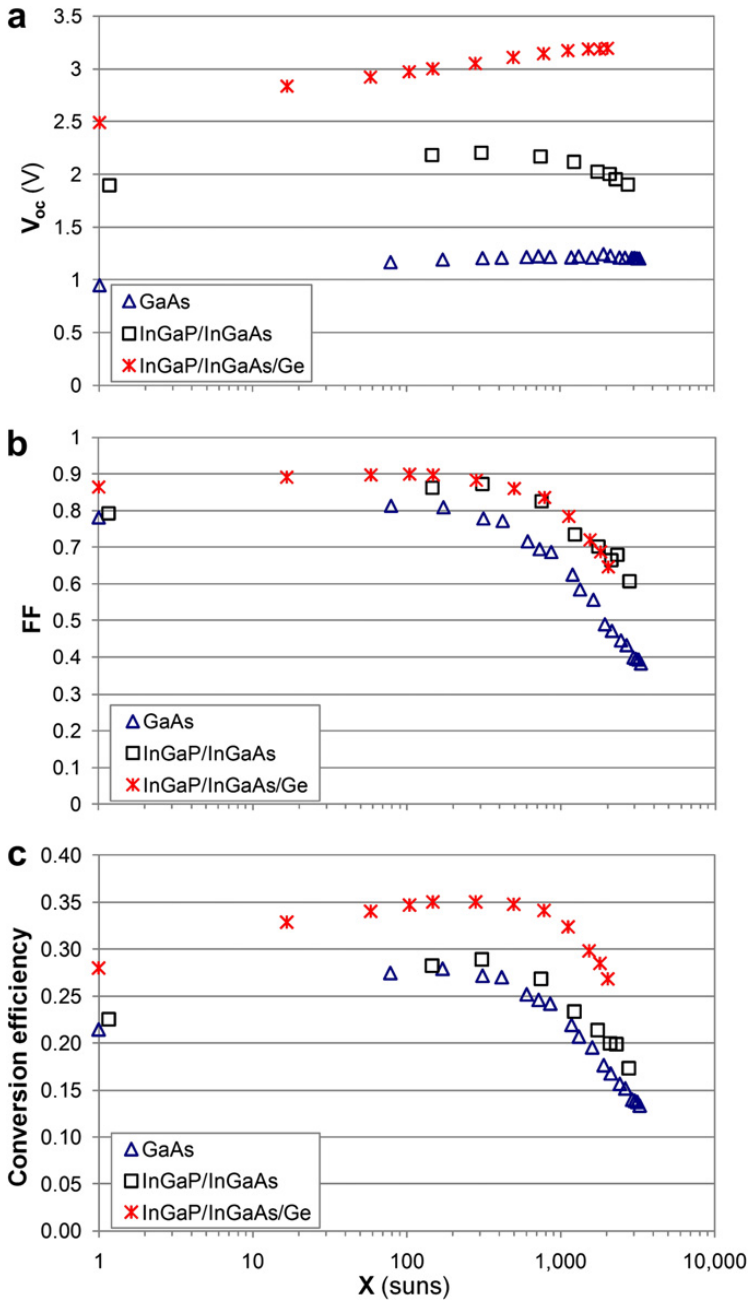

Figure 2.7: Plots of photovoltaic characteristics for different solar cells vs. concentration ratio: a. Top: Open-circuit voltage. b. Mid-height: Fill factor. c. Bottom: Conversion efficiency [Vos2012].

2.5) and the product of the open circuit voltage and short circuit current. It is typically better than 75% for good quality MJ solar cells. It is also a measure of the performance of a solar cell in terms of generated power and it should be as close as possible to 1: graphically, the FF is a measure of the *squareness* of the solar cell IV curve and is also the area of the largest rectangle which would fit in the curve.

Plots of V_{oc}, FF and conversion efficiency are shown in Fig. 2.7 up to concentration factor of a few thousands [Vos2012]. V_{oc} vs. $\times$ is reported in 2.7a for different type of cells. V_{oc}

decreases with increasing temperature and the deviations from linearity observed at very high concentration on V_{oc} (the plot is logarithmic) largely resulted from the temperature increase of the cells. However this deviation occurs at concentration factors which are not investigated in this work.

Fill factors are plotted in Fig. 2.7b. The maximum value of FF occurs for concentration ratios in the range 50-200 suns. It decreases gradually with increasing $\times$ above 200 suns, mainly because of the increase in the resistive losses which are proportional to the series resistance R_s of the cell and to the square of the short-circuit current.

As stated by the equation 2.7, cell efficiency depends on short-circuit current I_{sc} and on incident solar power P_{in}, which are both supposed to vary linearly with $\times$. Considering that V_{oc} increases as $\ln(\times)$, the cell efficiency defined should also increase logarithmically in the case FF remains nearly constant. No significant decrease in V_{oc} was noticed for both the 3J and 1J cells up to concentration ratios exceeding 2000 or 3000 suns, the decrease in efficiency observed for concentration ratios higher than 500 suns in 2.7c mainly resulting from the decrease in FF associated with the increased resistive losses.

Later in Chapters, we will pay attention on systems working in the range 500-1000 suns, even if some types of existent III-V cells have been already tested and characterized under natural sunlight concentrated up to about 3000 suns as shown in Fig. 2.7. Despite most commercial CPV systems are operative at maximum concentrations of about 500 suns the idea is that III-V solar cells could probably operate under concentrations of some thousands in future commercial CPV systems. The systems we will describe could be surely adaptable to higher concentrations.

2.3.2 Arrays of solar cells

The physical properties described above are referred to a solar cell working as single circuit. Usually in a CPV system several solar cells are arranged in electrical connections to produce specific output values of power and current. When a CPV system is designed also the number of cells to interconnect is determined both considering the cell efficiency at real working conditions and the amount and the distribution of light impinging on it. The spatial arrangement of the cells depends on the chosen optical scheme (i.e. point focus or dense array).

In both cases the electrical connection commonly used is a combination of traditional series and parallels. Since we will deal with dense array systems, a short discussion about this configuration and the related issues is appropriated.

Speaking of dense arrays, there are two main problems to face in order to maximize efficiency: the *maximum power point tracking* and the *power matching*. The first is the search for the maximum power point (mpp) along the total IV curve of the array, while the second is the choice of the appropriate type of connections with respect to the working

condition, i.e. the distribution of the incident solar radiation on each cell, temperature, type of cell, to ensure the maximum power transfer to the load.

For an array realized with N cells connected in series or in parallel, the power transferred to the load can be written as:

$$P = \sum_{j=1}^{N} V_j \cdot I_j \tag{2.8}$$

where j stands for the j-th cell and the couple (V_j; I_j) is the j-th cell working point. The power produced by an array represents a point on the IV curve of the entire equivalent circuit. Maximum electrical power and efficiency can be defined in analogy with the case of a single cell, as:

$$P_{max} = \sum_{j=1}^{N} V_{mpp_j} \cdot I_{mpp_j} \tag{2.9}$$

$$\eta_{max} = \frac{P_{max}}{P_{in}} = \frac{\sum_{j=1}^{N} V_{mpp_j} \cdot I_{mpp_j}}{P_{in}} \tag{2.10}$$

where the j-th $\times$ dependence is implicit and the mpp index refers the maximum power point of the j-th cell of the array (instead of the max index used before). When N cells are connected in parallel, the voltage across the cell combination is always the same and the total current from the combination is the sum of the currents in the individual cells:

$$I_0(V_0) = \sum_{j=1}^{N} I_j(V_j) \tag{2.11}$$

$$V_1 = \cdots = V_N = V_0 \tag{2.12}$$

When identical cells are series connected, the equation describing the circuit are:

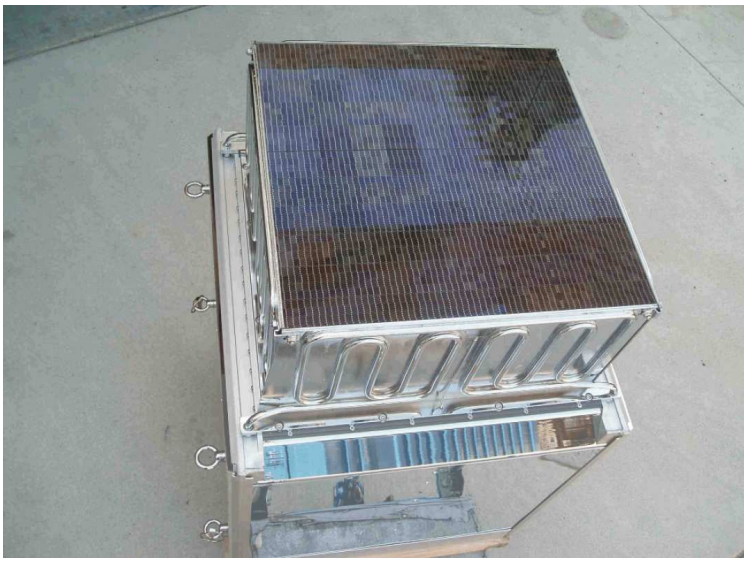

Figure 2.8: Multi-junction 33kW dense array receiver realized and tested in Australia [Ver2006].

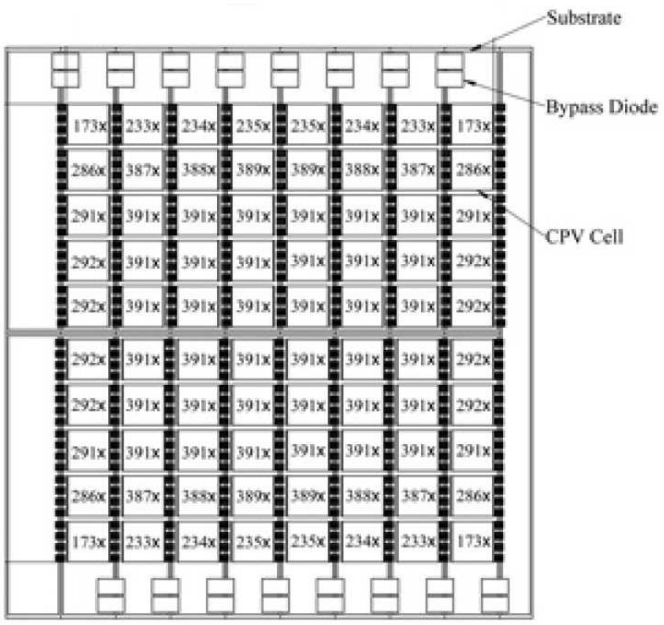

Figure 2.9: Scheme of dense array receiver coupled to a nonimaging flat concentrator [Cho2012]. Mean concentration values, diodes and substrate are indicated.

$$V_0(I_0) = \sum_{j=1}^{N} V_j(I_j) \tag{2.13}$$

$$I_1 = \cdots = I_N = I_0 \tag{2.14}$$

In such a case the current through the cells is the same and the overall voltage is found by adding the voltages at a particular current.

Examples of schemes and realized CPV dense array are in Fig. 2.8 and Fig. 2.9. The MJ receiver in Fig. 2.8 has been tested outdoor in an australian site and it is composed of approximately 1500 MJ solar cells [Ver2006]. The parallel and series interconnections between cells and between modules were selected to optimize power output, considering the light non-uniformity at the receiver level and to accommodate the voltage range of an existing inverter on site. Figure 2.9 shows a scheme of dense array receiver developed in another research work, under relatively high solar concentration ratio [Cho2012]. The impinging mean concentration on each single cell, the substrate and the bypass diodes are indicated. The diodes are useful to prevent the dangerous mismatches described in the next.

2.4 Effects of non uniform illumination in CPVs

The Equations 2.8-2.14 are valid for every PV array applying the classical connections. However, the degradation in current and voltage produced by differences in incident illumination depends on the spatial location of the cells. It is a minor issue when a

concentrating optics is associated to a single cell but it is fundamental in case of dense array receiver where cells are densely packed in a single element.

2.4.1 Non-uniform irradiance profile on single cells

The issue relative to spatial light uniformity is widely known for single cells [Fra2003],[Kat2006],[Her2012]. A cell under non-uniform illumination, as produced by many point focus concentrator systems, experiences a drop in both open-circuit voltage and efficiency compared to a cell under uniform illumination, despite both the cells could receive identical total illumination.

Figure 2.10 shows a multi-junction cell pictured schematically [Leu2001]. The MJ cell can be approximated by cells stacked together in parallel (vertical axis) so that the total current is the sum of the currents through each component. At high concentrations, the inhomogeneity causes the degradation of the fill factor deforming the total IV curve close to the maximum power point, the reduction in efficiency becoming larger with increasing centralized illumination profile. The necessity is to ensure a spatial flux uniformity over the area of the device exposed to the radiation.

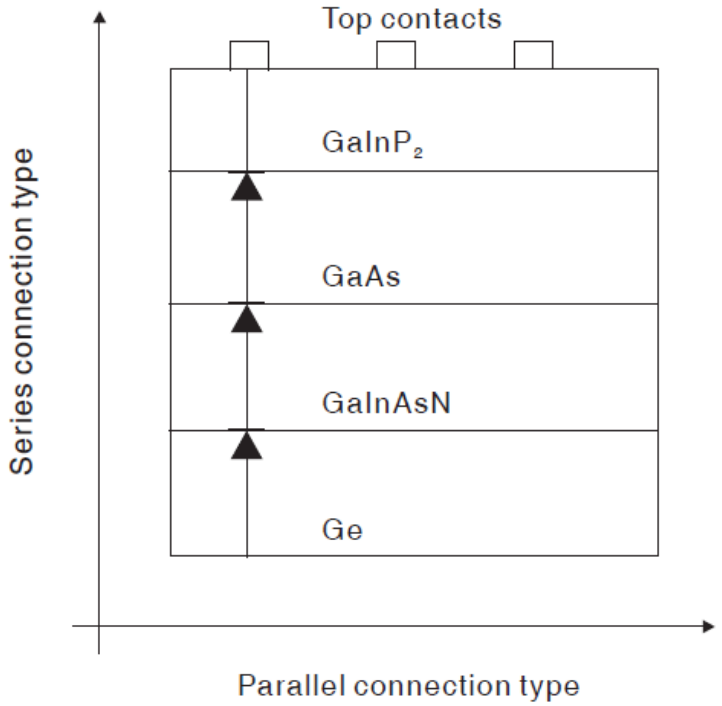

Figure 2.10: Scheme of series and parallel connections inside a triple-junction cell [Leu2001]

2.4.2 Uniformity problem over a dense array

Since MJ cells are much smaller than the whole assembly if organized in a dense array, it is reasonable to consider each single cell as almost uniformly illuminated. Problems related to the non uniformity on the single cells can be thus neglected. When the interconnected cells have identical electrical characteristics and they all experience the same irradiance and temperature, each cell ideally produces the same amount of output current and voltage. The IV curve of the array has the same shape as for the individual cell with the total V_{oc} and I_{sc} increased proportionally to the number of series and parallels as already explained.

Mismatch losses are caused by the interconnection of cells which do not have identical properties or when equal cells experience different conditions from one another. It is well known that when a cell array is subject to not uniform illumination, series connections give rise to mismatches among the cells, mainly because the output current is proportional to the concentration factor (Eq. 2.3). Since the current in the series has to be the same (Eq. 2.14), the current mismatch leads to a severe degradation in system performance, as well as danger of cell damage. The worst illuminated cell produces less current than the maximum power current of the other cells. The high power dissipation in the worst illuminated cell can cause irreversible break due to reverse-bias operation and overheating. A common method to protect cell arrays from reverse bias damage under uneven illumination is to install bypass diodes in parallel to each cell or string of cells. Nevertheless, this solution does not fully recover the power lost due to current mismatch. Simulations and theoretical models allow us to calculate the overall IV curve for array under high concentrations in the presence of current mismatches [Min2010] [Coo2013] and optimize the circuit model to adopt for the receiver.

The series mismatch is difficult to avoid since the PV cells typically offer low voltage (around 3 Volt for III-V MJ cells) and therefore they need to be connected in series to produce an overall high voltage of the module. In fact, a solar array must provide a high enough voltage to enable its inverter to operate at an efficient level and to minimize ohmic losses. Similarly it is important to make sure that the system can never go above the maximum voltage permitted by code (600 V in the U.S. for a residential PV plant).

If individual cells could provide high voltage and low current, then they could be connected in parallel rather than in series, still providing a reasonably high module output voltage. This latter arrangement would lead to voltage matching rather than current matching within the module. Since cell voltage is less sensitive to illumination, voltage matching should produce lower performance degradation under non-uniform illumination, compared to the series connection used in conventional dense array modules. The receiver modeling we implemented is based in these considerations.

The solution proposed to this problem involve mainly the introduction of refractive optics and of modified array interconnections (see Section 1.6). Alternative ways of redesigning the

primary collector have been poorly investigated despite the good results recently obtained in some researches. Just to mention, Chong et al. [Cho2012] proposed a planar modular concentrator coupled to the array in Fig. 2.9. The optimized result of solar illumination distribution is shown in Figures 2.11a and b. The flux pattern consists of a flat top area in the central region of flux distribution where the solar concentration ratio is constant and it is named as uniform illumination area with peak intensity of 391 suns.

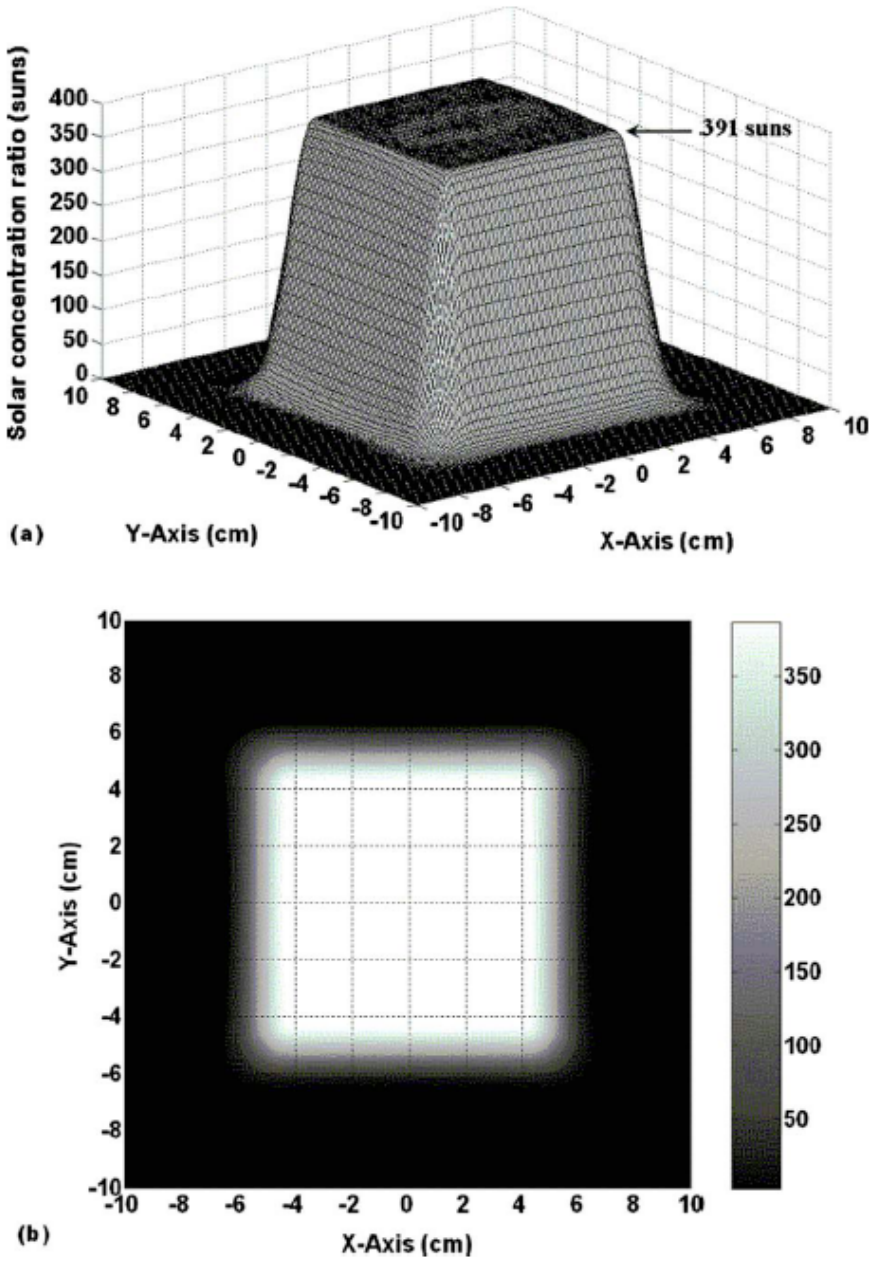

Figure 2.11: The optimized result of solar illumination distribution in both: a) 3-D and b) 2-D views [Cho2012].

However, the concentrator proposed by Chong et al. has some limitations for applications in dense array CPVs. The planar modular concentrator is made by several small flat mirrors which have to be mounted and aligned before being orientated with the use of line-tilting driving mechanism. Moreover, the final spot suffers of the projection effect of the single mirrors. The flat elements do not create an image of the Sun on the receiver but they just reflect its rays producing multiple mirror images that overlap at the target. The size of the single image increases depending on the positioning of the mirror generating the image itself and the shape becomes distorted, these effects increasing with the distance of the mirror from the center of the whole assembly. This projection effect is further worsened by the divergence solar angle. For this reason, such a system is not able to both have big collecting area and high concentration ratio, without embedding a huge number of mirrors. At the same time, its performance is better for longer structures: increasing focal distance can in fact improve the average solar concentration ratio in the uniform illumination area but most of the time the percentage of energy in uniform illumination area will be sacrificed. Thus, a trade-off between the average solar concentration ratio in the uniform illumination area and total energy in the uniform illumination area has to be evaluated to obtain the best performance.

Chapter 3

Optics to enhance the efficiency of a CPV system

As seen in Chapter 1, dishes are commonly large concave mirrors with paraboloidal or spherical geometries, monolithic or segmented depending on dimensions and constructive materials. Apertures of several square meters make the mirrors difficult to be built monolithically and their surfaces are often approximated with a mosaic arrangement of small flat or slightly curved mirrors. Moreover, the longer the focal length, the greater are the mechanical problems related to stability, because the whole system has to move continuously while tracking the Sun daily. Other restrictions are imposed by geometrical optics itself since concave mirrors with standard geometries produce an intrinsically circular solar image, being the Sun an extended circular shaped source. We will see in the following Sections that the irradiance distribution inside the spot produced by a standard mirror surface has a bell shaped profile, its steepness depending on the optical parameters.

In this Chapter we propose a new optical concept to solve the mismatches problems mentioned in Chapter 2 relative to CPV dense array systems. The new approach allows to design an innovative single stage CPV dense array system (with no secondary optics) for high irradiance uniformity and high concentration. A numerical algorithm based on analytical models for both the optics and the receiver has been conceived and coded in Interactive Data Language IDL® to optimize the reflective surface for squaring and smoothing the irradiance distribution on the receiver. Ray tracing techniques have been employed for the optical modeling of the nonimaging elements and for the generation of the irradiance distribution on the receiver. The receiver has been designed together with the optics maintaining simple and standard electrical connections. The mechanics for the optical frames have been designed for easiness of construction and with the aim of maintaining the optical performance. The system proposed is suitable for small/medium residential energy supply or to be also connected in a grid for utility scale PV plants.

3.1 Controlled optics for a prescribed squared irradiance

The concept of creating free-form optics for a prescribed irradiance pattern is certainly not new in nonimaging optics, but it has been mainly applied to design secondary refractive elements generally much smaller than the primary optics. The idea here exposed is to develop primary reflective elements based on a well known analytical theory of aberrations. In the framework of the opto-mechanical and optical research for astrophysical applications, sophisticated optics called "active" and "adaptive" are fruitfully employed to correct the optical aberrations in telescopes. These technologies are relative recent and they allow the telescopes to work with great precision.

In telescopes and, more in general, in every imaging systems used in astrophysics where an image is created, the optics have the main purpose to exactly reproduce the object characteristics and to preserve both its optical and photometric features. In big telescopes mirrors, controlled deformations are introduced by actuators to balance the optical aberrations which contribute to degrade the incoming wavefront from an observed source. The distortions in the final image are caused by several factors, some external to the telescope (i.e. the atmospheric turbulence) some due to the optics itself (i.e. gravitational or wind effects which led to optics deviation from its ideal shape).

What we mainly propose here is a sort of "reverse" approach of the concept applied in astronomical telescopes, in order to perform a technological transfer process from the astrophysical techniques mentioned above to the solar concentrators technology for energy production. The guideline is to apply deformations to the concentrating mirrors not to correct aberrations in the solar wavefront rather to introduce them, degrading the solar image to generate a square/rectangular spot with prescribe irradiance distribution. This condition would give certainly a better match between the concentrated flux and the dense arrays features.

Looking at the solar concentrators, the proposed method could be usefully extended and implemented for the following goals:

- to tailor the irradiance distribution for the adopted receiver, thus introducing aberrations;
- to correct optical aberrations in particular configurations, as in tower systems to boost the concentration up to its limit.

Hereafter, we focus on the first purpose explaining the method in detail with the aim of optimizing a CPV dense array concentrator.

3.1.1 Irradiance and spot diameters for spherical mirrors

The image size and its irradiance profile depend on the concentrator parameters and to a first approximation, if diffraction effects are negligible, very simple formulas of geometrical optics describe this dependence. When dealing with dense array systems the dimensions of the optics range from one to several meters. In a paraboloidal mirror with focal ratio f (ratio between focal length and diameter), being D the entrance aperture diameter, F the focal length and φ the solar angular dimension, the image diameter d after correcting all the aberrations is given by:

$$d \simeq \varphi f D = \varphi F \tag{3.1}$$

The Sun can be considered as a finite source with an angular diameter of around 0.53°, neglecting its shape variations caused be the altitude changing during the day. Considering the receiver exactly on the focal plane, i.e. the distance l between the receiver and the mirror vertex being equal to the focal length $l = F$, as the concentration factor C depends by definition on the image dimension, it useful to recall that:

A. C scales as D^2;

B. for mirrors with the same D, C is inversely proportional to F^2.

For circular apertures, these relations can be easily deduced combining Eq. 1.2 and Eq. 3.1 to obtain the following:

$$C = \frac{D^2}{d^2} = \varphi^{-2} f^{-2} \propto f^{-2} \tag{3.2}$$

Fig. 3.1 shows that d does not substantially change with D if F remains constant. The spot is formed at the focal plane which coincides with the receiver and the scale of each panel is the same in all the cases (50 mm). The source is modeled to irradiate 1 sun at the mirror aperture. Units shown in the legend are then Watts per millimetres squared.

The case of fixed D and variable F is shown in Fig. 3.2. d increases with F which in the example reported assumes the value 3000 mm, 4000 mm and 5000 mm, from left to right,

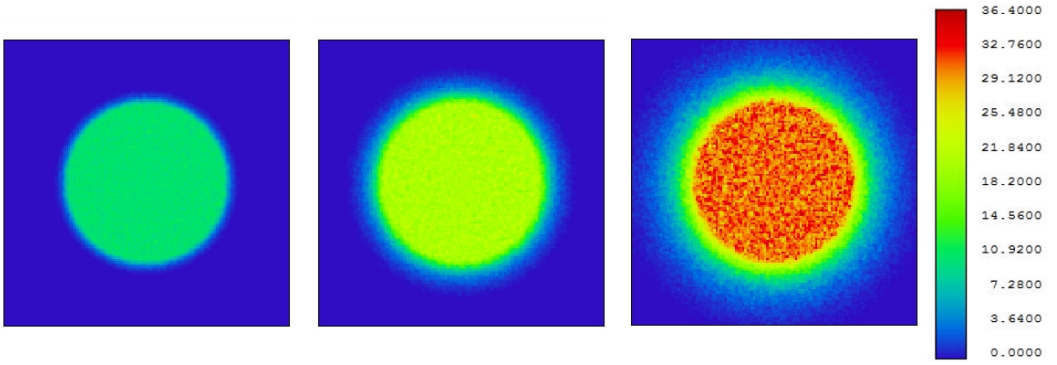

Figure 3.1: Simulated spot for different D and constant F. From left to right, D values are: 3000 mm, 4500 mm and 6000 mm.

while $D = 3000$ mm in all the cases. Concentration ratio drops as f^{-2} accordingly to the equation 3.2.

The previous examples show that irradiance uniformity and high concentrations can be achieved by an imaging mirror around its focal zone. However, it must be taken into account that the cells presently available on the market can work efficiently for concentrations between few hundreds and few thousands of suns. The concentration produced by an imaging mirror could be too high for these cells. A common technique to obtain suitable concentration ratios is to use out-of-focus imaging optics. The mean working parameter C is generally decided before the design of whole systems depending on the cells used. An investigation of the irradiance in case of receiver not located exactly on the focal plane is thus needed.

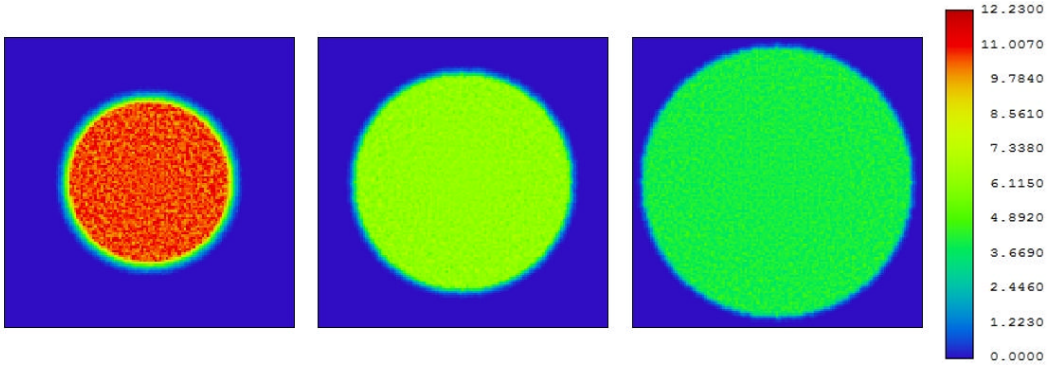

Figure 3.2: Simulated spot for different F and constant D. From left to right, F values are: 3000 mm, 4000 mm and 5000 mm.

When a mirror with paraboloidal or spherical shape has to be designed to work as concentrator, the easiest way to adjust the concentration ratio is by shifting properly the receiver distance after fixing some optical parameters. The off-focus mode, which results in $l \neq F$, is the operating state commonly used in dense array systems to reach the concentration required and it can equally be employed to change the concentration at which a system works (for example for testing different receivers). The same effect of changing the flux at the receiver, in case of fixed receiver distance, could be theoretically obtained supposing to change F by "bending" the mirror, i.e. changing the mirror curvature in order to tune the mean concentration at the fixed distance l. Fig. 3.3 shows the spot for mirrors with the same $D = 3000$ mm and with different F (so different curvatures), the latter chosen in order to reproduce mean concentrations of 5000× (the same reached in focus), 2500×, 1000× and 500×. In the simulations the image plane has been located at $l = 4800$ mm. Smaller concentrations are obtained for larger F. The spot diameter changes since F varies (l remains constant) and the irradiance uniformity is almost perfect in focused mode, then it degrades getting better again for lower concentrations. Figures 3.3 and 3.4 show how irradiance uniformity depends on focal length once D and the receiver plane have been fixed.

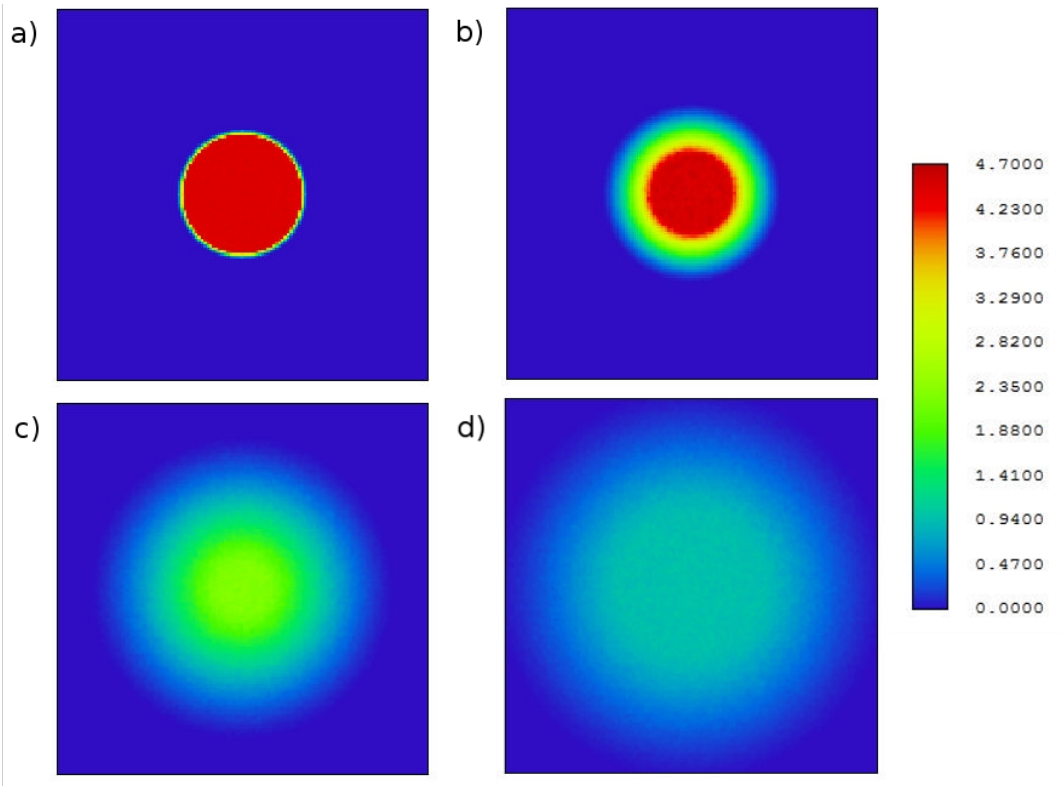

Figure 3.3: Spot dimension for constant D and different F (different curvatures), corrisponding to C mean values of 5000×, 2500×, 1000×, 500× from a) to d). The entrance irradiance is constant (1 sun) for all the cases.

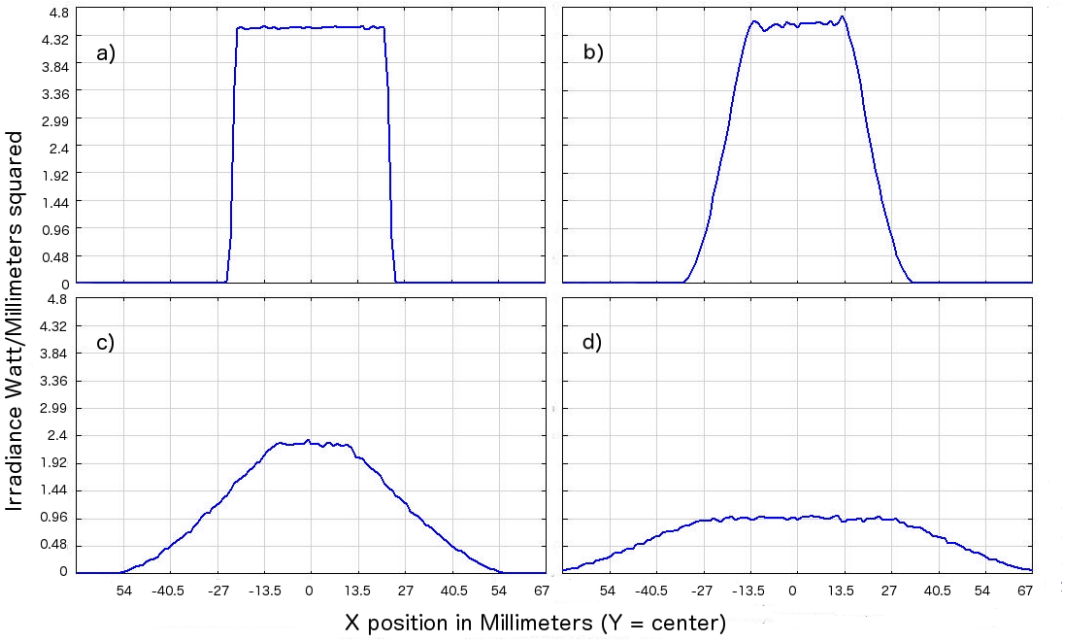

Figure 3.4: Irradiance profile for for constant D and different F (different curvatures) corrisponding to C mean values of 5000×, 2500×, 1000×, 500× from a) to d). The entrance irradiance is constant (1 sun) for all the cases. The x-cross section irradiance is evaluated at the central y-row of the Figures 3.3.

The best irradiance profile is represented by the shape of the curve in the focus mode in Fig. 3.4a, where the tails of the curve are negligible if compared to the extended central plateau. A spot diameter $d = 44$ mm can be deduced by the same figure, in agreement with the Eq. 3.1 substituting $f = 1.6$, despite no aberrations have been corrected. The reason for the small aberrations influence is the large focal length.

3.1.2 Zernike polynomials to describe surfaces

To describe the mirrors shape and to perform the optimization we introduce here the *Zernike polynomials*, an analytical tool largely used in optics to model surfaces. These are a set of functions often expressed in polar coordinates (ρ, θ), where ρ is the normalized radial coordinate ranging from 0 to 1 and θ is the azimuthal angle ranging from 0 to 2π. It is a useful tool to characterize functions and data on a circular domain then widely used for issue related to lens design. The polynomials form an orthogonal basis on the unit circle and real surfaces can be represented by linear combinations of them. Each of the Zernike polynomials consists of three components: a normalization factor, a radial dependent component and an azimuthal dependent component. The radial components are polynomials derived from the Jacobi polynomials, whereas the azimuthal component is sinusoidal. There exist several different normalization and numbering schemes for these polynomials. As in the well know paper by Noll [Nol1976], the Zernike polynomials can be written as:

$$Z_{even,j} = \sqrt{n+1} R_n^m \rho \sqrt{2} \cos m\theta \tag{3.3}$$

$$Z_{odd,j} = \sqrt{n+1} R_n^m \rho \sqrt{2} \sin m\theta \tag{3.4}$$

$$Z_j = \sqrt{n+1} R_n^0(\rho) \tag{3.5}$$

where m is the azimuthal frequency and n is the radial degree, both are integer and the condition $m \leq n$, $n - |m| =$ even must be satisfied. Equations 3.3 and 3.4 exist for $m \neq 0$ while equation 3.5 for $m = 0$. The double indexing scheme is useful for unambiguously describing the functions. The radial polynomials are:

$$R_n^m(\rho) = \sum_{s=0}^{(n-m)/2} \frac{(-1)^s (n-s)!}{s! \left[\frac{n+m}{2} - s\right]! \left[\frac{n-m}{2} - s\right]!} \rho^{n-2s} \tag{3.6}$$

Table 3.1 and Figure 3.5 show the 2D and 3D maps of the polynomials up to the 6th radial order. The polynomials are ordered vertically by radial degree and horizontally by azimuthal degree. These representations are useful to visualize the geometry of the deformation introduced by a specific term. The magnitude of the deformations is directly related to the coefficients associated with the polynomials, as we will describe in the following Section.

In ground based astronomical observations, a flat wavefront coming from a source is deformed by the atmospheric turbulence and other effects. With a combination of a certain

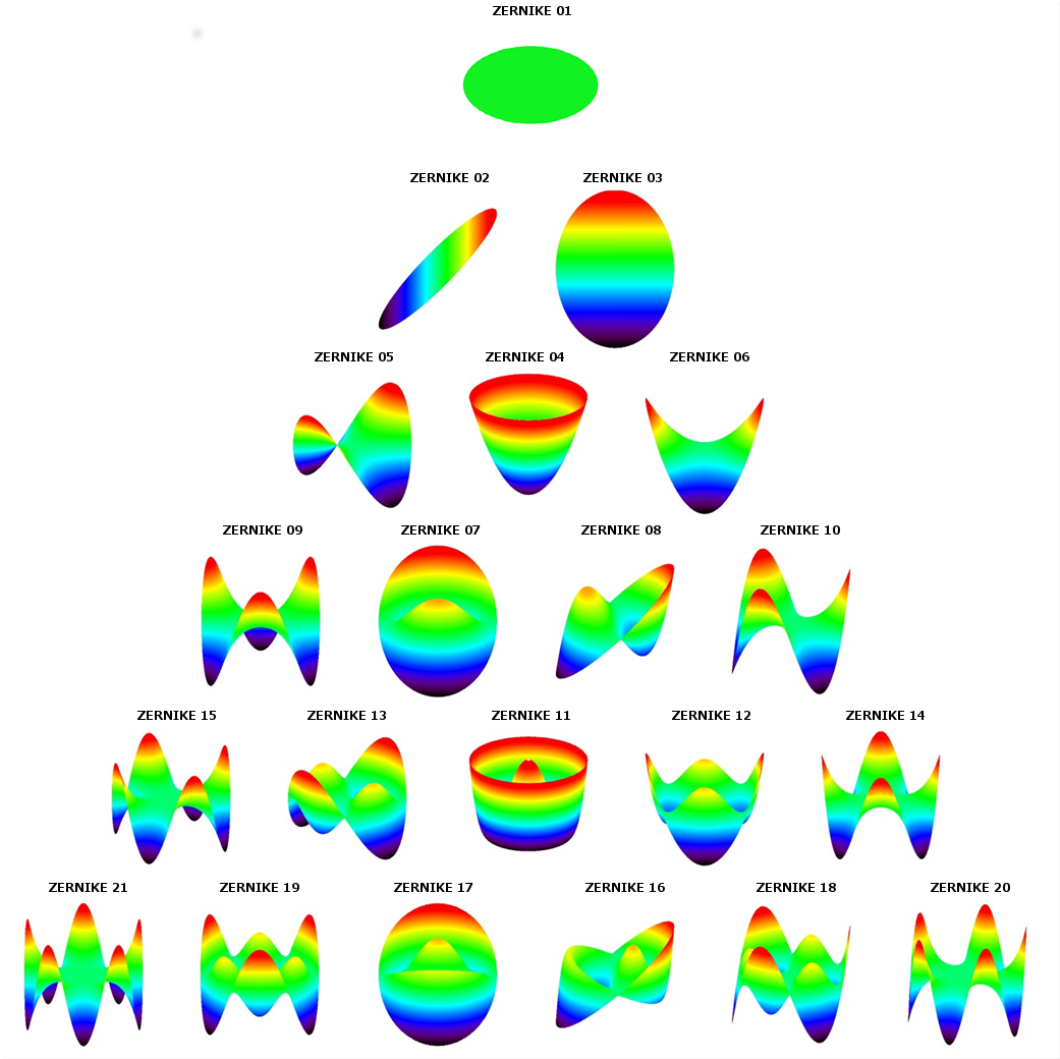

Figure 3.5: 3D representation of the first 21 polynomials.

number of Zernike modes, quantified by the numerical values of the associated coefficients, it is possible to model the form of the deviation experienced by the ideal plane wave. More in general, we could say that these functions can describe arbitrarily complex surfaces.

Despite dense array solar concentrators have some analogies with telescopes as for geometries, mechanics and tracking, the design of these two devices has different drivers. This suggested us to exploit the Zernike model in reverse: the irradiance distribution properties needed by a PV concentrator can be reached by the design of a primary mirror starting from a spherical or paraboloidal shape and superimposing a finite combination of Zernike modes.

Radial degree (n)	**Azimuthal frequency (m)**					
	0	1	2	3	4	5
0	Z1 (Piston)					
1		Tilts Z2 Z3				
2	Defocus Z4		Astigmatism (3° order) Z5 Z6			
3		Coma (3° order) Z7 Z8		Z9 Z10		
4	Spherical (3° order) Z11		Z12 Z13		Z14 Z15	
5		Z16 Z17		Z18 Z19		Z20 Z21

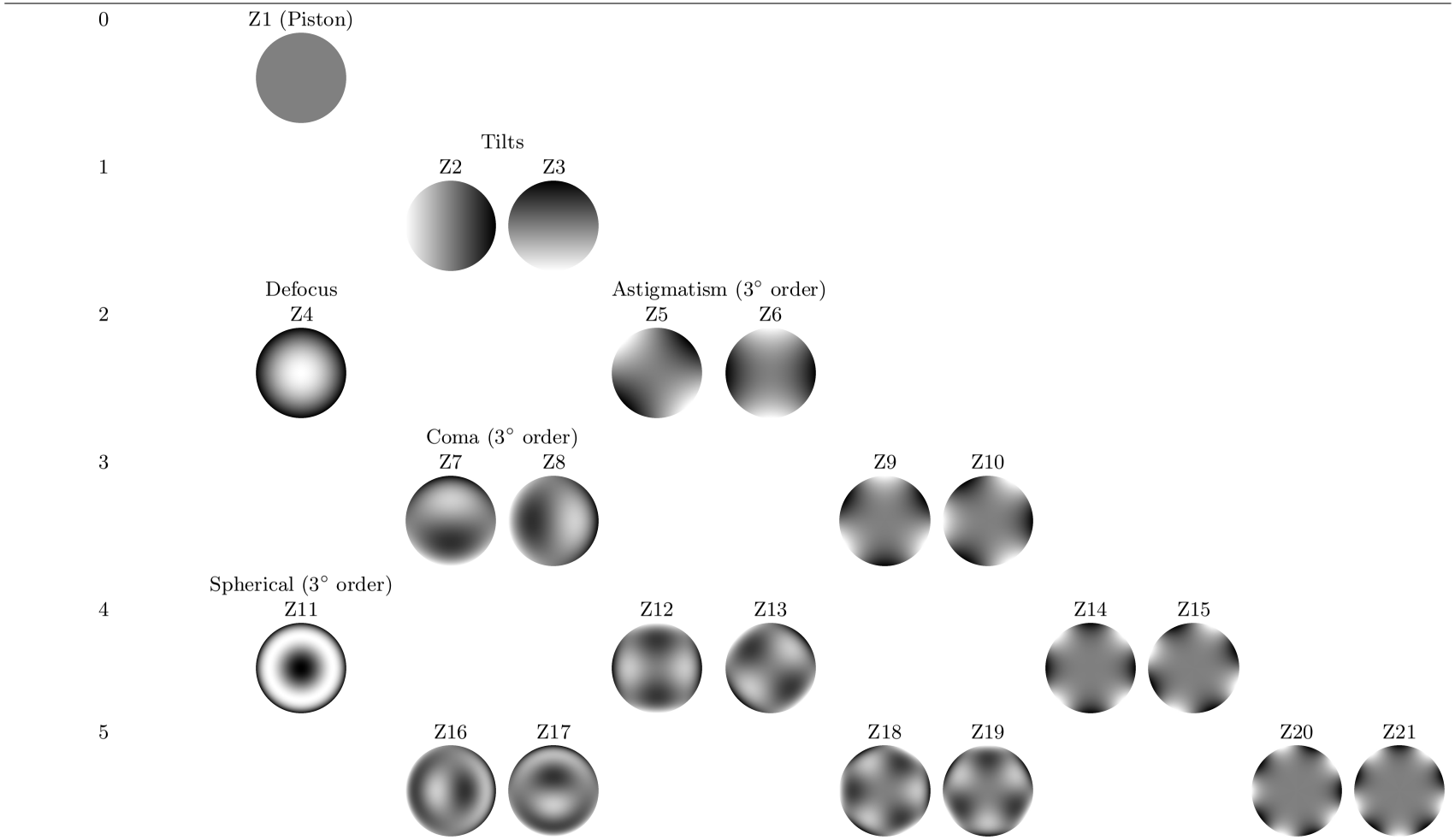

Table 3.1: 2D representation of the first 21 polynomials.

3.1.3 Optical concept for a single mirror focusing on-axis

An analysis we performed with the ray tracing software Zemax® showed that, starting from a spherical mirror, very few deformations described by Zernike modes can improve the irradiance uniformity and solve the problem of squaring the circular solar image.

Considering an imaging mirror in presence of deformations, its surface z (the so-called *sag*) can be approximated by the following formula:

$$z = \frac{cr^2}{1+\sqrt{1-(1+k)c^2r^2}} + \sum_{i=1}^{N} A_i Z_i(\rho,\theta) \tag{3.7}$$

where N is the series polynomial number, A is the coefficient associated to the i^{th} polynomial, r is again the radial coordinate in the chosen units, ρ and θ are the polar coordinates already defined. The Eq. 3.7 depends on the geometry by the curvature c and the conic constant k. The first term in the equation represents an ideal conic surface, spherical for $k = 0$, while the second term represents the deformations described as Zernike polynomials. The number of polynomials needed for a good surface modeling grows together with the number of deformations on different scales.

We identified three main polynomials useful for a single spherical mirror focusing on axis: the 4^{th}, the 11^{th} and the 14^{th}. Fig. 3.6 shows how the solar spot produced at a fixed distance by a out-of-focus spherical mirror can be modified by introducing controlled deformations related to the three Zernike polynomials mentioned above. This model can be however extended to mirrors with an off-axis focus: in that case the number of Zernike modes involved in the spot shaping is higher.

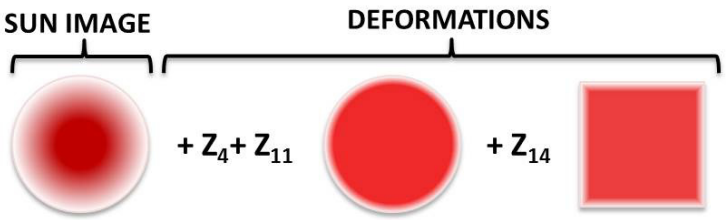

Figure 3.6: A scheme of the effects introduced on the solar image by deformations related to the Zernike indicated.

These modes are shown in 2D and 3D in Table 3.2. The deformation associated with the 4^{th} mode (*defocus*) basically enlarges the image and contributes to spread the light quite similarly to a receiver plane shift. The 11^{th} mode (*third order spherical*) contributes to redistributing the rays maintaining an image radial symmetry and changing the image irradiance profile. These two polynomials do not have any impact on the spot shape since they have no azimuthal dependence. A deformation corresponding to the 14^{th} polynomial (*vertical quadrafoil*) contributes to square a circular spot along two preferential directions rotated 45 degree, depending on the coefficient sign. The effect of this specific deformation is less evident if the mirror is in focus mode: that is the reason for a combined use of the

modes 14^{th} and 4^{th}. Alternatively, the same effect of this combination can be obtained by positioning the receiver slightly behind or above the correct focal plane and avoiding (partially or completely) the deformations related to the 4^{th} mode.

Zernike Mode		
4^{th}	11^{th}	14^{th}
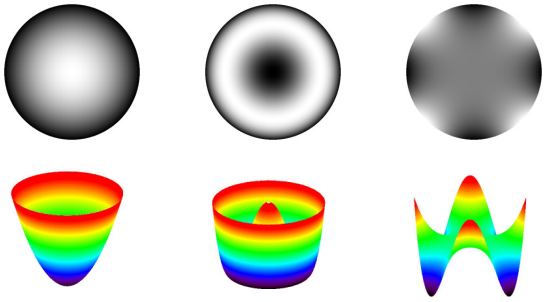		

Table 3.2: Zernike modes that contribute in a spherical mirror to make the solar spot square.

The size of the spot depends on the desired concentration factor. Since it is easier for a single mirror to produce a square uniform image when the defocus is bigger, this means that the lower the concentration factor the better the method works.

3.2 Design choices and modeling tools

It is possible to conceive reflective systems which perform at high level of irradiance uniformity on a fixed distant plane manipulating the spot shape. The desired effect can be obtained by designing concentrators with several mirrors opportunely optimized and focusing on the same point. In such a case, the final illumination pattern impinging on the receiver is the sum of the incoherent illumination patterns produced by each single mirror.

To optically model the system, an end-to-end code of routines has been written on purpose. Each step of the modeling and the results have been tested with the optical design software Zemax® as reference. A whole optimization with Zemax® would have been also possible by the Zemax Programming Language macros. The code includes two main subgroups of routines for individually modeling the optical part and the receiver. A third group of procedures calculates the tolerances for the optical/mechanical parameters.

3.2.1 System dimensioning

Since this research activity has been carried out with the specific goal of finding new solutions in the field of clean micro-generated distributed electricity, the dish has been conceived as a power system suitable for the market of medium residential contexts or small farms, then for a production of around 10 KWe. Utility scale applications could be anyway considered by connecting an array of several of these systems in a field, also scaling the single elements for a higher energy output.

To dimension the system, a series of concepts have been taken into account. In a single mirror the focal ratio should approach f/0.5 in order to maximize the concentration, but also to allow a more compact structure. Previous considerations (see Figures 3.1 - 3.4) show that a concentrator in focus mode with $l = F$ would give a very high concentration ratio and a good irradiance uniformity. Unfortunately there are two main reasons to avoid this condition: the flux collected could be too high for the cells working range (at present up to few thousands of suns); the deformations introduced by the Zernike modes are more efficient in reproducing the image features required when a defocus occurs. The defocus mode is then preferred despite the higher image initial disuniformity. In this condition also a small extra-obscuration is introduced by a larger detector imposed by the image enlargement. At the same time the energy density goes down as the defocus grows, in contrast with the technology developing trend which aims at obtaining cells working at higher and higher fluxes. Finally, very big dishes have more problems related to aligning, tracking, stability also because the collector has to move simultaneously with its receiver which is built-in in the mechanical structure.

To mitigate some of these issues, we selected an optical design already used in Stirling applications as well as in some ground based optical telescopes. The mosaic optics commonly used in CPV dishes has been here replaced by few monolithic optics mounted on the same structure close together. The developed configuration is a 7-mirrors combination made by a central mirror and a ring of six mirrors in hexagonal arrangement around it. Figures 3.7 presents the optical layouts of the proposed system. The z-axis is the direction of the incoming rays and it is perpendicular to the central mirror vertex. This optical condition of alignment with the solar direction should be the nominal working state.

A multi-mirror configuration can be useful to solve the issue of modeling a unique huge mirror avoiding the mosaic of hundreds small reflective elements (see [Cho2012][SolSys]). Nevertheless it should fulfill a series of requirements to be efficient as the maximum pupil filling, a cylindrical symmetry and the constructive homogeneity of the mirrors. The best configuration in this sense, in case of mirrors with the same aperture, is the hexapolar grid. In the hexapolar configuration, the elements are placed on rings so that the $(n+1)^{th}$ ring contains six elements more than the n^{th} ring, the central ring having only one element. In Fig. 3.7B the mirrors of the second ring have been labeled from 2 to 7 counter-clockwise .

Considerations about the concentration ratios and the mechanical compactness have been made also in comparison with similar existing prototypes and plants, mainly located in Australia. The mirror size has been decided to be not bigger than 2-3 meters diameter, to avoid construction difficulties. The diameter of the single mirror has been chosen to be 2600 m, for a total system size of 7800 m. The detector distance has been set to 4800 m in order to have a low *detector distance/ total diameter* ratio (parameter similar to the focal ratio in imaging systems) of 0.6 thus allowing a very compact system. The mirrors aperture have

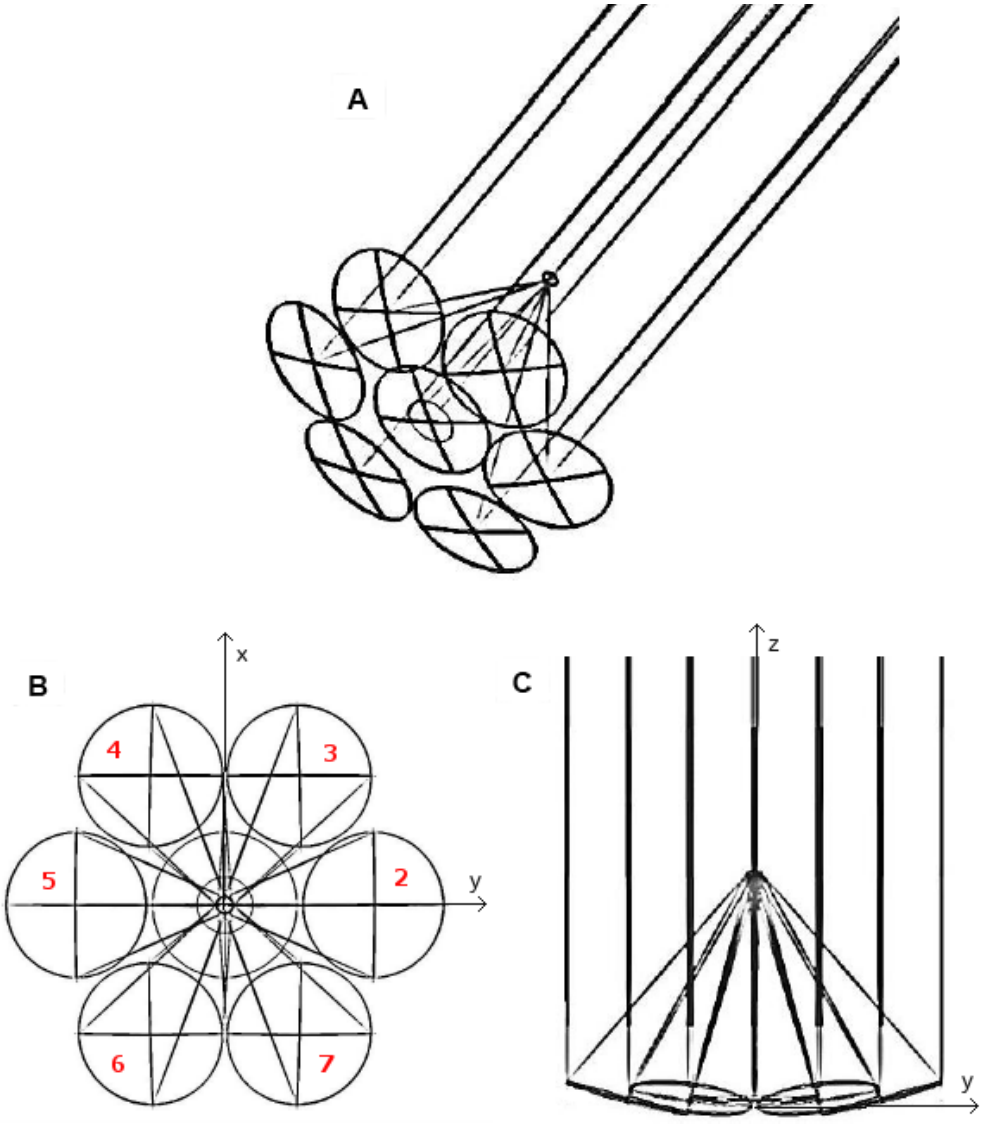

Figure 3.7: Optical layouts of the geometry proposed in two planes: A) 3D layouts, B) x-y plane, C) y-z plane.

been set circular for a total collecting area of about 37 m^2. Two concentration ratios were investigated: 500× and 800×.

3.2.2 Optical Modeling

The concentrator has been initially designed with Zemax® putting flat mirrors with same circular aperture and diameter D on the same plane. Each mirror has been placed at d=2680 mm from the central mirror vertex to prevent shading effect in the mirrors of the second ring caused by the central mirror (Fig. 3.8).

The mirrors of the ring have been tilted respect to the central one in order to focus the chief rays at the center of the receiver plane placed at distance h from the central mirror vertex. Following the scheme in Fig.3.8, it is easy to obtain the law to calculate the tilt fulfilling this

optical condition. The incoming rays are parallel to the z-axis, while the mirrors vertexes lay in the x-y plane. This choice is optional, but it aims at simplifying the mechanical structure.

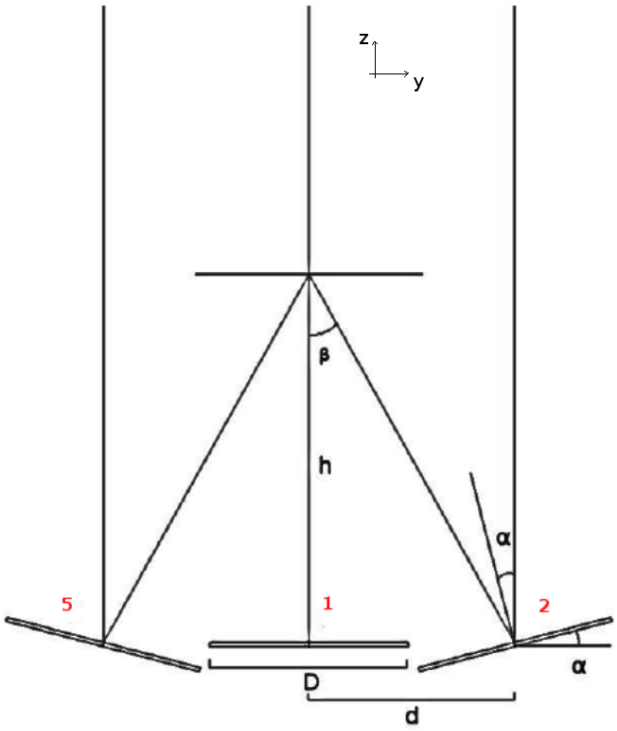

Figure 3.8: Tilting scheme for the mirrors in the ring.

In the Figure (Fig. 3.8), the first mirror of the external ring (♯2) is positioned along the positive y axis and the mirror ♯5 in the negative one. The tilt angle α for these mirrors having the vertexes in the y-z plane, :

$$\alpha = -\frac{\left(\frac{\pi}{2} - \tan^{-1}\left(\frac{h}{d}\cdot \operatorname{sgn} d\right)\right)}{2}\cdot \operatorname{sgn} d \tag{3.8}$$

where the $\tan^{-1}\left(\frac{h}{d}\cdot|d|\right)$ is the β angle in the figure, and sgn is the sign function.

For the other mirrors in the ring not located in the y-z plane, there are two tilt angles in the reference chosen, which are the projections of α into the y-z and x-z planes. These angles can be calculated by the following formulas:

$$\alpha_x = -\left|\tan^{-1}\left(\frac{\sin\alpha\cdot\cos\phi}{\cos\alpha}\right)\right|\cdot \operatorname{sgn} y_s \tag{3.9}$$

$$\alpha_y = -\left|\cos^{-1}\left(\frac{\cos\alpha}{\cos\alpha_x}\right)\right|\cdot \operatorname{sgn} x_s \tag{3.10}$$

where ϕ is the azimuthal angle of the mirror accounted clockwise starting from the mirror in the positive y axis and (x_s, y_s) are the coordinates of the mirror vertex considered in the same reference. The angle α_y lays in the y-x plane as the angle α, while α_x in the x-z plane.

Once fixed the distance d in the hexapolar grid the parameters or the mirrors in the other ring can be immediately calculated. Each mirror of the first ring is positioned, for example, at an hexagon vertex. The value of position and tilt for the seven mirrors are listed in Table 3.3, where the distances are in millimeters and the angles in degrees.

	Mirr1	**Mirr2**	**Mirr3**	**Mirr4**	**Mirr5**	**Mirr6**	**Mirr7**
X pos (mm)	0.000	0.000	2320.880	2320.880	0.000	-2320.880	-2320.880
Y pos (mm)	0.000	2680.000	1340.000	-1340.000	-2680.000	-1340.000	1340.000
$\alpha_{\mathbf{x}}(^\circ)$	0.000	-14.588	-7.414	7.414	14.588	7.414	-7.414
$\alpha_{\mathbf{y}}(^\circ)$	0.000	0.000	12.599	12.599	0.000	-12.599	-12.599

Table 3.3: List of positions and tilt angles of the seven mirrors.

After positioning and tilting the plane mirrors, the initial optical parameters have been set by a ray tracing analysis performed in Zemax®. The initial curvatures have been optimized so that the mirrors could produce a spot with a size comparable with the mean geometrical concentration chosen. The concentration ratio has been defined as the total mirrors area perpendicular to the solar direction divided by the total area of the receiver, supposing a receiver and a spot ideally with the same size. With this definition we neglected the obscuration of the central mirror due to the receiver and its possible inactive areas. The tilt of the external mirrors reduce by 5% the collecting area of the whole system from 37.17 m^2 to about 35.25 m^2. For both the configurations with concentration 500× and 800× the parameters in Table 3.3 remain valid as they are calculated from geometrical evaluations independent from the optical features.

The Zernike coefficients which correspond to the deformations useful to satisfy our requests of shape and uniformity have been individuated after fixing the initial curvature as described. The coefficients needed for the central mirror are the three described in Section 3.1.3. Other modes (from 5^{th} to 8^{th}) are necessary for the six off-axis mirrors to form the suitable spots. In this way, the superimposition of all the generated spots forms a picture with the desired features.

	Mirr1	**Mirr2**	**Mirr3**	**Mirr4**	**Mirr5**	**Mirr6**	**Mirr7**
Z4	Z4(1)	Z4(2)	Z4(2)	Z4(2)	Z4(2)	Z4(2)	Z4(2)
Z5	0.000	0.000	-Z6(2)$\cdot\cos 30^\circ$	Z6(2)$\cdot\cos 30^\circ$	0.000	-Z6(2)$\cdot\cos 30^\circ$	Z6(2)$\cdot\cos 30^\circ$
Z6	0.000	Z6(2)	-Z6(2)$\cdot\sin 30^\circ$	-Z6(2)$\cdot\sin 30^\circ$	Z6(2)	-Z6(2)$\cdot\sin 30^\circ$	-Z6(2)$\cdot\sin 30^\circ$
Z7	0.000	Z7(2)	Z7(2)$\cdot\sin 30^\circ$	-Z7(2)$\cdot\sin 30^\circ$	-Z7(2)	-Z6(2)$\cdot\sin 30^\circ$	Z7(2)$\cdot\sin 30^\circ$
Z8	0.000	0.000	Z7(2)$\cdot\cos 30^\circ$	Z7(2)$\cdot\cos 30^\circ$	-Z7(2)	-Z6(2)$\cdot\cos 30^\circ$	Z7(2)$\cdot\cos 30^\circ$
Z11	Z11(1)	Z11(2)	Z11(2)	Z11(2)	Z11(2)	Z11(2)	Z11(2)
Z14	Z14(1)	Z14(2)	Z14(2)	Z14(2)	Z14(2)	Z14(2)	Z14(2)

Table 3.4: Correlation between the Zernike coefficients of the seven mirrors.

Symmetry properties have been imposed for the six mirrors in the external ring. These mirrors have the same curvature radius and same Zernike coefficients 4^{th}, 11^{th} and 14^{th}. As consequence, the Zernike coefficients are linked by the geometrical relations shown in

Table 3.4. Opposite mirrors are equal but rotated by π. The final optical model in this way results to be made of only four different surfaces. It could be certainly possible to identify more coefficients to improve the performance: however, in the case of free-form surfaces or of surfaces obtained by deformation of an initial spherical one, the number of actuators would be smaller for a limited number of coefficients. This condition is more suitable both in constructive and calibration stages. Table 3.4 shows that the independent modes for our system are basically eight, three for the central mirror (Z4(1), Z11(1) and Z14(1)) and five for the lateral ones, all derived from the modes of the mirror ♯2 (Z4(2), Z6(2), Z7(2), Z11(2), Z14(2)) according to the relations shown in Table 3.4.

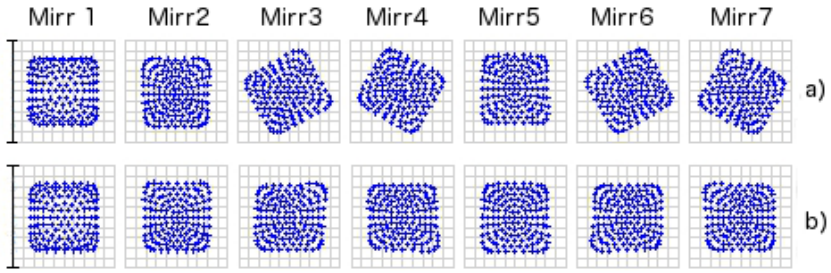

Figure 3.9: Effect introduced in the spot generated by each mirror by the introduction of a) a Z14 value rotated according to the mirror location and a) a common Z14 value.

The mirrors of the ring can not have all the same shapes even if this would be the best constructive condition. The 14^{th} Zernike mode in fact corresponds to a deformation able to modify the circular symmetry of the ray bundle into a square symmetry and it obviously has an azimuthal dependence. The simple rotation of a given surface would lead to a different analytical description for the surface itself in terms of Zernike coefficients, except for the coefficients with pure radial dependence. This means that a ring generated by replicating mirror ♯2 and simply rotating the replicas according to the position in the ring, would give a series of identical spot rotated as in Fig. 3.9a. A superimposition of these figures would not give the desired result. On the contrary, fixing the 14^{th} coefficient to the same value for all the surfaces gives the features in Fig. 3.9b.

3.2.3 Receiver Implementation

The receiver has been analytically designed and numerically simulated using a datasheet of commercially available high concentration cells 3C40 produced by AZUR SPACE [Azur] with a nominal efficiency of 39% at 500× (around 38% at 1000×) at ambient temperature. The reference cell has main features described in Table 3.5.

The receiver design has been implemented in IDL® to minimize the series connections mismatches even maintaining high degree of linearity and easiness of construction. The electrical scheme involves classical series and parallel connections balanced to match the quasi-square symmetry of the irradiance distribution. When multiple micro-cells are packed

one beside the other inter-spaces among the cells can not be avoided, despite these can be are really small if compared to the total array area. Supposing to neglect these gaps but taking into account only the cells active area (given in Section 3.5), a dense array of these cells could potentially reach efficiency slightly lower than 33% for 500× and 32% for 1000× under an even illumination. There are two version of considered cell but in the calculation we used the one without glass (blu line).

Base Material	GaInP/GaAs/Ge on Ge substrate
AR Coating	TiOx/Al2Ox
Chip size	5,59 x 6,39 mm^2= 35.25 mm^2
Active Cell Area	5,5 x 5,5 mm^2=30,25 mm^2

Table 3.5: Main features of the AZUR SPACE 3C40 cell implemented in the simulations

	$\mathbf{I_{sc}}$(A)	$\mathbf{V_{oc}}$(V)	$\mathbf{I_{max}}$(A)	$\mathbf{V_{max}}$(V)	$\mathbf{P_{max}}$(W)	**FF**(%)	$\boldsymbol{\eta}$(%)
500×	2.151	3.144	2.102	2.842	5.98	88.0	39.0
1000×	4.239	3.170	4.135	2.762	11.42	85.0	37.8

Table 3.6: Electrical parameters of the AZUR SPACE 3C40 cell at 500× and 1000×.

In addition to efficiency, the datasheet of the cell gives other output parameters for the two concentrations as reported in Table 3.6 necessary for the simulations to predict the cells power output at different illumination conditions.

The electrical performance has been analytically calculated by a routine implementing the equations 2.3-2.7 which model the cell output current and voltage as a function of light concentration, neglecting resistive effects. A temperature of $T = 25°$ has been considered and a reasonable value for the ideality factor $n_1 = 3.3$ has been assumed to treat the junctions as real. The other initial parameters used are in Table 3.6. Being the FF only dependent from the V_{oc}, it has been calculated using a classical empirical formula [Gre1981] approximated for zero resistivity:

$$FF(\times) = \frac{v_{oc}(\times) - \ln(v_{oc}(\times) + 0.72)}{1 + v_{oc}(\times)} \tag{3.11}$$

where $v_{oc}(\times)$ is the open circuit voltage normalized for the factor $\frac{n_1 KT}{q}$.

The Equations 2.3-2.7, together with data available for the cell and the fill factor model in Eq. 3.11, allow to calculate, to a first approximation, the nominal performance of the single cell as a function of the flux impinging on it. The value of $I_{sc}(1)$ and $V_{oc}(1)$ can be deduced from the data, inverting the Equations 2.3 and 2.4. Another assumption based on the datasheet is that V_{max} does not change significantly with the concentration ×, then we can consider it constant. In this way, calculating P_{max} from Eq. 2.6 and inverting Eq. 2.5, we obtain the maximal current of the cell at a given concentration.

The current and voltage calculation for series and parallels connections have been derived by the classical Equations 2.12 and 2.14. Attention has to be paid to series connected cells

since the output current in this case corresponds to the current produced by the worst illuminated cells of the series. No model has been implemented for the bypass diodes.

The choice of the exact number of cells to connect has been made starting from the concept that a receiver should have a certain area to perform at a certain concentration. The array design has to resemble, with the right connections, an irradiance distribution size mostly square and uniform but degrading in concentration toward the borders.

To simplify the scheme, we decided to construct the receiver starting from the same base unit, which is a string of series connected cells. The first design version is a detector made by 56 strings of 36 cells. The strings spatial positioning is shown in Fig. 3.11a where each string is represented by the narrow rectangle. There are 32 strings in the central bordered zone, which corresponds roughly to the maximum uniform area obtainable by the optimization, and 4 lateral zones made by 6 additional modules. The total number of cells is 2016. A similar design has been used for another receiver version that we explain soon after. This scheme allows cells in series to be irradiated with similar fluxes. At the same time, the strings and the groups contain the same number of elements thus guaranteeing small parallel mismatches. This scheme does not have cells at the corners, since the spillage losses in case of 500× have been evaluated in the order of 5%.

A scheme with many parallels leads to a lower dependence from irradiance gradients, but has the inconvenience to give high current and small voltages in output. Thus we developed a new connection concept to obtain the same power output with higher output voltage. The second detector version is shown in Fig. 3.10a and b: the basic string is made of 8 cells in series and the parallel connection are between blocks of strings. In practice, zones with the same number in Fig. 3.10b contain only series connected strings. The 8 blocks of strings obtained, numbered from 0 to 7, are then parallel connected. In this way it is possible to have a large amount of cells in series and then a small final current.

Figures 3.11a and 3.11b depict the third array version implemented for which we calculated the tolerance results shown in the next Chapter. The cells arrangement is the same described for the first version receiver (Fig. 3.11a) while the electrical connections are the following (Fig. 3.11b): cells in each strings and strings with the same color are series connected. The central zone is then made by 8 blocks of cells each containing 4 adjacent substrings (the subdivision of each colored areas have been omitted), while the lateral strings are series connected in concentric frames. The 14 resulting blocks are finally parallel connected.

The latter electrical scheme was used also for simulating the case with concentration 800×. In this case the cells of the base string are only 27 and the central zone is made by 24 strings since the higher concentration results in a smaller irradiated area.

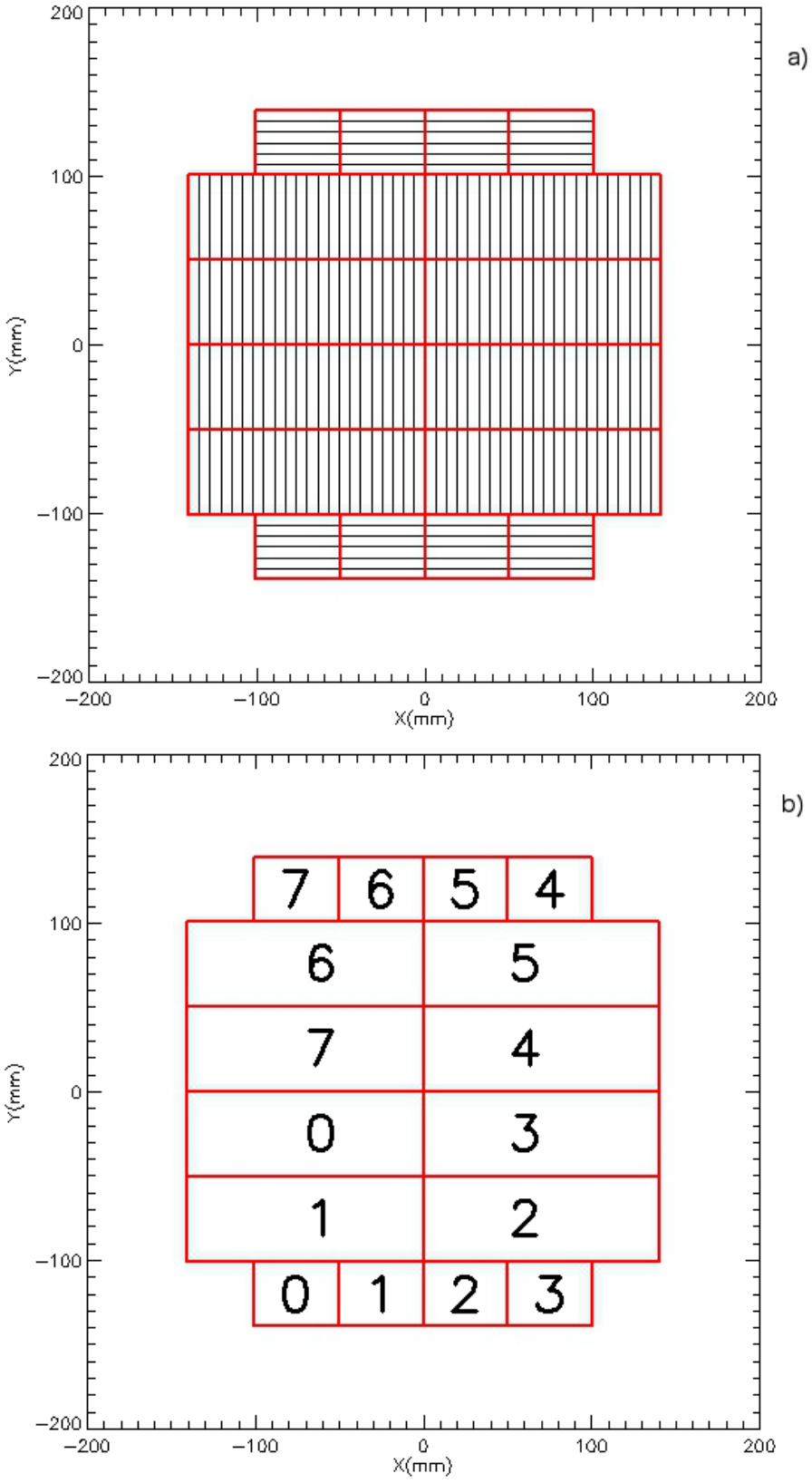

Figure 3.10: Second version of the receiver design at 500×. The a) panel shows the subdivision in strings. The b) panel shows the electrical connections: zone with the same number are series interconnected. The 8 resulting blocks are parallel connected.

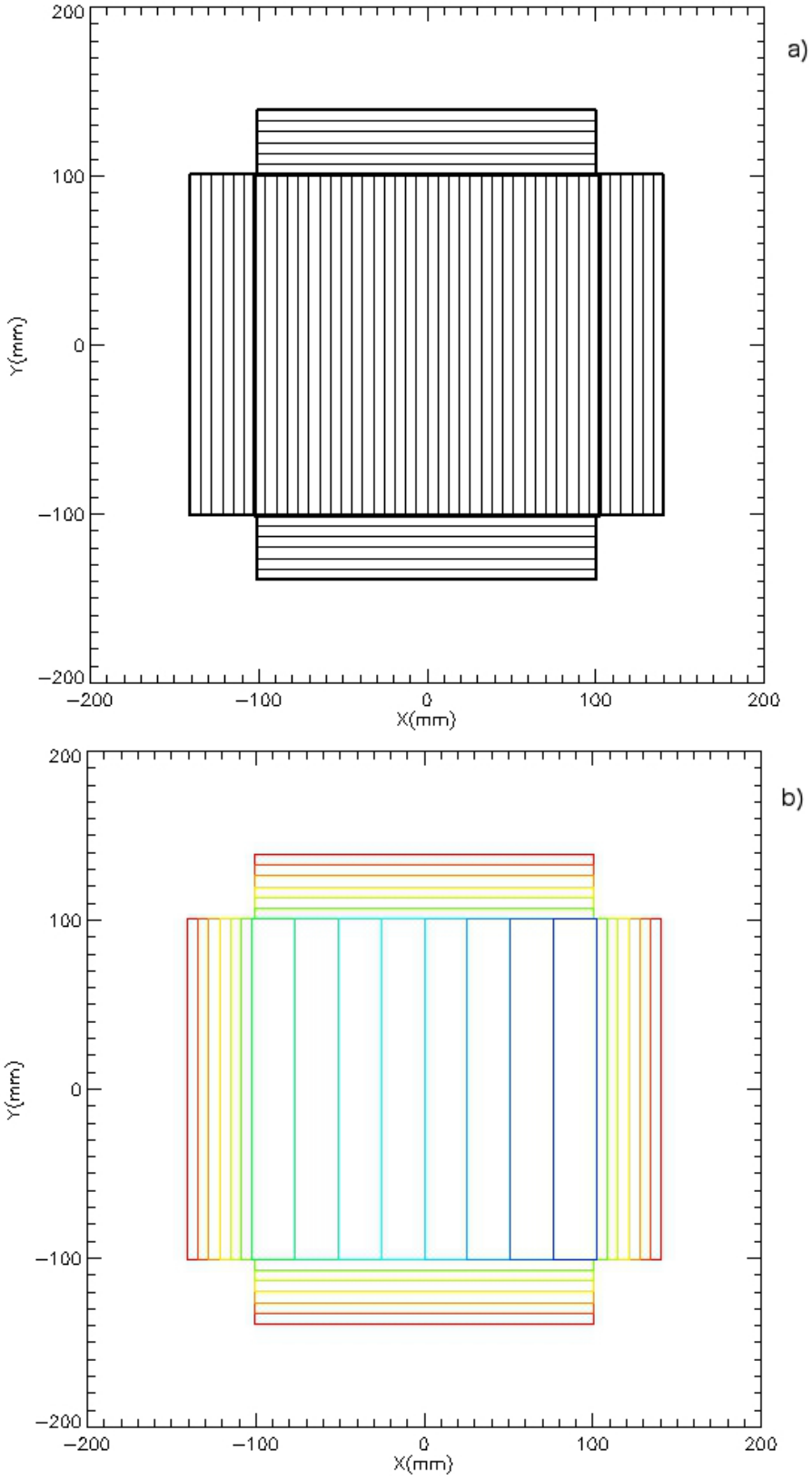

Figure 3.11: Third version of the receiver design at 500×. The a) panel shows the subdivision in strings. The b) panel shows which strings are series connected (zones with the same color). The 14 resulting blocks are parallel connected.

The parallel connected blocks are 12. Spillage losses at the corners are around 8-10% because we preferred to preserve the array symmetry avoiding to put cells in these areas. This choice prevents to further increase the series mismatches.

3.2.4 Optimization procedure

After completing the two blocks of simulation code, respectively for the optics and the receiver, we optimized the eight independent Zernike coefficients. A procedure optimizes the parameters by a downhill simplex method. The merit function to minimize has been defined as the negative efficiency of the receiver $(-\eta)$: each evaluation of this function requires to calculate the efficiency by the ray tracing procedure and the receiver modeling previously explained. We summarize the optimization steps as follows.

The initial values chosen for the parameters to be optimized are inserted in the optimization routine. The routine performs multidimensional minimization of a function $Func(x)$, where x is an n-dimensional vector, using a downhill simplex method requiring only function evaluations and not derivatives. Additional input for the routine are the fractional tolerance to be achieved in the function value as well as the range of the parameters variation. The optimization procedure transfers the parameters value to the ray-tracing procedures.

The ray-tracing code is the first block of procedures that simulates the optical scheme for the inserted parameters giving as output the nominal spot produced by a 7-mirrors optics dimensioned as seen. In the algorithm, the continuous optical surfaces of the mirrors have been approximated by a fixed number of subapertures. Each subaperture follows the ray-tracing method: the rays striking it are addressed toward the receiver following the classical reflection law. The Sun has been modeled as an homogeneous circular source with a diameter of 0.53°, thus applying a realistic divergence model. The number of rays traced from the Sun has been set in order to minimize subsampling errors. We supposed an ideal tracking conditions in which the central solar rays strikes the central mirror vertex parallel to the optical axis.

The second block simulating the receiver performance gets in input the image focused by the optics. The image is a matrix containing the local concentration on each receiver cell. The analytical model distinguishes between cells series and parallel connected, imposing the current of a series cells as the current produced by the worst illuminated cell. Subsequently, the current and voltage output for each series/parallel are summed to give the array output and the efficiency.

After calculating the efficiency of a specific optics coupled with the receiver, the procedure changes the parameters value iteratively in the range specified, calculating a new efficiency and comparing the values of the simplex obtained. When the minimum is found within the threshold, the routine returns an n-element vector corresponding to the function minimum value.

This kind of method could be applied to other type of receivers and it could be improved by extending the variable parameters (for example the curvature that we considered fixed) ever paying attention that the optimization converges in reasonable time.

3.2.5 Tolerances calculation

The tolerances calculation has been implemented to assess the feasibility of the proposed concentrator designs. Tolerances have been obtained for both optical and geometrical parameters. The results will be shown in the next Chapter, but here we briefly introduce the method used to obtain them.

We considered 25 parameters for each of the 4 different mirrors (the remaining surfaces are identical but simply rotated). 3 additional parameters are the two tracking angles and the receiver position along the z-axis for overall 178 parameters. The parameters include tilts and positions of the mirrors, their curvatures and the Zernike coefficients up to the 6^{th} radial order (from 4^{th} to 21^{th}). The reason for considering up to this order lays in the connection between the radial degree of the polynomials and the spatial scale of the deformations: the degree of a polynomial on a certain surface (which has a diameter of 2.6 m in the proposed design) roughly define the scale of the associated deformation so that, for example, a 6^{th} degree deformation on 2.6 m diameter would be around half meter wide (2.6/6 m = 0.43 m). It has been evaluated that higher degree of deformations, occurring on spatial scales smaller than about the calculated scale, can be reasonably controlled by surface polishing of suitable materials (aluminum, molded plastics, etc.). The tolerances have to be calculated also for polynomials with nominal null coefficients since all the polynomials included are necessary to model the irregularities up to the spatial scale chosen.

The nominal image produced by the optics with the optimized parameters and the corresponding receiver efficiency have been calculated and stored as term of comparison. We chose a reasonable interval in which the parameters can vary and a the minimum tolerable efficiency. The tolerated efficiency degradation is equally split among all the parameters, assuming that their effects are intercorrelated. Degraded efficiency is calculated for the minimum and maximum values of a given parameter, keeping nominal values for all the other parameters: if the degraded efficiency is acceptable, the minimum and maximum values of the given parameter are adopted as tolerances for that parameter; otherwise the variation range of the parameter is reduced and the process is repeated until convergence. After computing the tolerances for each parameter separately, the global effect is evaluated by perturbing all the parameters simultaneously, in a random fashion and according to the computed tolerances, and evaluating the corresponding degraded efficiency.

Chapter 4

Optimization results: the SOLARIS concentrator

In the previous Chapter the method for optimizing the efficiency of a CPV dense array system by controlling the optical deformations has been presented in detail. The optimization led to the conceptual design of a new system called "SOLARIS (SOLAR Image Squaring) Concentrator" that has been patented in Italy. The patent is owned by both the University of Bologna and the National Institute of Astrophysics (INAF), the two research institutes involved in the project. It has been filed with the reference number TO2014A000016. Main subjects of the patent are both the innovative concentrating optics and the method for the numerical optimization of the reflective surfaces. Theoretical procedures described at the end of this Chapter, to test/calibrate the reflective shapes and to align the mirrors on Sun, as well as the receiver and the mechanical design are also part of the patent.

4.1 System performance and mechanical design

In the following Sections we will show the simulated performance of the designed 7-mirror concentrator, also in comparison with the performance of a monolithic imaging paraboloidal mirror dimensioned for the same collected radiation and average concentration ratio. Thanks to the collaboration with the technical INAF staff, a mechanical structure for supporting the optics has been developed as described later in the Sections.

4.1.1 Results of the optical optimization

The concentrator design has been optimized by the routines described in Section 3.2.4, minimizing a merit function related to the electric conversion efficiency. The output values shown in Table 4.1 have been obtained by optimizing the efficiency of the third-type receiver described in Section 3.2.3 designed for the two concentrations 500× and 800×. The coefficients of the other mirrors have been easily calculated with the relations in Table 3.4.

	Z4(1)	Z11(1)	Z14(1)	Z4(2)	Z6(2)	Z7(2)	Z11(2)	Z14(2)
500×	1.1235	0.1365	0.0982	1.4858	-0.6158	0.2225	0.0032	-0.2172
800×	1.1027	0.0703	-0.1076	1.0526	-0.7142	0.2794	0.0190	-0.1436

Table 4.1: Values in mm of the Zernike coefficients optimized for the third-type receiver, at the two considered concentrations.

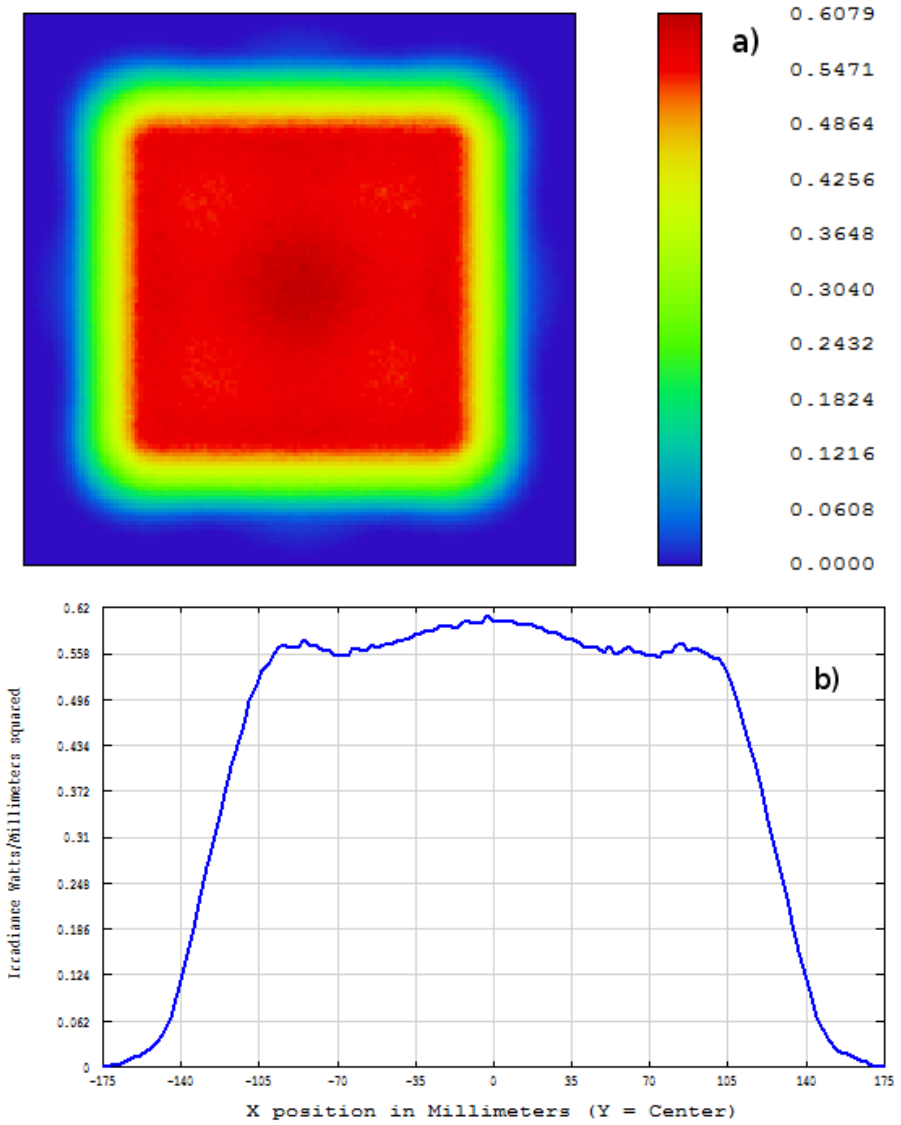

Figure 4.1: 2D (a) and x-cross section (b) irradiance produced by the optics coupled to the third-type receiver and optimized for concentration 500×. The physical size of the figures is 350 mm. Units in the color bar are Watt/cm^2.

The irradiance features obtained by the efficiency optimization of the third-type receiver are reported here. The bi-dimensional and the x-cross section irradiance produced by the optimized optics have been simulated by Zemax® for the two concentration ratios and they are shown in Fig. 4.1 and Fig. 4.2. The x-cross section irradiance is evaluated on the central row parallel to the x-axis of the bi-dimensional irradiance pattern. The physical size of all the Figures is 350 mm, while the color bar in the bi-dimensional Figures describes irradiance

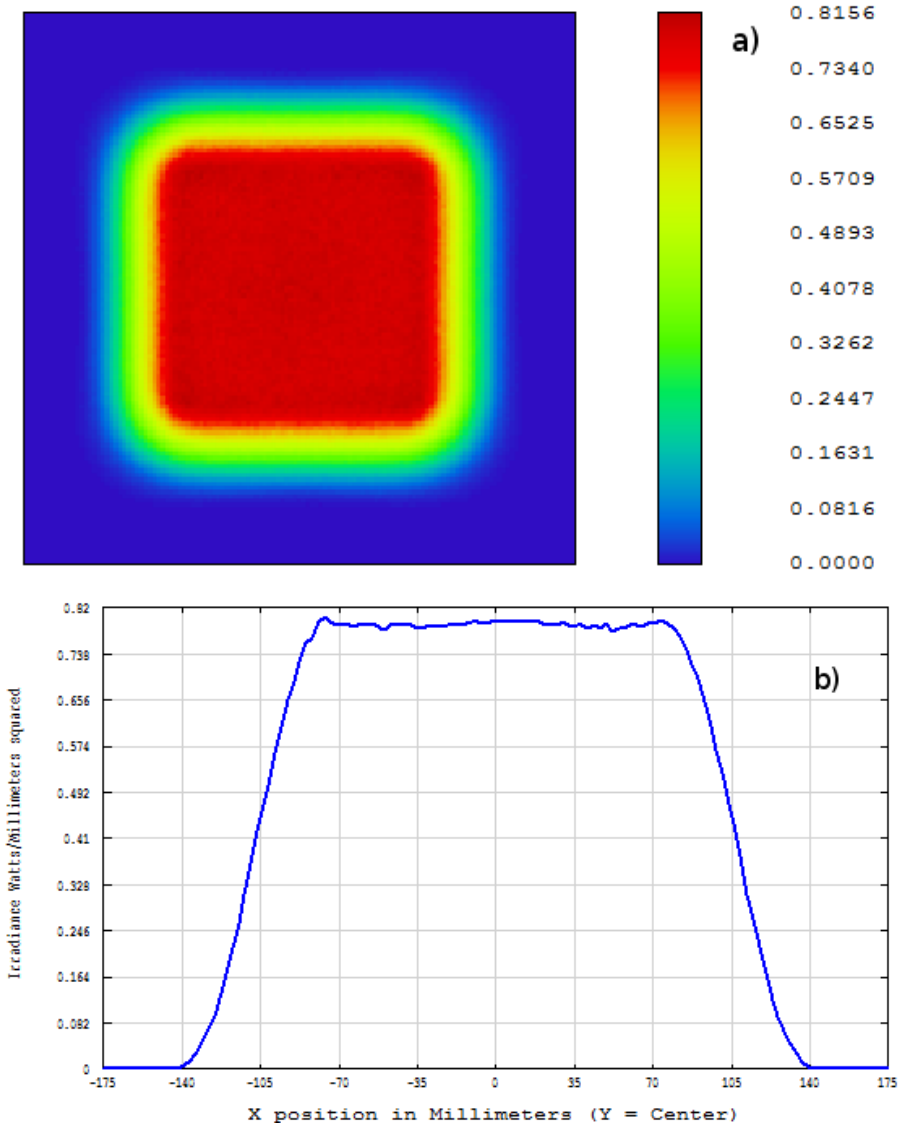

Figure 4.2: 2D (a) and x-cross section (b) irradiance produced by the optics coupled to the third-type receiver and optimized for concentration 800×. The physical size of the figures is 350 mm. Units in the color bar are Watt/cm^2.

values in Watt/cm^2. All the simulations have been performed with 1 sun irradiance at the concentrator entrance aperture, which is a value used in Standard Test Conditions (STC).

In Table 4.2, the performances of the receivers described in Section 3.2.3 are listed. The efficiency η has been defined as the output power of the receiver divided by the total power collected by the optics. The optimized systems have a conversion efficiency of about 30% in all the cases with 500× and of 28% in the only analysed case with 800×. The second case is interesting for the development of new generation cells because it shows that the method proposed gives good results also at higher concentrations. Moreover, the higher the concentration the smaller is the number of cells employed in the receiver. The case with concentration 800× includes only 1152 cells, almost the half of the cells needed for the concentration 500× (2016 elements).

The relative efficiency η_{rel} in the Table has been defined considering not all the collected power but only the effective power impinging on the array, i.e. accounting for spillage losses at the corners/edges. This parameter is useful to evaluate the average cells performance in the array. In three of the four cases, its value is above 31% and it must be compared with the maximum theoretical efficiency reported in Section 3.2.3 for the active part of the cell considered, i.e. 33% for concentration 500× and 32% for 1000×. This means that the cells in the arrays, under the irradiance produced by the optimized optics, work really close to their nominal performance.

	$\mathbf{I_{out}}$(A)	$\mathbf{V_{out}}$(V)	$\mathbf{P_{out}}$(W)	η(%)	$\eta_{\mathbf{rel}}$(%)
Receiver 1 (500×)	98.7	105.2	10288.0	29.2	30.5
Receiver 2 (500×)	50.5	204.6	10324.8	29.7	31.6
Receiver 3 (500×)	25.3	409.2	10354.5	29.4	31.2
Receiver 3 (800×)	32.6	302.6	9868.1	28.0	31.4

Table 4.2: Electrical performance obtained after the optimization run with the three receivers implemented.

Looking at the results in Table 4.2, the main difference between the three receivers analysed in the case with concentration 500× lays in the output parameters values. Even if the total power produced is quite similar in all the cases (slightly higher than 10 KWe), the output current and voltage are very different. The third receiver has been designed specifically with a high number of series connections to obtain a high voltage value (409.2 V) suitable for the available inverters and with small current (25.3 A) for limiting the resistive losses. This condition is convenient from an electrical point of view, but it leads to smaller tolerances as we will see in Section 4.1.3.

4.1.2 Comparison with the monolithic paraboloid

We show in this Section a comparison between the performance of a monolithic paraboloid mirror coupled with the third-type receiver and the efficiency of our optics with the same receiver. The monolithic mirror has been dimensioned for having the same effective aperture of our mirrors (35.25 m^2) and with a focal ratio very similar to the ratio *receiver distance/total diameter* of our system. The paraboloid curvature has been set to a convenient value with the aim of having average concentrations of 500× and 800× at the receiver plane.

Bi-dimensional and x-cross section irradiances produced by the monolithic optics have been simulated by Zemax® for the two concentrations mentioned above, but the results are shown in Fig. 4.3 only for the concentration 500×. The physical scale and the irradiance color bar have the same meaning as before.

The best receiver for the spot given by the paraboloidal mirror would be a receiver with a radial symmetry, with series connected rings of cells. Such a receiver is practically unfeasible with square/rectangular cells. The problem of using traditional rectangular receivers coupled with paraboloids rises because of the spillage losses caused by the obscuration of some

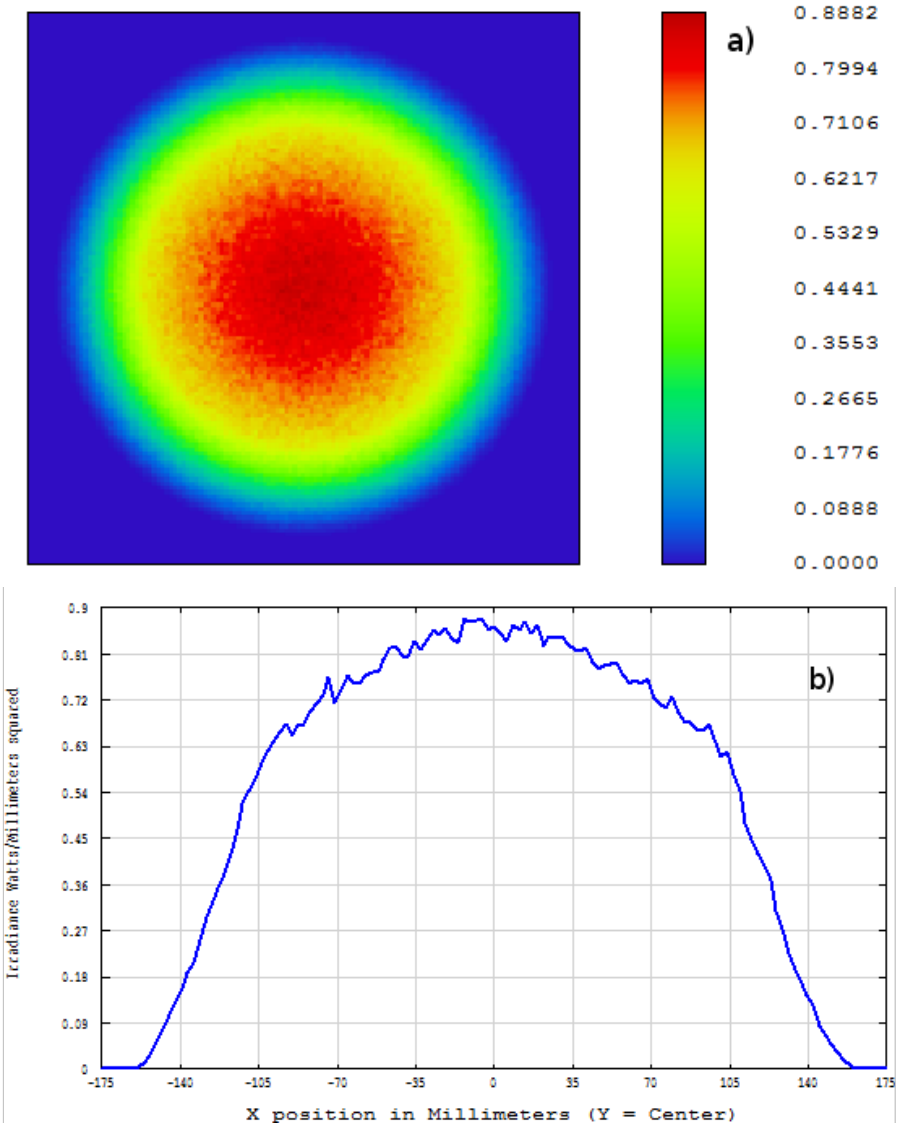

Figure 4.3: 2D (a) and x-cross section (b) irradiance produced by the monolythic paraboloid at concentration 500×. The physical size of the figures is 350 mm. Units in the color bar are Watt/cm^2.

cells. The rectangular electrical scheme does not match the circular irradiance pattern: the external modules are completely useless since the darkened cells exclude from the electrical production all the cells series connected to them.

The efficiency of the third-type receiver in Fig. 3.11 calculated with the spot produced by the monolithic mirror is slightly above 16% and 13% respectively for the two concentration mentioned. Compared to this simple optics, our system increases the efficiency by a factor of 2. The performance of a segmented mirror approximating the monolithic paraboloid, another common scheme, would be similar to the monolithic mirror if the segmented system was not provided with a secondary optics or the single facets were not adjusted on the mechanical frame to modify the spot shape.

4.1.3 Tolerances

The tolerances have been calculated with the algorithm explained in Section 3.2.5. We will show in detail only the tolerances calculated for the concentration 500× with the third version receiver, giving some qualitative indications for the other cases. The parameters related to each mirror are in Table 4.3 while the ones related to the receiver position are in Table 4.4. Three out of seven mirrors have been omitted from the Table since their tolerances corresponds respectively to the values calculated for the first three mirrors in the ring.

The last row in the table is the root square sum (RSS) of the Zernike coefficients and it is one of the most important tolerance indicators in our analysis since it represents the tolerated surface sag deviation. For all the mirrors, this parameter is in the order of tenths of a millimeter. The tracking errors shown in Table 4.4 seems quite small if compared to other CPV concentrators (normally in the order of thousandths of a radian or more). In any case, the tracking accuracy can be achievable with standard tracking solutions commonly employed in telescopes since these systems can also reach subarcseconds tolerances. Good pointing and active tracking systems are already developed also for solar concentrators [Fon2011], but their performances should be further improved to allow our tolerances. The shape deviation tolerated is also compatible with the manufacturing irregularities of candidate materials (molded plastics or aluminum) for the deformed/deformable mirrors.

The calculation have been performed setting a threshold of 3% on the efficiency, i.e. tolerating a degradation of the performance from 29.4% down to 26.4%. This value has been chosen as reasonable for this type of systems, but it can be varied depending on the required performance. In general, for small perturbations, the tolerance on a parameter scales linearly with the threshold value.

The tolerances are strictly related to the electrical scheme implemented in the receiver. Considering an efficiency degradation threshold of 1%, the values calculated with the first detector described in Section 3.2.3 led to approximately the same values as reported in Tables 4.3 and 4.4. This means that calculating the tolerances with the 3% threshold for the first detector would lead to values much more relaxed than those listed in the Tables. On the other side, the first receiver is made mainly by parallel connections that prevent series mismatches when the uniformity of the nominal spot degrades: this condition produces higher output current respect to the other receivers considered, the output power being approximately the same in all cases.

Units	Parameter	Mirr1		Mirr2		Mirr3		Mirr4	
		nominal value	tolerance	nominal value	tolerance	nominal value	tolerance	nominal value	tolerance
	Z4	1.1235	0.0625	1.4858	0.0625	1.4858	0.0313	1.4858	0.0313
	Z5	0.0000	0.0625	0.0000	0.0313	0.5334	0.0625	-0.5334	0.0625
	Z6	0.0000	0.2500	-0.6158	0.0625	0.3079	0.0313	0.3079	0.0313
	Z7	0.0000	0.0313	0.2225	0.0156	0.1113	0.0156	-0.1113	0.0156
	Z8	0.0000	0.0313	0.0000	0.0156	0.1927	0.0156	0.1927	0.0156
	Z9	0.0000	0.0313	0.0000	0.0313	0.0000	0.0156	0.0000	0.0156
	Z10	0.0000	0.0313	0.0000	0.0156	0.0000	0.0313	0.0000	0.0313
	Z11	0.1365	0.0078	0.0032	0.0156	0.0032	0.0156	0.0032	0.0156
	Z12	0.0000	0.0156	0.0000	0.0078	0.0000	0.0078	0.0000	0.0078
mm	**Z13**	0.0000	0.0156	0.0000	0.0078	0.0000	0.0078	0.0000	0.0078
	Z14	0.0982	0.0156	-0.2173	0.0313	-0.2173	0.0156	-0.2173	0.0156
	Z15	0.0000	0.0156	0.0000	0.0156	0.0000	0.0156	0.0000	0.0156
	Z16	0.0000	0.0156	0.0000	0.0039	0.0000	0.0078	0.0000	0.0078
	Z17	0.0000	0.0039	0.0000	0.0078	0.0000	0.0078	0.0000	0.0078
	Z18	0.0000	0.0156	0.0000	0.0078	0.0000	0.0078	0.0000	0.0078
	Z19	0.0000	0.0078	0.0000	0.0078	0.0000	0.0078	0.0000	0.0078
	Z20	0.0000	0.0156	0.0000	0.0156	0.0000	0.0156	0.0000	0.0156
	Z21	0.0000	0.0156	0.0000	0.0078	0.0000	0.0156	0.0000	0.0156
	radius of curv.	10101.0000	25.0000	11480.1000	25.0000	11480.1000	12.5000	11480.1000	12.5000
	tilt x	0.0000	0.0004	-0.2546	0.0002	-0.1294	0.0002	0.1294	0.0002
rad	**tilt y**	0.0000	0.0009	0.0000	0.0001	0.2199	0.0002	0.2199	0.0002
	tilt z	0.0000	0.0017	0.0000	0.0017	0.0000	0.0017	0.0000	0.0017
	offset x	0.0000	5.0000	0.0000	2.5000	2320.8800	2.5000	2320.8800	2.5000
mm	**offset y**	0.0000	2.5000	2680.0000	2.5000	1340.0000	2.5000	-1340.0000	2.5000
	offset z	0.0000	25.0000	0.0000	3.1250	0.0000	3.1250	0.0000	3.1250
mm	$\sqrt{\sum \mathbf{Z^2}}$		**0.2762**		**0.1122**		**0.0957**		**0.0957**

Table 4.3: Tolerances calculated for the parameters of the mirrors.

Units	Parameter	All Mirrors	
		nominal value	tolerance
rad	**tracking error x**	0.0000	0.000109
	tracking error y	0.0000	0.000014
mm	**receiver offset z**	4800.0000	2.5000

Table 4.4: Tolerances calculated for the receiver parameters.

4.2 Mechanical design

The mechanical requirements of the structure for the proposed application can be divided into kinematic and geometrical. The system has to follow the Sun daily so it must be provided with an alt-azimuth tracking system. Nevertheless, considering the Sun as an infinite distant source, the rotational axis position is not relevant respect to the optical focus of the system. The tracking has to span 90° in altitude and 180° in azimuth. All these features are compatible with simple systems presently available for astronomical use.

The mechanical shaded model is shown in Fig. 4.4. From the analysis of the Zernike polynomials, the desired deformations on the mirrors can be calibrated by a restricted number of actuators positioned on a certain number of control point. For the designed systems, these points are located radially on three circumferences every 10° as shown in Fig 4.5. The rings and the fixation points are shown in two structural schemes in the Figures 4.6 and 4.5. However, the number of the controlling points depends on the type of deformations desired, i.e. on the number of Zernike coefficients involved in the surface shaping.

A way to obtain the final surfaces is to use spherical mirrors and to set the deformations by the actuators. Another approach involves freeform mirrors already shaped with the final form desired, the actuators being used only to calibrate the shape errors once the mirrors have been placed on their own support. All these mirrors could be made for example by aluminium sheets, since this material is particular suitable for its lightness and its ductility. Molded plastic could be also suitable material (if compatible with the tolerances needed) after the deposition of a high reflective layer.

After mechanical manufacturing for creating the mirror shape and the fixation points, the surfaces will probably require a new refining for obtaining the needed optical features. High reflectivity could be achieved by surface lapping or by electro-deposition of a thin nickel layer.

The support of the mirror has been conceived as an aluminium truss structure since it is light and easy to construct and it prevents ribs on the mirrors. Also the receiver support could be made of aluminium: its cross section should be as small as possible to limit shadowing effect on the central mirror. The optics frames are mounted on the truss structure, designed to fulfill the mechanical stability requirements and to host two pipes

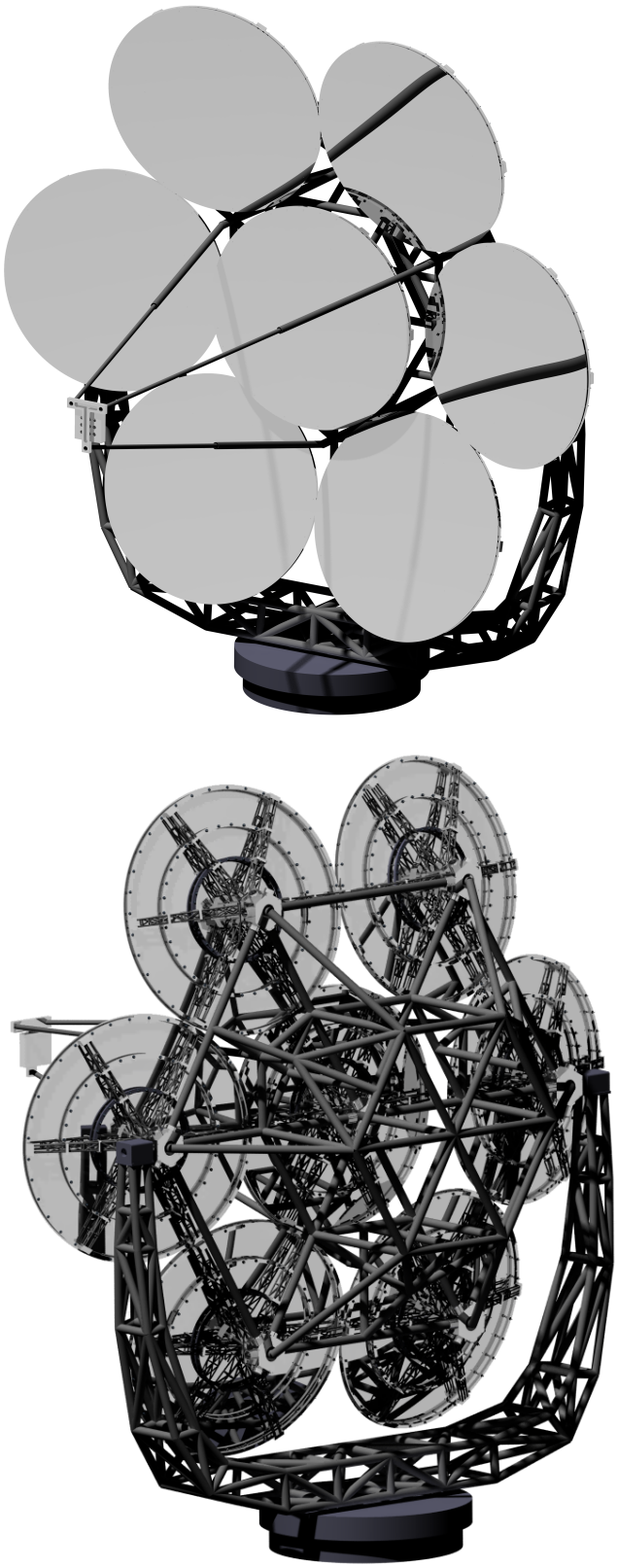

Figure 4.4: Shaded models of the SOLARIS Concentrator: a) front side, b) rear side.

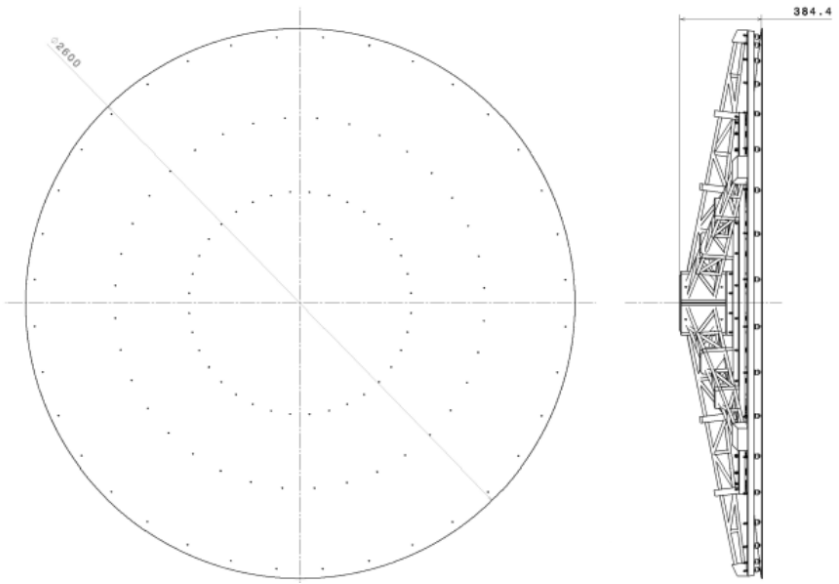

Figure 4.5: Scheme of the control points and lateral view of the optics support.

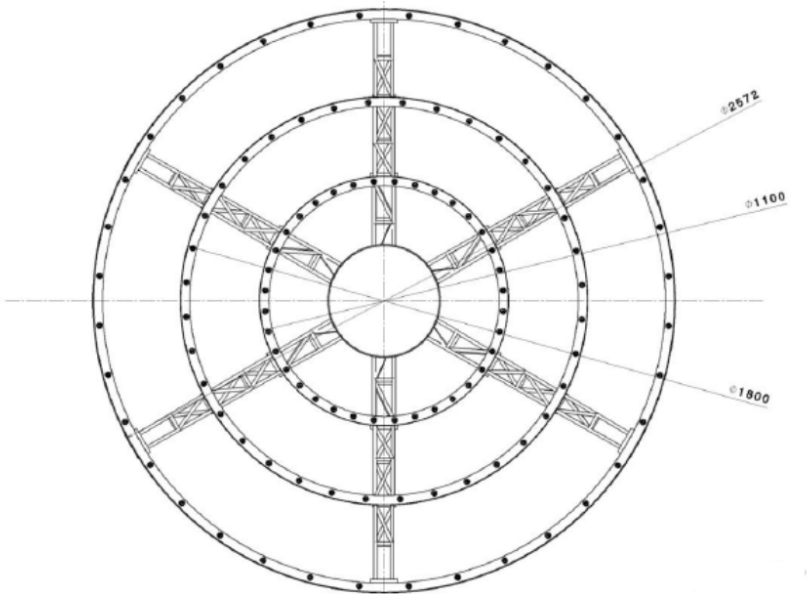

Figure 4.6: Front view of the optics support

to conduct the electrical cables and two pipes for the cooling fluid. The choice of using a cooling system for the cells is necessary for dense array receivers to remove the residual heat caused by radiation not converted into electricity. Moreover, this heat can be introduced into a cogeneration cycle thus increasing the global system efficiency.

4.3 Deformations control and alignment methods

In the realization phase of the system described above, particular attention should be paid to the optics manufacturing and to the accurate positioning of the mirrors on the

mechanical structure. For this reason, we theoretically conceived two procedures to test the mirrors shape and to align the supports correctly so that the optical and geometrical parameters of the system result within the desired tolerances. The two steps are: the mirrors positioning on their own supports and the calibration of their nominal shape; the alignment on Sun of each mirror on the whole structure.

4.3.1 Testing the optical shapes

The first phase can be performed in laboratory and it requires a point light source, a beam splitter, a Shack-Hartmann (SH) wavefront sensor [Sha1971] with a suitable number of subapertures as shown in Fig. 4.7. The details of the zone around the camera is zoomed in Fig. 4.8. The procedure can be sketched as follows:

- the point source is positioned in the exact curvature center of the mirror;
- if the mirror is perfectly spherical, the rays are reflected back toward the beam splitter, which redirects the rays toward the SH sensor;
- the camera acquires the image which can be used to recognize the wavefront shape and the mirror surface map;
- the actuators are tuned iteratively until the measured surface map matches its nominal value (within the tolerances).

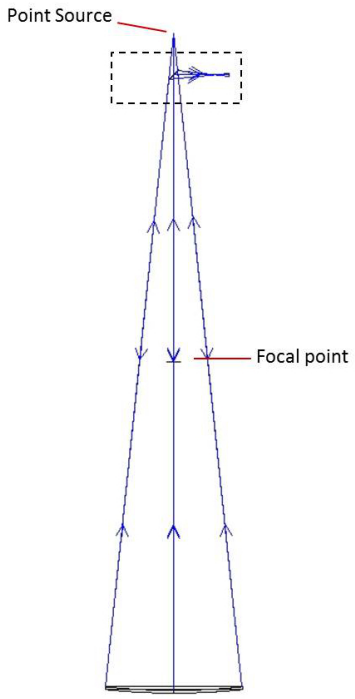

Figure 4.7: Optical scheme of the shape testing instrumentation.

To accelerate the calibration procedure, an interaction matrix records the SH sensor reaction to the specific movement of each single actuator. This matrix has to be inverted and used to transform the SH sensor signal into incremental corrections to apply to the actuators.

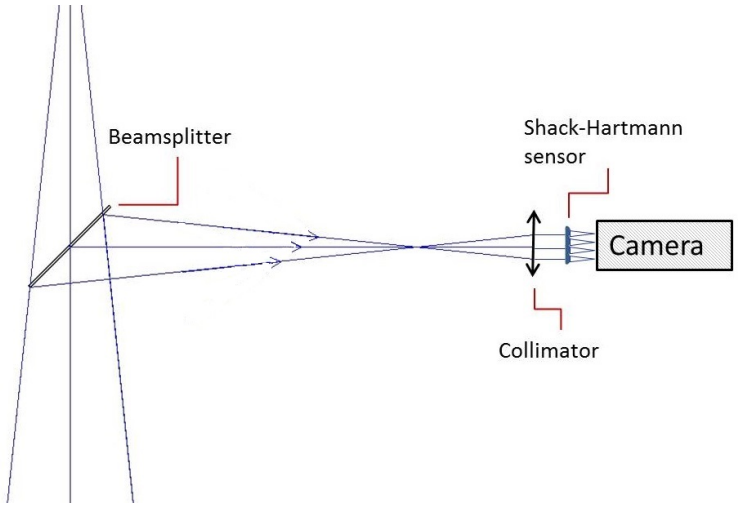

Figure 4.8: Zoom-in of dashed rectangle in Fig. 4.7 showing the wavefront sensor.

4.3.2 Outdoor alignment procedure

The alignment steps should be done outdoor having the Sun or the full Moon in the sky. A mask dimensioned as the receiver and realized in a material resistant to temperatures of a few hundreds degrees is needed (Fig. 4.9). Concentric frames of pinholes on the mask transmit part of the light impinging on the receiver plane to diodes or other electronic light-sensitive devices. Such a tool allows to sample the irradiance distribution produced by the optics. The procedure is divided into different steps:

- once the mirrors have been set on their own supports as described in Section 4.3.1, they are mounted on the global mechanical structure;
- the mask is positioned at the receiver distance;
- six out of seven mirrors are obscured by removable covers;
- the whole system tracks the Sun/the Moon so that the uncovered mirror can produce its spot on the mask;
- the irradiance distribution is sampled by the diodes;
- if the distribution differs from the nominal value, the mirror positions are adjusted iteratively until the desired irradiance is obtained (within the tolerances desired).

As in Section 4.3.1, an interaction matrix is used to record the diodes reaction to the parameters to align. This matrix is then inverted and used to translate the measured signal into corrections for the mirror positioning.

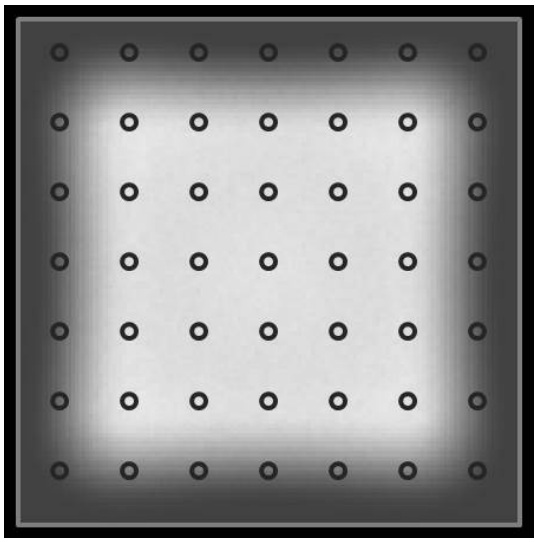

Figure 4.9: Mask for the outdoor alignment procedure. The number and the position of the pinholes are indicative and must be chosen depending on the spot dimension.

Conclusions and discussion

In this thesis work we developed a new method for designing optics for solar concentrators. In this technological scenario, the issues related to the optical design have a crucial role. In particular, dense array photovoltaic applications need an accurate control on both shape and irradiance of the collected light spot to perform at high efficiency. These systems are experiencing in the last years growing interest (from market and research) as feasible solutions in the production of cost competitive electricity on demand, especially in very sunny environments and off-grid communities. The development of solar cells that can work at higher and higher irradiance imposes a technological jump also from an optical point of view, to let these systems work at the same performance of the employed cells.

The proposed method is based on controlling the optical shapes so that the spot produced by the mirrors can resemble the optimal features for the chosen receiver without including secondary optics. The deformations to apply to spherical reflective surfaces have been analytically modeled by the Zernike polynomials and the deformed mirrors have been simulated by ray tracing routines written on purpose. At the same time, different schemes of dense array receivers have been designed using reference cells with known features and simulated by implementing simple electrical models for photovoltaic devices. The deformed optics have been then numerically optimized to maximize the performance of the concentrator as a function of the coupled receiver.

The method has been fruitfully employed to solve the prescribed irradiance problem at high concentration in a novel design of CPV dense array receiver system, called SOLARIS concentrator. This concentrator has been conceived not only in its optical part: a receiver scheme and a preliminary model for the mechanical structure have been designed. Both the method and the specific application developed have been patented in Italy.

The concentrator is a single stage multi-mirror system made by 7 monolithic optics placed in an hexapolar arrangement and all focusing on the same receiver. The main advantage of this choice is to have a systems with few optics to manage respect to the complex segmented dish optics usually employed in this technology. The main design has a mean concentration ratio $500\times$. The deformations applied to the optics allow them to produce a solar spot resembling a square shape with smoothed corners. The irradiance pattern inside the spot obtained is highly uniform. At this concentration, the optimized optics can boost the conversion

efficiency of the whole receiver up to 30%, almost the same performance of the single cell used in the calculations which is around 33%. The receiver has been designed as simple as possible, using exclusively strings of identical cells in series. The strings are then organized in parallels or series connections, with a Cartesian configuration and not involving bypass diodes in the design.

From an optical point of view, different considerations can been done to extend the purposes and the applications of the method conceived. Similar systems with different concentrations can be surely designed ever keeping in mind that the deforming method we introduced acts more efficiently in squaring and smoothing the spot for lower concentration ratios (i.e. high defocus). This behavior goes unfortunately against the trend of designing concentrating systems working at increasing concentrations since the research in cells technology is directed in this sense. Despite this limitation, we demonstrated that our method is however efficient at significantly high concentration ratios.

Method improvements could be done by a further investigation of the convenient deformations to introduce, exploring for example the effects related to Zernike polynomials of higher degrees. The selected deformations and the optical configuration used in this work are indeed only an example of the method proposed: other concentrators could be designed by adding deformations or changing the geometrical/optical parameters in function of the spot features desired. Systems with single or multiple mirrors (different or not) could be implemented and different geometrical configurations explored. Also the mirrors aperture could be varied in shape and size depending on the amount of output power needed or on the economical/constructive constraints. The final spot could result from a superimposition of images not necessarily centered in the same point, as in the studied cases. Moreover, all the mentioned parameters could be treated as additional variables to be optimized in the procedures. Another interesting application could result form both exploring the performance of deformable optics and very simple reflective secondary optics to recover possible light losses at the receiver borders or to relax the tolerances (thus enhancing the acceptance angle).

A great advantage of employing actively deformable optics could be given by the tuning of the concentration ratio. Using convenient deformable materials, flexible systems could be obtained that could embed different type of receivers exploiting the same optics. Also from the receiver point of view, great improvements could be obtained in terms of electric efficiency, involving optimized electrical schemes or thinking to future monolithic receivers.

Finally, an extension of this method could be also helpful in solving thermal problems. Thermal concentrators do also need a certain uniformity in the light collected to optimally transfer the energy to the exchanging fluid. On the other side, the proposed technique could be implemented in a "direct"' way, i.e. introducing controlled deformations to correct possible optical aberrations thus boosting the concentration up to its limit. This idea could

be developed, for example, in future solar tower plants where the intrinsic geometrical configuration with fixed focus and moving mirrors prevent the heliostats to collect the light into the smallest possible spot during its daily tracking of the Sun.

Acknoledgements

This research activity has been financially supported by a MIUR PhD grant and a CARISBO fellowship within the research framework on renewable sources, energy spare and distributed micro-generation.

I'm deeply grateful to Emiliano Diolaiti for his competence and temperance, but above all for the good ideas on which this research is based, and to Bruno Marano for the encouragement and his precious advice. My thanks go also to Matteo Lombini, Adriano De Rosa, Giuseppe Cosentino, Italo Foppiani, Carmelo Arcidiacono and Giovanni Bregoli for their technical and human support and to Laura Camanzi, Roberto Nani and the ABreMar office for their essential help during the patent application (especially when time was running out...). A special thank to Laura Schreiber for being "l'impiegata perfetta" and to Paolo, Carmela and Giuliana for their smile. Last but not least, all my gratitude goes to my beloved family, above all to Alessandro for the unconditional love and patience he has given. I should thank other people that surely contributed to this thesis. They faithfully believed in me even when I felt I couldn't do it. The list would be long to be written but I'm sure they know who they are.

Bibliography

[Azur] Azur Space website. Available at: http://www.azurspace.com

[DirInd] Direct Industry website. Available ay: www.directindustry.com

[Electro] The Elecropaedia website. Available at: http://www.mpoweruk.com

[NrelWeb] NREL website. Avialable at: http://rredc.nrel.gov/solar/spectra/am1.5/

[PVinsider] PV-insider website. Avialable at: http://www.pv-insider.com\cpv

[Qenerg] Qualenergia website. Available at: www.qualenergia.it

[Soitec] Soitec website. Available at: www.soitec.com/en/technologies/concentrix

[SolSys] Solarsystems website. Available at: www.solarsystems.com.au

[Spectro] Spectrolab website. Available at: www.spectrolab.com

[Ant2007] Antón I. and Sala G., The EUCLIDES concentrator, in *Concentrator Photovoltaics*, Springer Series in Optical Sciences, vol. 130, pp. 279-299, 2007.

[Bai2012] Baig H., Heasman K.C and Mallick T.K., Non-uniform illumination in concentrating solar cells, *Renewable and Sustainable Energy Reviews*, vol. 16, n. 8, pp. 5890-5909, 2012.

[Ben2005] Benítez P. and Miñano J.C., Concentrator optics for the next-generation photovoltaics, in *Next Generation Photovoltaics: High Efficiency through Full Spectrum Utilization*, A. Marti, A. Luque, ed. Taylor & Francis, CRC Press, London, 2004.

[Ben2010] Benítez P. and Miñano J.C., Zamora P., Mohedano R. et al., High performance Fresnel-based photovoltaic concentrator, *Opt. Express*, vol. 18, pp. A25-A40, 2010.

[Bru1996] Brunotte M., Götzberger A. and Blieske U., Two-stage concentrator permitting concentration factors up to 300x with one-axis tracking, *Solar Energy*, vol. 56, n. 3, pp. 285-300, 1996.

[Bur1975] Burkhard D.G and Shealy D.L., Design of reflectors which will distribute sunlight in a specified manner, *Solar Energy*, vol. 17, n. 4, pp. 221-227, 1975.

[Cha2011] Chayet H., Kost O., Moran R. and Lozovsky I., Efficient, Low Cost Dish Concentrator for a CPV Based Cogeneration System, *AIP Conference Proceedings*, vol. 1407, pp. 249-252, 2011.

[Cho2010] Chong K.K., Wong C.W., Siaw F.L. and Yew T.K., Optical Characterization of Nonimaging Planar Concentrator for the Application in Concentrator Photovoltaic System, *J. Sol. Energy Eng.*, vol. 132, n. 011011, 2010.

[Cho2012] Chong K.K. and Siaw F.L., Electrical characterization of dense-array concentrator photovoltaic system, *PVSEC Congress Proceedings*, Frankfurt, 2012.

[Coo2013] Cooper T., Pravettoni M., Cadruvi M., Ambrosetti G. et al., The effect of irradiance mismatch on a semi-dense array of triple-junction concentrator cells, *Solar Energy Materials and Solar Cells*, vol. 116, pp. 238-251, 2013.

[Cov2005] Coventry J.S., Performance of a concentrating photovoltaic/thermal solar collector, *Solar Energy*, vol. 78, n. 2, pp. 211-222, 2005.

[Dom2010] Domínguez C., Antón I. and Sala G., Multijunction solar cell model for translating I-V characteristics as a function of irradiance, spectrum, and cell temperature. *Prog. Photovolt: Res. Appl.*, vol. 18, n. 4, pp. 272-284, 2010.

[Feu2001] Feuermann D and Gordon J., High-concentration photovoltaic designs based on miniature parabolic dishes, *Solar Energy*, vol. 70, n. 5, pp. 423-430, 2001.

[Fon2011] Fontani D., Sansoni P., Francini F., Jafrancesco, D. at al., Pointing sensors and sun tracking techniques, *International Journal of Photoenergy*, n. 806518, 2011.

[Fra2006] Fraas L., Avery J., Huang H., Minkin L. et al., Demonstration of a 33% Efficient Cassegrainian Solar Module, *Proceeding of the 2006 IEEE 4th World Conference on Photovoltaic Energy Conversion*, vol.1, pp.679-682, 2006.

[Fra2003] Franklin E., Coventry J. Effects of highly non-uniform illumination distribution on electrical performance of solar cells, *Proc. Solar Australian and New Zealand Solar Energy Society*, 2003.

[Fri2010] Friedman D.J., Progress and challenges for next-generation high-efficiency multijunction solar cells, *Current Opinion in Solid State and Materials Science*, vol. 14, n. 6, p. 131-138, 2010.

[Fu2011] Fu L., Leutz R. and Annen H.P., Evaluation and comparison of different designs and materials for Fresnel lens-based solar concentrators, *Proc. SPIE 8124, Nonimaging Optics: Efficient Design for Illumination and Solar Concentration VIII*, vol. 81240E, 2011.

[Gia2010] Giannuzzi A., Sansoni P., Fontani D., Francini F. et al., Image optimization for a linear CPV system, in *EUROSUN Congress Proceedings*, Graz, 2010.

[Gia2011] Giannuzzi A., Fontani D., Pierucci G., Francini F. et al.,Secondary Optics Design For Mitigating Tracking Errors In A Linear CPV System, *PVSEC Congress Proceedings*, Hamburg, 2011.

[Gre1981] Green M.A., Solar cell fill factors: General graph and empirical expressions, *Solid-State Electronics*, vol. 24, n. 8, pp. 788-789, 1981.

[Gre2013] Green M.A., Emery K., Hishikawa Y., Warta W.et al., Solar cell efficiency tables (version 42), *Prog. Photovolt: Res. Appl.*, vol. 21, n. 5, pp. 827-837, 2013.

[Har1976] Harper D., Hildebrand R., Stiening R. and Winston R., Heat trap: an optimized far infrared field optics system, *Appl. Opt.*, vol. 15, n. 1, pp. 53-60, 1976.

[Her1995] Hermann C. and Sapoval B., *Physics of semiconductors*, Springer Verlag, New York, 1995.

[Her2008] Hernández M, Cvetkovic A., Benítez P. and Miñano J.C. High-performance Kohler concentrators with uniform irradiance on solar cell, *Proc. SPIE 7059, Nonimaging Optics and Efficient Illumination Systems V*, 705908, 2008.

[Her2012] Herrero R., Victoria M., Domínguez C., Askins, S. et al., Concentration photovoltaic optical system irradiance distribution measurements and its effect on multi-junction solar cells, *Prog. Photovolt: Res. Appl.*, vol. 20, n. 4, pp. 423-430, 2012.

[Kat2006] Katz E.A., Gordon J.M. and Feuermann D., Effects of ultra-high flux and intensity distribution in multi-junction solar cells, *Prog. Photovolt: Res. Appl.*, vol. 14, n. 4, pp. 297-303, 2006.

[Kin2006] Kinsey G.S., Sherif R.A., Cotal H.L., Pien P. et al., Multijunction Solar Cells for Dense-Array Concentrators, P*Proceeding of the 2006 IEEE 4th World Conference on Photovoltaic Energy Conversion*, vol.1, pp. 625-627, 2006.

[Leu1999] Leutz R., Suzuki A., Akisawa A. and Kashiwagi T., Design of a nonimaging Fresnel lens for solar concentrators, *Solar Energy*, vol. 65, n. 6, pp. 379-387, 1999.

[Leu2001] Leutz R., Suzuki A., Akisawa A. and Kashiwagi T., Flux Uniformity and Spectral Reproduction in Solar Concentrators Using Secondary Optics, in *Proceedings ISES Solar World Congress*, Adelaide, 2001.

[Loc2010] Löckenhoff R., Kubera T. and Rasch K.D, Water Cooled TJ Dense Array Modules for Parabolic Dishes, *6th Int. Conf. on Concentrating Photovoltaic Systems*, Freiburg, 2010.

[Luq1998] Luque A., Sala G. and Arboiro J.C., Electric and thermal model for non-uniformly illuminated concentration cells, *Solar Energy Materials and Solar Cells*, vol. 51, n. 3-4, pp. 269-290, 1998.

[Men2010] Menegolo A., *Fotovoltaico a Concentrazione: controllo e puntamento*, M. Sc. Thesis, Padova, 2010.

[Min2010] Minuto A., Timo G., Groppelli P. and Sturm M., Concentrating photovoltaic multijunction (CPVM) module electrical layout optimisation by a new theoretical and experimental mismatch analysis including series resistance effects, in *Photovoltaic Specialists Conference (PVSC), 35th IEEE*, pp. 3081-3086, 2010.

[Nol1976] Noll R., Zernike polynomials and atmospheric turbulence, *J. Opt. Soc. Am.*, vol. 66, n. 3, pp. 207-211, 1976.

[Nrel2012] Opportunities and Challenges for Development of a Mature Concentrating Photovoltaic Power Industry, *NREL Technical Report*, 2012.

[Phi2012] Philipps S.P., Guter W., Welser E., Schne J. et al., Present Status in the Development of III-V Multi-Junction Solar Cells, *Next Generation of Photovoltaics: New Concepts*, Springer Verlag, New York, 2012.

[Pra2011] Pravettoni M., Barbato M., Cooper T., Pedretti A. et al., InPhoCUS (Inflated Photovoltaic Ultra-light Mirror Concentrators): First Results Of The Project And Future Perspectives, *AIP Conference Proceedings*, vol. 1407, pp. 154-157, 2011.

[Rab1975] Rabl A., Comparison of solar concentrators, *Solar Energy*, vol. 18, no. 2, pp. 93-111, 1976.

[Rie1996] Ries H., Gordon J.M. and Lasken M., High-flux photovoltaic solar concentrators with kaleidoscope-based optical designs, *Solar Energy*, vol. 60, n. 1, pp. 11-16, 1996.

[Roy2007] Royne A. and Dey C., Design of a jet impingement cooling device for densely packed PV cells under high concentration, *Solar Energy*, vol. 81, n. 8, pp. 1014-1024, 2007.

[Sal2011] Salemi A., Eccher M., Miotello A. and Brusa R.S., Dense array connections for photovoltaic systems, *Prog. Photovolt: Res. Appl.*, vol. 19, n. 4, pp. 379-390, 2011.

[Sha1971] Shack R.V. and Platt B.C., Production and use of a lenticular Hartmann screen, *J. Opt. Soc. Am.*, vol. 61, pp. 656-660, 1971.

[Tae1976]
Thekaekara M. P., Solar Radiation Measurement: Techniques and Instrumentation, *Solar Energy* vol. 18, n. 4, pp. 309-325, 1976.

[Ver2006] Verlinden G.P, Lewandowski S., Bingham C., Kinsey G. et al., Performance and Reliability of Multijunction III-V Modules for Concentrator Dish and Central Receiver Applications, *Proceeding of the 2006 IEEE 4th World Conference on Photovoltaic Energy Conversion*, vol. 1, pp. 592-597, 2006.

[Vos2012] Vossier A., Chemisana D., Flamant G. and Dollet A., Very high fluxes for concentrating photovoltaics: Considerations from simple experiments and modeling, *Renewable Energy*, vol. 38, n. 1, pp. 31-39, 2012.

[Wie2012] Wiesenfarth M., Helmers H., Philipps S.P., Steiner M. et al., Advanced concepts in concentrating photovoltaics (CPV) *Proc. of 27th European Photovoltaic Solar Energy Conference and Exhibition*, pp.11-15, Frankfurt, 2012.

[Win1969] Winston R., Light Collection within the Framework of Geometrical Optics, *Journal of the Optical Society of America*, vol. 6, n. 2, pp. 245-247, 1969.

[Win2003] Winston R. and O'Gallagher J., Nonimaging Concentrators (Optics), in *Encyclopedia of Physical Science and Technology (Third Edition)*, Academic Press, New York, pp. 507-522, 2003.

[Win2005] Winston R., Miñano J.C. and Benítez P., *Nonimaging optics*, Elsevier, 2005.

[Zhu2011] Zhu L., Boehm R., Wang Y., Halford C. et al., Water immersion cooling of PV cells in a high concentration system, *Solar Energy Materials and Solar Cells*, vol. 95, n. 2, pp. 538-545, 2011.

[Zub2009] Zubi G., Bernal-Agustn J.L and Fracastoro G.V., High concentration photovoltaic systems applying III-V cells, *Renewable and Sustainable Energy Reviews*, vol. 13, n. 9, pp. 2645-2652, 2009.